DIPLOMARBEIT

BREITBANDIGES REFLEKTOMETER

AUSGEFÜHRT ZUM ZWECKE DER ERLANGUNG DES AKADEMISCHEN GRADES EINES DIPLOM-INGENIEURS UNTER DER LEITUNG VON

UNIV. PROF. GOTTFRIED MAGERL
UND
DI MARKUS MAYER

INSTITUT FÜR ELEKTRISCHE MESS- UND SCHALTUNGSTECHNIK
INST. NR. 354

EINGEREICHT AN DER TECHNISCHEN UNIVERSITÄT WIEN
FAKULTÄT ELEKTROTECHNIK VON

RAINER HORNSTEIN
MATR. NR. 9625681
WIENERSTRASSE 4
2285 LEOPOLDSDORF

WIEN, IM APRIL 2002

DIPLOMA THESIS

BROADBAND REFLECTOMETER

PERFORMED AT THE

INSTITUTE OF ELECTRICAL MEASUREMENTS AND CIRCUIT DESIGN

VIENNA UNIVERSITY OF TECHNOLOGY

SUPERVISED BY

UNIV. PROF. GOTTFRIED MAGERL
AND
DI MARKUS MAYER

DONE BY

RAINER HORNSTEIN
WIENERSTRASSE 4
2285 LEOPOLDSDORF

VIENNA, APRIL 2002

Acknowledgement

I would like to thank all members of the microwave engineering group of the Institute for Electrical Measurement and Circuit Design at the Vienna University of Technology. Special thanks to Univ. Prof. Gottfried Magerl, my advisor DI Markus Mayer and DI Holger Arthaber and DI Dieter Smely for their support with practical experience and their participation in inspiring discussions that led to new ideas for the realisation of my work.

Also special thanks to my student colleagues Jürgen Leeb and Volker Neubauer for supporting me with tips and hints for simulations and the practical implementation of my work.

Abstract

The aim of this work was to study the possibility of the realisation of a reflectometer that should be used in a low impedance measurement system for microwave devices. For that reason the reflectometer should be built in a 50 ohm version to test the principle of measurement. If this test is passed successfully the reflectometer could be adapted to be used in the low impedance measurement system.

This work concentrates on the 50 ohm implementation of the reflectometer. A sampled transmission line reflectometer turned out to be the best solution to this measurement problem.

The thesis starts with the structure of a sampled transmission line reflectometer. Referring to this the theory of reflection coefficient determination is explained. This also contains the theoretical basis for the used hardware and the algorithms. The next chapter is on the development and results of the hardware design. After that the implementation of the software is described and some according simulation results are shown. The main part is completed by measurement results made with the developed reflectometer. At the end there is a summary that sums up the properties of the chosen implementation and the important facts to adapt the reflectometer to a low impedance measurement system.

In the appendix there are descriptions of additionally developed software tools, mechanical drawings and required documents for the hardware development.

Kurzfassung

Zweck dieser Diplomarbeit war es die Möglichkeiten der Realisierung eines Reflektometers für ein niederohmiges Messsystem für Mikrowellenbauteile zu untersuchen. Um dies durchzuführen wurde das Reflektometer zuerst als 50 Ohm Variante entwickelt, um das Messprinzip zu testen. Wenn diese Testergebnisse zufriedenstellend ausfallen, kann das Reflektometer für ein niederohmiges Messsystem adaptiert werden.

Diese Arbeit konzentriert sich auf den Aufbau der 50 Ohm Variante des Reflektometers. Als beste Möglichkeit stellte sich das Konzept eines Sampled Transmission Line Reflektometers heraus.

Die vorliegende Diplomarbeit beginnt mit der prinzipiellen Struktur eines Sampled Transmission Line Reflektometers. Basierend darauf wird die Ermittlung des Reflektionskoeffizienten erklärt. Dies umfasst auch die Theorie der benötigten Hardware Komponenten und der verwendeten Algorithmen. Im nächsten Abschnitt werden die Entwicklung und die Ergebnisse der Hardwareentwicklung erläutert. Anschließend folgt ein Kapitel über die verwendeten Algorithmen und zugehörige Simulationsergebnisse. Der Hauptteil endet mit den Ergebnissen einer Messung die mit dem entwickelten Reflektometer durchgeführt wurde. Am Ende der Arbeit folgt eine Zusammenfassung der Eigenschaften der gewählten Realisierung und es werden die wichtigsten Punkte für die Adaption zur Verwendung in einem niederohmigen Messsystem besprochen.

Im Anhang befinden sich die Beschreibungen von zusätzlich entwickelten Software-Tools, mechanische Zeichnungen und benötigte Unterlagen für die Hardware-Entwicklung.

Contents

List of Acronyms

Abs	Absolute Value
Basic®	Microsoft Visual Basic® Version 6.0
DAB	Digital Audio Broadcasting
DUT	Device Under Test
GHz	Gigahertz
GPIB	General Purpose Interface Bus
GSM	Global System for Mobile Communication
HP	Hewlett Packard
HW	Hardware
Im	Imaginary Part
MHz	Megahertz
PCB	Printed Circuit Board
Re	Real Part
RF	Radio Frequency
SMA	RF Connector Type
SMD	Surface Mounted Device
SOLT	Calibration Method (Short-Open-Load-Thru)
SW	Software
TEM	Transversal Electro Magnetic
TRL	Calibration Method (Thru-Reflect-Line)
UMTS	Universal Mobile Telecommunication System
VNA	Vector Network Analyser
Microwave Office®	Microwave Office 2001® (Version 4.01)
MatLab®	MatLab® Version 5.3

List of Formula Symbols

φ_i	Reflection Coefficient Angle
ξ_i	Intermediate Value for the Calibration Coefficient Determination
κ	Condition Number
η_i	Intermediate Value for the Calibration Coefficient Determination
ζ_i	Intermediate Value for the Calibration Coefficient Determination
ε_{EFF}	Effective Dielectric Constant
δ	Ripple Factor in dB
Γ_R	Real Part of the Reflection Coefficient
γ_R	Real Part of the Transformed Reflection Coefficient
Γ_I	Imaginary Part of the Reflection Coefficient
γ_I	Imaginary Part of the Transformed Reflection Coefficient
$\underline{\mathbf{\Gamma}}$	Reflection Coefficient Vector
Γ	Complex Reflection Coefficient
$\underline{\boldsymbol{\gamma}}$	Transformed Reflection Coefficient Vector
β_i	Intermediate Value for the Calibration Coefficient Determination
α_i	Magnitude of the Calibration Value
Z_{IN}	Input Impedance of a Certain Termination
Z_{0O}	Odd Impedance
Z_{0E}	Even Impedance
Z_0	Nominal Impedance
x	Lateral Position
w_i	Weighting Factor
W	Width of Coupled Lines
V_{R0}	Complex Magnitude of the Reflected Wave
V_R	Reflected Wave
V_{I0}	Complex Magnitude of the Incident Wave
V_I	Incident Wave
$\underline{\mathbf{V}}_0$	Intermediate Value for the Calibration Coefficient Determination
T	Triple of Optimal Positions
S	Distance between Coupled Lines
R	Linear Ripple Factor
Q_i	Transformation Value for the Optimisation
q_i	Centre Point
P_i	Power at a Certain Position
p_i	Power Ration
$\mathbf{P}$	Power Matrix
N	Number of Sections
n	Minimum Number of Sections
M	Number of Frequencies for the Optimisation
m	Frequency Index
k_O	Variable of the Elliptic Integral for Odd Mode Impedance
$K_{k,j}$	Intermediate Value for the Calibration Coefficient Determination
k_i	Transformation Value for Optimisation
k_E	Variable of the Elliptic Integral for Even Mode Impedance
i	Index
H_k	Intermediate Value for the Calibration Coefficient Determination
G_k	Intermediate Value for the Calibration Coefficient Determination
$\mathbf{G}$	Reflection Coefficient Matrix
f_U	Upper Frequency Limit of the Directional Coupler
f_L	Lower Frequency Limit of the Directional Coupler

F_0	Centre Frequency of the Directional Coupler
f	Frequency
E_k	Intermediate Value for the Calibration Coefficient Determination
D	Distance between Coupler Tip and Transmission Line
$c_{i,j}$	Calibration Value
C_0	Speed of Light in Free Space
C	Width of the Coupler Tip
$\mathbf{C}$	Transformed Coefficient Matrix for the Reflection Coefficient Determination
b_i	Imaginary Part of the Calibration Value
B	Height of the Substrate
$\mathbf{B}$	Coefficient Vector for the Reflection Coefficient Determination
a_i	Real Part of the Calibration Value
$\mathbf{A}$	Coefficient Matrix for the Reflection Coefficient Determination
$\lvert\Gamma\rvert$	Magnitude of the Reflection Coefficient
$\lvert\gamma\rvert$	Magnitude of the Transformed Reflection Coefficient
ε_R	Relative Dielectric Constant
β_0	Wave Number at the Centre Frequency
Γ_0	Magnitude of the Complex Reflection Coefficient
λ	Wavelength
β	Wave Number
α	Loss Factor
γ	Complex Propagation Coefficient
φ	Angle of the Complex Reflection Coefficient

1 Introduction

1.1 Motivation

The reflection coefficient is a very important parameter for the interstage matching in high frequency and microwave circuit applications. A good matching between the different circuit stages is important for a good efficiency of the whole circuit. Therefore, it is important to be able to measure the reflection coefficient for different applications in the high frequency and microwave field. For these various applications located in different frequency ranges a simple measurement system that can be used in a wide frequency range is needed.

The most common method to measure the reflection coefficient is using a vector network analyser (VNA). But in many cases this is not necessary or takes some disadvantages along. The greatest disadvantages of a VNA are the price and size, which makes it very uneconomic for reflection coefficient measurements and very difficult to transport. Another disadvantage that goes along with the principle of measurement of a VNA makes it impossible to measure the reflection coefficient while the circuit is in use. As an example if the output of an amplifier is terminated with a certain load the output reflection coefficient of the amplifier can not be measured because the port of the VNA cannot be connected between the amplifier output and the termination.

The background to this thesis is the development of a reflectometer for a low impedance measurement system. This reflectometer should be useable for transistor measurements in the frequency range given below. The low impedance is necessary because the input and output impedances of power transistors are very low. If these impedances are measured with a low impedance measurement system the measurement error is much small than measuring them with a standard measurement system. Since the principle of measurement was not tested yet it was decided to build up a reflectometer that has a nominal impedance of 50 ohm which makes it easier to use commercially available test equipment. The content of this thesis is the development of the 50 ohm reflectometer and the according measurements to find basic information for the implementation of the low impedance reflectometer.

The broadband reflectometer that was developed in this thesis should meet all the requirements, which arise from the problems explained above. The main applications for the reflectometer are in the range of mobile communications. Therefore, the frequency range was chosen from 800 MHz up to 6.5 GHz what covers GSM, UMTS and DAB up to frequencies of the 3rd harmonic frequency of those applications.

According to all the requirements above different methods for measuring the reflection coefficient are possible. The most interesting is the six-port measurement technique and the sampled transmission line reflectometer. Both methods use scalar power measurements for determining the complex reflection coefficient. The classical method invented by G. F. Engen has the great disadvantage, that it is only usable in a small frequency range. The sampled transmission line reflectometer does not have this disadvantage and also fulfills all other requirements demanded above. So this was found to be the best solution to this measurement problem.

1.2 Overview of the Measurement System

The sampled transmission line reflectometer that was implemented in this diploma thesis uses five couplers that sample the power of the standing wave on certain positions. From these scalar power measurements the complex reflection coefficient of the device under test (DUT) is determined.

The six main components of the reflectometer are: the signal source, the directional coupler, the standing wave probe, the multipositionswitch, the powermeter and the control computer which are shown in the block diagram in Fig. 1.1.

The shown reflectometer principally works as follows: The signal source delivers the power that is used to arise a standing wave on the transmission line that is built up by the directional coupler and the standing wave probe. The directional coupler is used to measure the incident wave power for normalisation. The local power on the transmission line is sampled with the standing wave probe on five certain positions. Because just one power meter is used a multi position switch toggles between the output of the directional coupler and the five outputs of the standing wave probe. The control computer is responsible for the control of the signal source, the power meter and the multiposition switch. From the scalar power measurements the control computer determines the reflection coefficient and displays it to the user.

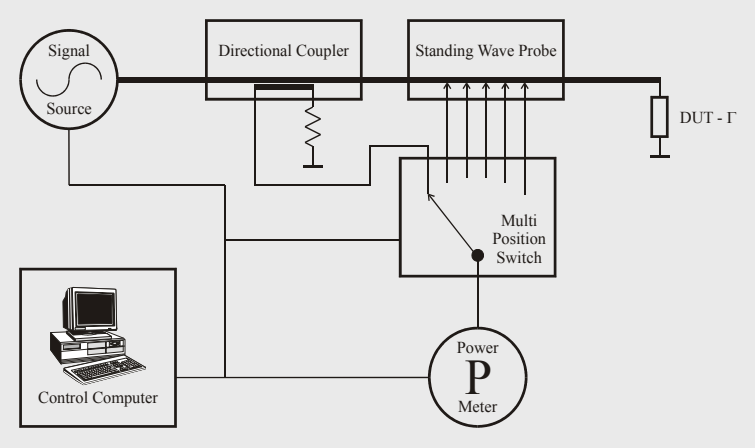

Fig. 1.1 - Measurement System for the Reflection Coefficient

1.3 Implemented Components

For the signal source, the powermeter and the multipositionswitch commercially available components were used. The control computer is a standard PC.

My task was to develop and implement the directional coupler and the standing wave probe and find a proper algorithm to determine the reflection coefficient. For this determination a calibration algorithm for the reflectometer had to be found as well. How this work was done and the achieved measurement results are the contents of this thesis.

2 Theory

The theory chapter of this thesis is divided into three subchapters: the basic theory of reflection coefficient measurements, the theory of the hardware components and the theory of the algorithms. All theory subchapters base on the concept of the sampled transmission line reflectometer as shown in the introduction.

2.1 Basic Theory of Reflection Coefficient Measurements

This subchapter intends to introduce the reader to the most basic theory on standing waves and reflection coefficient measurements. For this reason it is divided into two parts. The first part starts with the physical structure where standing waves occur and ends with a mathematical expression of the power of the standing wave on a certain position on the transmission line. This mathematical description is used in the second part where the determination of a certain reflection coefficient is shown in a graphical way. Based on this determination method, the difference between narrowband- and broadband measurements will be explained.

2.1.1 Standing Waves

A more detailed explanation of standing waves with additional background information can be found in [1], which is also the basis for this chapter.

Physical Description of Standing Waves

The physical structure for the occurrence of standing waves is shown in Fig. 2.1. At least three elements are needed to arise a standing wave: a signal source, a transmission line and a device under test (DUT) that has a certain input reflection coefficient. The signal source generates the incident wave that travels along the transmission line to the device under test. Due to the input reflection coefficient of the DUT a part of the incident wave is reflected at the reference plane and travels back to the source as reflected wave. The input reflection coefficient Γ of the DUT can be derived from the transmission line impedance and the input impedance of the DUT as shown in equation (2-1).

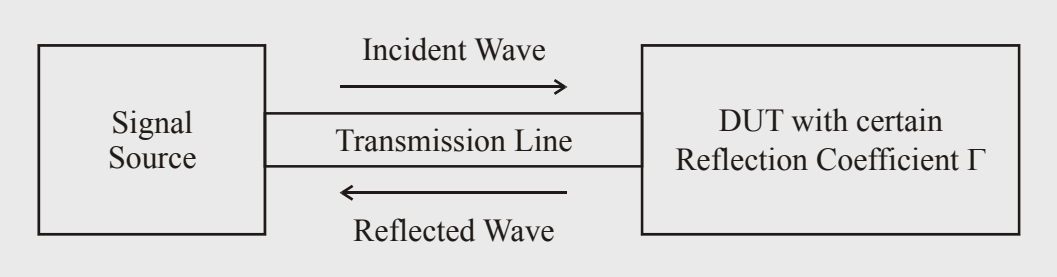

Fig. 2.1 - Physical Structure for Standing Waves

On the transmission line the incident and the reflected wave interfere and a standing wave pattern arises. Since the incident and the reflected wave depend on the reflection coefficient, also the standing wave pattern depends on the reflection coefficient. The mathematical basis for these relations will be explained in the next subsections.

Mathematical Description of Standing Waves

Before the mathematical basis is explained the transmission line impedance is defined as Z_0 and the input impedance of the DUT is defined as Z_{IN}. Using these definitions one can determine the reflection coefficient with expression (2-1). Γ_0 stands for the magnitude and φ for the angle of the complex reflection coefficient Γ.

$$\Gamma = \Gamma_0 \cdot e^{j\varphi} = \frac{Z_{IN} - Z_0}{Z_{IN} + Z_0} \qquad (2\text{-}1)$$

For the mathematical description a structure as shown in Fig. 2.2 is used. The reference plane is between the transmission line and the input port of the DUT. According to the position of the reference plane the x-values along the transmission line are negative.

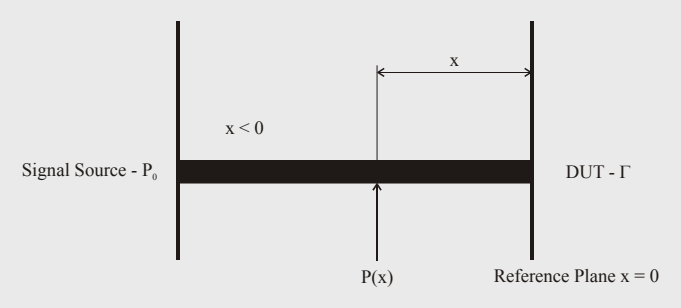

Fig. 2.2 - Physical Structure for the Standing Wave Description

For the incident wave voltage $V_I(x)$ equation (2-2) and for the reflected wave voltage $V_R(x)$ equation (2-3) can be used.

$$V_I(x) = V_{I0} \cdot e^{-\gamma x} \qquad (2\text{-}2)$$

$$V_R(x) = V_{R0} \cdot e^{+\gamma x} \qquad (2\text{-}3)$$

$$\gamma = \alpha + j\beta \qquad (2\text{-}4)$$

$$\beta = \frac{2\pi}{\lambda} = \frac{2\pi \cdot f \cdot \sqrt{\varepsilon_r}}{c_0} \qquad (2\text{-}5)$$

V_{I0} and V_{R0} are the complex magnitudes of the incident and reflected wave respectively. The complex propagation coefficient γ consists of the real part α, which counts for the loss on the transmission line, and β, the wave number. The relation between these parameters is given in equation (2-4).

Fig. 2.3 shows the incident and reflected wave for a certain reflection coefficient ($0.8 \cdot e^{+j180°}$) at a frequency of 7 GHz on a lossless transmission line. Since the phase of the reflection coefficient is 180°, we can determine the amplitude of the reflected wave at the reference plane by multiplying the incident wave by -0.8. In this example the amplitude of the incident wave at the reference plane is -0.5, which results in an amplitude of the reflected wave of 0.4.

If we assume a lossless transmission line we can substitute γ by $j\beta$. This leads from equations (2-2) and (2-3) to equations (2-6) and (2-7). This simplification can be made, because the loss on such short transmission lines is very small, and as a benefit the mathematical description becomes much clearer.

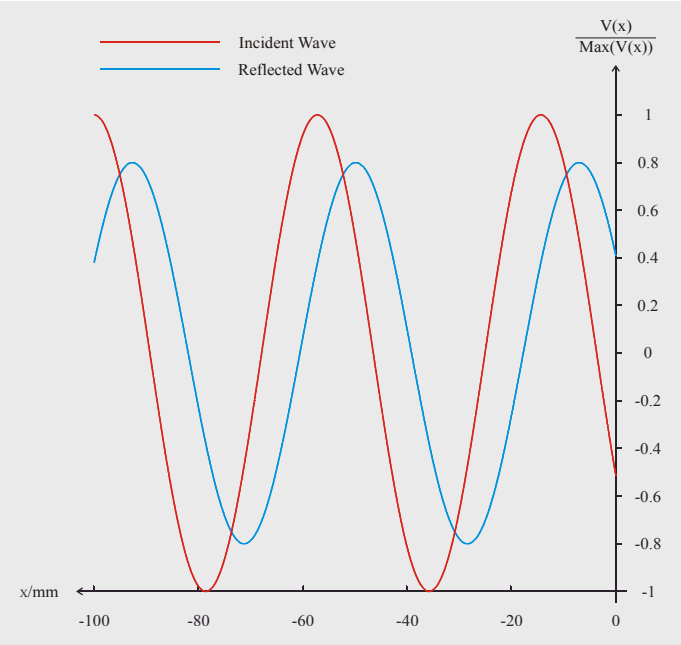

Fig. 2.3 - Incident- and Reflected Wave

The voltage on the transmission line *V(x)* is given by the sum of the incident and reflected wave voltages. Using another definition for the reflection coefficient given by equation (2-8) one can eliminate V_{R0} and show the direct dependence of the standing wave pattern on the reflection coefficient (2-10).

$$V_I(x) = V_{I0} \cdot e^{-j\beta \cdot x} \tag{2-6}$$

$$V_R(x) = V_{R0} \cdot e^{+j\beta \cdot x} \tag{2-7}$$

$$\Gamma = \frac{V_R(0)}{V_I(0)} = \frac{V_{R0}}{V_{I0}} \tag{2-8}$$

$$V(x) = V_I(x) + V_R(x) = V_{I0} \cdot e^{-j\beta \cdot x} \cdot \left(1 + \frac{V_{R0}}{V_{I0}} \cdot e^{+j2\beta \cdot x}\right) \tag{2-9}$$

$$V(x) = V_{I0} \cdot e^{-j\beta \cdot x} \cdot \left(1 + \Gamma \cdot e^{+j2\beta \cdot x}\right) = V_{I0} \cdot e^{-j\beta \cdot x} \cdot \left[1 + \Gamma_0 \cdot e^{+j(2\beta \cdot x + \varphi)}\right] \tag{2-10}$$

In Fig. 2.4 the standing wave pattern according to the incident and reflected wave of the last example is shown. From equation (2-10) one can see that the standing wave is periodically with half the wavelength, which also can be seen in Fig. 2.4. For a frequency of 7 GHz half the wavelength is 21.4 mm for free space conditions. The magnitude in this figure is normalized to the maximum magnitude of the incident wave. Since the power is proportional to the square of the magnitude of the voltage, one can use equation (2-11) to formulate equation (2-12) for the local power of the standing wave at a certain position of the transmission line.

$$P(x) = |V(x)|^2 = V(x) \cdot V^*(x) \tag{2-11}$$

$$P(x) = P_0 \cdot \left|1 + \Gamma \cdot e^{+j2\beta \cdot x}\right|^2 = P_0 \cdot \left[1 + |\Gamma_0|^2 + 2 \cdot \Gamma_0 \cdot \cos(2\beta \cdot x + \varphi)\right] \tag{2-12}$$

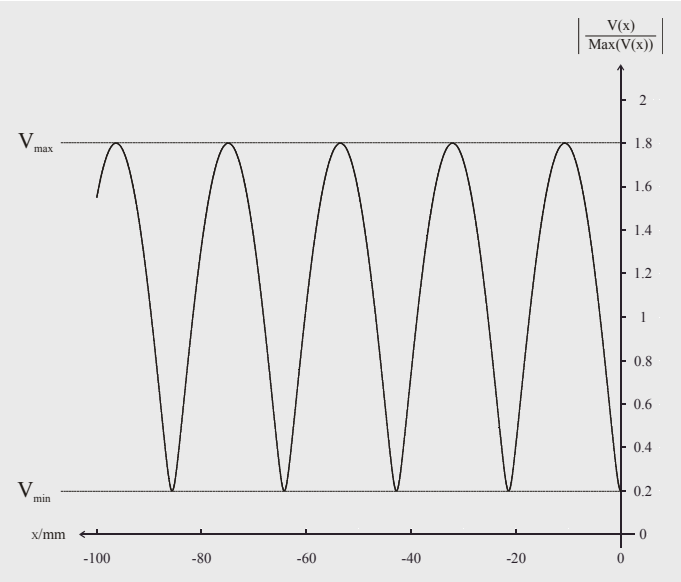

Fig. 2.4 - Standing Wave Pattern

To determine the magnitude of the reflection coefficient one can use a very easy expression given in equation (2-13). For this determination only the minimum- and maximum voltages of the standing wave are used. Equation (2-13) shows that a decrease of the difference between minimum and maximum voltages of the standing wave decreases the reflection coefficient magnitude. Therefore a measurement error has much more influence to a smaller difference between minimum- and maximum voltages than to a bigger one. For that reason reflection coefficients with larger magnitudes can be determined more accurately than such with smaller magnitudes.

$$\Gamma_0 = \frac{V_{max} - V_{min}}{V_{max} + V_{min}} \qquad (2\text{-}13)$$

At the end of this subchapter there is a comparison of the standing wave pattern for three different reflection coefficients depicted in Fig. 2.5.

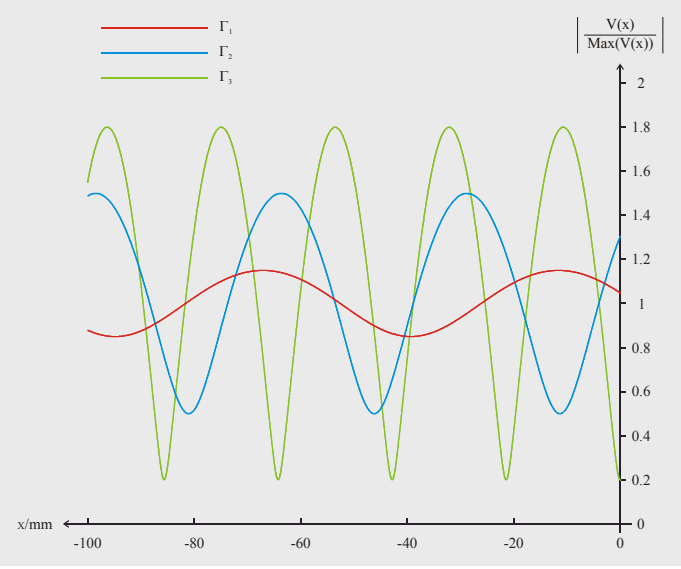

Fig. 2.5 - Standing Wave Pattern for Different Reflection Coefficients

The standing wave patterns for following three reflection coefficients are shown:

- $\Gamma_1 = 0.8 \cdot e^{+j180°}$ at f = 7 GHz
- $\Gamma_2 = 0.5 \cdot e^{+j63°}$ at f = 4.3 GHz
- $\Gamma_3 = 0.15 \cdot e^{+j285°}$ at f = 2.7 GHz

What should be noted in Fig. 2.5 are the different magnitudes, for the different reflection coefficients. The second important point is the lateral expansion of the standing wave pattern according to the frequency. Both characteristics are important for the determination of the reflection coefficient, which will be explained in the next subsection.

2.1.2 Reflection Coefficient Measurement

This subsection explains the determination of the reflection coefficient from local power measurements of the standing wave, initially for a single frequency, showing the narrowband case and finally for a wider frequency range, showing the broadband case. Applying the narrowband method to the broadband case this will lead to problems. How these problems can be solved will be shown in subsection 2.2.3.

This subsection is based on [2] and [3]. In these publications also references to more detailed publications on this topic can be found, because this chapter only contains the most basic aspects on reflection coefficient measurements.

Narrowband Measurement

Before a principal method for determining the reflection coefficient is discussed, the measurement structure, shown in Fig. 2.6, should be explained. Principally it is equal to the structure in Fig. 2.1. What is new are the measurement ports and their exact positions along the transmission line. At each of these ports which have an exact position (x_1 to x_3) the according scalar power (P_1 to P_3) of the standing wave pattern is sampled. The power P_0 is the output power of a directional coupler that measures the incident wave power. Since this power should be the same along the whole lossless transmission line the exact position of the directional coupler is unimportant.

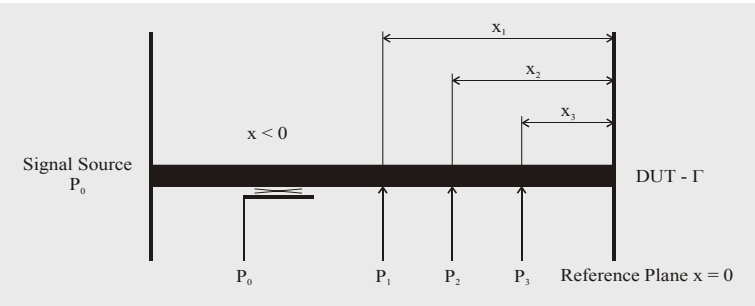

Fig. 2.6 - Measurement Structure - Reflection Coefficient Measurement

Using the second term of equation (2-12) expression (2-14) can be formulated for the ratio of the power at a certain sampling point to the power of the incident wave. In this expression i is used as an index for the powers and the according positions. If $e^{-j2\beta \cdot x_i}$ is substituted by q_i one can see that every possible value of Γ lies on a circle with q_i as the centre point and $\sqrt{\frac{P_i(x_i)}{P_0}}$ as the radius. As every q_i has a magnitude of 1, every q_i lies on the unit circle.

$$\left|\frac{P_i(x_i)}{P_0}\right| = \left|e^{-j2\beta \cdot x_i} + \Gamma\right|^2 = \left|q_i + \Gamma\right|^2 \qquad (2\text{-}14)$$

The reflection coefficient can be determined if at least three different circles fulfilling equation (2-14) are plotted in a smith chart. The point of intersection of those circles is the correct reflection coefficient. This is shown in an example: the reflection coefficient is chosen as $\Gamma_1 = 0.8 \cdot e^{+j180°}$ and the frequency is 7 GHz. The according standing wave pattern is plotted in Fig. 2.7. The dashed lines mark the positions, where the powers of the standing wave pattern are sampled.

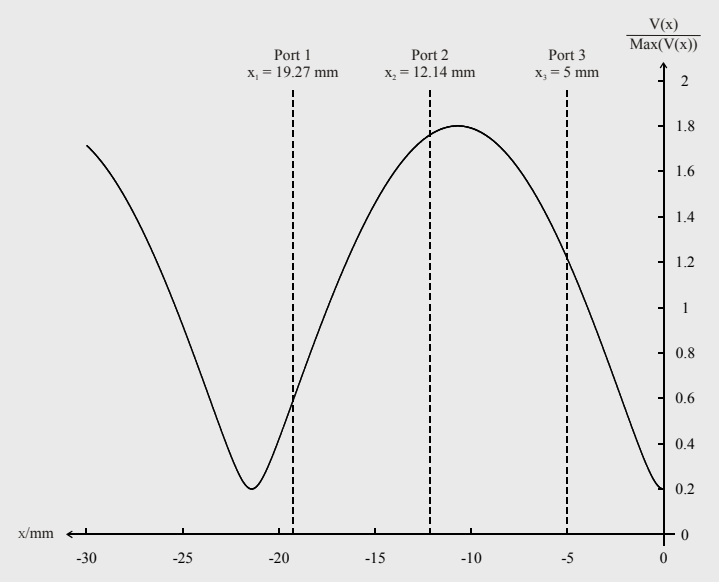

Fig. 2.7 - Standing Wave Pattern and Sampling Points

Firstly the *q*-points on the unit circle of the smith chart have to be found. If $x = 0$ the sampling point lies at the reference plane and the according *q*-point equals the short circuit point. If x is counted as in the measurement structure the *q*-points are found at an angle of $2\ \beta \cdot |x_i|$ anticlockwise starting from the short circuit point. To determine the reflection coefficient unequivocally at least three circles are needed. The procedure explained above is graphically shown in Fig. 2.8.

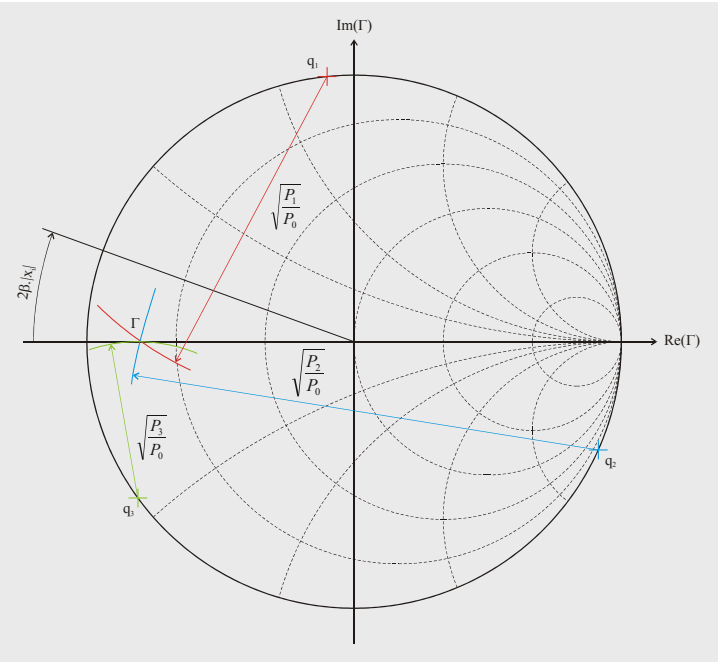

Fig. 2.8 - Determination of the Reflection Coefficient

Inspecting this determination method one can see that at least three sampling points along the transmission line are needed. Together with the fact that the circumference of the unit circle of the smith charts is $\frac{\lambda_0}{2}$, best accuracy is achieved if the probes are equally spaced with a distance of $\frac{\lambda_0}{6}$ between two adjacent probes, so that there are no slurring intersections of two circles. A slurring intersection would happen if the distance between two probes is very small because then their centres are very close on the unit circle and the radius of the circles is nearly the same because nearly the same standing wave power is sampled on the transmission line.

This determination method is graphically shown in Fig. 2.8 for the example values given above. The sampling ports are placed at the ideal positions of 5 mm, 12.14 mm and 19.27 mm, which are shown in Fig. 2.7 by the dashed lines. The first distance is just an offset that is chosen arbitrarily. Important is the distance of $\frac{\lambda_0}{6}$ = 7.14 mm between two consecutive sampling ports. As a result the correct reflection coefficient of $0.8 \cdot e^{+j180}$ is determined.

The method described above is just to show the principle of the determination and what is important when placing the sampling ports for the power measurement. The two implemented algorithms for the determination of the reflection coefficient are explained in detail in subchapter 2.3.

Broadband Measurement

Using the determination method explained above for a wider frequency range will lead to some problems. As mentioned above the optimum distance between two adjacent probes should be $\frac{\lambda_0}{6}$. Since λ_0 depends on the frequency this criterion can only be fulfilled for a single frequency. This spacing is chosen to avoid slurring intersections of two circles. But this will also be fulfilled in a narrow frequency range around the centre frequency f_0 for which this distance is not exactly met. So the above method can also be used in a limited frequency range around the centre frequency.

Problems occur, if the frequency is a multiple of $1.5 \cdot f_0$. Then the positions of two probes, which are correctly spaced for f_0, will coincide on the unit circle. A short example using the equations (2-15) to (2-19) should make this easily understandable. We choose x_1 arbitrarily, x_2 and x_3 are chosen as in equation (2-15) and (2-16), respectively.

$$x_2 = x_1 + \frac{\lambda_0}{6} \qquad (2\text{-}15)$$

$$x_3 = x_1 + 2 \cdot \frac{\lambda_0}{6} \qquad (2\text{-}16)$$

If the measurement frequency is chosen as $f_1 = 1.5 \cdot n \cdot f_0$, we can calculate λ_1 using equation (2-17). The according angles are then given by equation (2-18). In the special case of φ_3 we can show with equation (2-19) that this angle is equal to angle φ_1.

$$\lambda_1 = \frac{\lambda_0}{1.5 \cdot n} \qquad (2\text{-}17)$$

$$\varphi_i = 2\beta_1 \cdot x_i \qquad (2\text{-}18)$$

$$\varphi_3 = 2\beta_1 \cdot x_3 = 2\beta_1 \cdot x_1 + 2 \cdot \frac{2\pi}{\lambda_0} \cdot 1.5 \cdot n \cdot 2 \cdot \frac{\lambda_0}{6} = \left(2\beta_1 \cdot x_1 + n \cdot 2\pi\right) mod\left(2\pi\right) = 2\beta_1 \cdot x_1 = \varphi_1 \qquad (2\text{-}19)$$

This means that there are just two different centres and radii for three sampling points. So a uniqueness problem occurs and because of that the optimum distance for f_0 cannot be used for a measurement frequency of $f_1 = 1.5 \cdot n \cdot f_0$.

To avoid this problem at broadband measurements more than three probes, which are not equally spaced, have to be used. Those probes have to be placed in such a way, that at least three probes do not coincide on the unit circle for every frequency of the measurement range. But not any of those non-equal spacings is as good as the other. There is an optimum for the use in a wide frequency range. A method for determining this optimum will be discussed in subsection 2.2.3.

2.2 Hardware Theory

As already mentioned in the introduction two components of the sampled transmission line reflectometer were implemented by myself. Those components were the directional coupler and the standing wave probe. The standing wave probe was built by myself because it is not commercially available. The reason for building the directional coupler is that commercial available ones are very expensive and since the reflectometer should be a low cost implementation, a cost-effective realisation was needed.

The theory that is needed for the implementation of the directional coupler and the standing wave probe contains many different aspects. Therefore only the minimum of theory that is needed to build up these components will be presented in this subchapter. If the reader is interested in more details or in the theoretical background he is advised to look it up in the references, because the whole theory would blast this subchapter. For easier comprehensibility the theory of the standing wave probe is divided into two parts, firstly one part for a single coupler and secondly a part for the optimum spacing of the couplers.

2.2.1 Directional Coupler

The theory of coupled lines and the directional coupler is based on [4]. The first part of this subsection is on the properties of coupled lines that are needed to derive the physical layout of the directional coupler. The second part is on the determination of the characteristic parameters of a directional coupler.

Symmetrical Coupled Lines

Talking on coupled lines someone has to distinguish odd- and-even mode impedances, Z_{0O} and $Z_{0E,}$ respectively, which are responsible for the amount of coupling and the directivity. These two impedances are related to the transmission line impedance Z_0 by equation (2-20). The value of the odd- and even-mode impedance is influenced by the characteristics of the substrate and the physical shape of the coupling structure.

$$Z_0 = \sqrt{Z_{0E} \cdot Z_{0O}} \qquad (2\text{-}20)$$

What is important for the development of the directional coupler is how the physical shape of two coupled lines can be calculated from the odd- and even-mode impedance. This is important, because these two impedances are the results of a determination algorithm for the directional coupler that will be explained at the end of this subsection.

As a function of elliptical integrals of k_O and k_E, the odd- and-even mode impedances can be written as shown in equation (2-21) and (2-22), respectively. The relationship between k and k' is given in equation (2-25).

$$\frac{Z_{0E}\cdot\sqrt{\varepsilon_R}}{30\cdot\pi}=\frac{K(k_E')}{K(k_E)} \qquad (2\text{-}21)$$

$$\frac{Z_{0O}\cdot\sqrt{\varepsilon_R}}{30\cdot\pi}=\frac{K(k_O')}{K(k_O)} \qquad (2\text{-}22)$$

Since the evaluation of the elliptical integrals is very complicated equations (2-23) and (2-24) are used as approximations with an error of less than 0.1%. Which equation has to be used depends on the value of *k*.

$$\frac{K(k)}{K(k')}=\frac{\pi}{ln\left(2\cdot\frac{1+\sqrt{k'}}{1-\sqrt{k'}}\right)},\ \text{if } 0\le k^2\le 0.5 \qquad (2\text{-}23)$$

$$\frac{K(k)}{K(k')}=\frac{1}{\pi}\cdot ln\left(2\cdot\frac{1+\sqrt{k}}{1-\sqrt{k}}\right),\ \text{if } 0.5\le k^2\le 1 \qquad (2\text{-}24)$$

$$k'=\sqrt{1-k^2} \qquad (2\text{-}25)$$

By a combination of equations (2-21), (2-22) and (2-23) or (2-24) the values of k_E and k_O can be evaluated from the odd- and even-mode impedance. The width *w* of both coupled lines and the distance *s* between them referring to the height *b* of both substrates can be calculated using equations (2-26) and (2-27). The two substrates are needed because of stripline technology that is used for a proper implementation of the directional coupler. The reasons for that and the description of stripline technology will be explained later. As the substrate height *b* is known the dimensions of *w* and *s* of the coupling structure can be determined.

$$\frac{w}{b}=\frac{2}{\pi}\cdot tanh^{-1}\left(\sqrt{k_E\cdot k_O}\right) \qquad (2\text{-}26)$$

$$\frac{s}{b}=\frac{2}{\pi}\cdot tanh^{-1}\left(\frac{1-k_O}{1-k_E}\cdot\sqrt{\frac{k_E}{k_O}}\right) \qquad (2\text{-}27)$$

The accompanying physical material parameters are shown in subsection 3.1.1. What has to be mentioned is, that all equations are for ideal material, what means that there is no loss in the substrate, and that the lines are infinite flat perfect conductors. The so determined parameters have to be adapted to the real material parameters by a empirical method.

Directional Coupler

After a study of reference [4] a nonuniform broadband TEM directional coupler was chosen to be best suitable as directional coupler. This type of coupler is applicable in a wide frequency range which is its most important property. More details on choosing the directional coupler and the different development steps are stated in subsection 3.1.2. The principal structure of a symmetrical multisection nonuniform directional coupler is shown in Fig. 2.9. It is built of several sections that have different line widths and spacings, according to the different odd and even-mode impedances of each section.

Every section causes different coupling such that the overall coupling and the directivity should be equal over the whole frequency range. The structure of the coupler is symmetrical with respect to the vertical and horizontal axes that are plotted dashed in Fig. 2.9. For the

measurement of the length of the coupler there are two different scales. On the one hand there is the *u*-axis that measures the length in degrees and is used for the determination of the odd- and even mode impedances and on the other hand there is the *x*-axis that measures the length in mm and is used to calculate the physical dimensions of the coupler. As shown by θ all the elements have the same length.

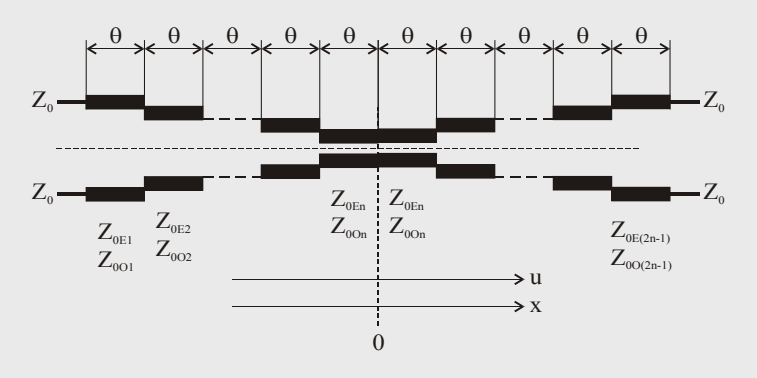

Fig. 2.9 - Structure of the Directional Coupler

For the determination of the odd- and even-mode impedances of the different sections of the coupler a weighting function is used. This weighting function is precalculated and listed in tables in [4]. We will come back to these tables later. The values of the weighting function are symmetrical with respect to the vertical axis of the directional coupler. They are different for different sections. The principal weighting function over the u-axis is shown in Fig. 2.10.

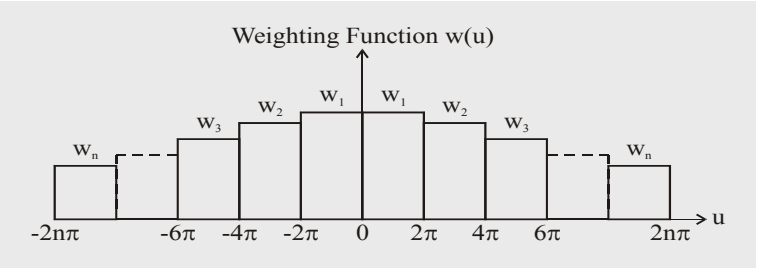

Fig. 2.10 - Weighting Function for the Directional Coupler

The first step in the development procedure is to define the lower f_L and upper frequency f_U of the application frequency range. Further the wanted coupling *C* and the ripple factor δ that describes the ripple of the coupling versus frequency have to be defined in dB. With equations (2-28) to (2-30) the voltage-coupling factor *R,* the centre frequency f_0 and the bandwidth ratio *B* can be determined.

$$R = 10^{-\frac{C}{20}} \qquad (2\text{-}28)$$

$$f_0 = \frac{f_L + f_U}{2} \qquad (2\text{-}29)$$

$$B = \frac{f_U}{f_L} \qquad (2\text{-}30)$$

With this characteristics the values of the normalized impedances Z_{0O} and Z_{0E} can be looked up from table 6.1 on pages 200 to 207 in reference [4] or in Appendix A. These impedances are used to determine the weighting factors. In the table the number of used sections *N* can be found too. Using equation (2-31) the minimum number of sections *n* can be determined.

$$n = \frac{N+1}{2} \qquad (2\text{-}31)$$

From the values of the normalised impedance $Z_{0E}(i) = Z_{0Ei}$ given in the table the values of the weighting coefficients w_1 to w_n can be determined using equation (2-32). For the value of $Z_{0E}(0)$ the nominal impedance Z_0 of the coupler has to be used.

$$w_i = \frac{\pi}{4 \cdot R} \cdot ln \frac{Z_{OE}(n-i+1)}{Z_{OE}(n-i)} \text{ for } i = 1 \text{ to } n \qquad (2\text{-}32)$$

Since all values for the calculation of the even-mode impedances of the directional coupler on certain positions are defined now, one can determine them with equation (2-33) where equation (2-34) is already substituted in the last expression.

$$\frac{1}{2} \cdot ln \frac{Z_{0E}(u)}{Z_0} = \frac{R}{\pi} \cdot \int_{-\frac{d}{2}}^{u} w(u) \cdot p(u) \cdot du = -\frac{R}{\pi} \cdot \int_{-\frac{d}{2}}^{u} w(u) \cdot \frac{sin^2\left(\frac{u}{2}\right)}{\frac{u}{2}} \cdot du \qquad (2\text{-}33)$$

$$p(u) = \frac{sin^2\left(\frac{u}{2}\right)}{\frac{u}{2}} \qquad (2\text{-}34)$$

As the coupler is symmetrical with respect to the vertical and horizontal axis at position 0 only the values for $u < 0$ have to be calculated. The variable $w(u)$ is the weighting value for a certain position u that can be determined according to Fig. 2.10.

The limits of u are given by $-2 \cdot \pi \cdot n \le u \le 2 \cdot \pi \cdot n$. For the evaluation of equation (2-33) the value of $\frac{d}{2}$ is set to $2 \cdot \pi \cdot n$. This also shows the relation between the x- and u-axis, which is given in equation (2-35).

$$x = \frac{u \cdot d}{4 \cdot \pi \cdot n} \qquad (2\text{-}35)$$

The overall length d can be calculated from the centre frequency by equation (2-36), where ε_R is the relative dielectric constant of the used substrate.

$$d = \frac{n \cdot \pi}{\beta_0} = \frac{n \cdot c_0}{2 \cdot f_0 \cdot \sqrt{\varepsilon_R}} \qquad (2\text{-}36)$$

With the calculations above the even-mode impedance at a certain position on every section of the coupler can be derived. Using equation (2-20) the odd-mode impedance can be calculated. Furtheron, with equations (2-26) and (2-27) the physical shape of the directional coupler can be determined.

2.2.2 Coupler

The theory of the coupler is very simple. The design idea goes back to [5]. In this implementation the coupler just consists of a stub that is capacitively coupled to the transmission line as shown in Fig. 2.11.

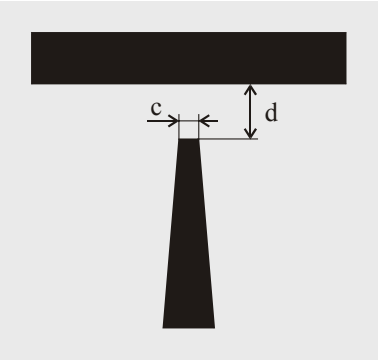

Fig. 2.11 - Dimensions of the Coupler Tip

As the coupling is capacitive there are two main parameters that are responsible for the coupling:

- Distance *d* between the main line and the coupler tip
- Width *c* of the coupler tip

If the distance *d* is decreased or the width *c* is increased the coupling increases and vice versa, but there are two constraints of these parameters. The distance between transmission line and coupler tip is constrained by the production process. The width of the coupler is constrained by the averaging of the measured power, this means since the power changes with the position on the transmission line and the coupler is not infinitely small the measured power is averaged over the width of the coupler tip. The algorithms for the determination of the reflection coefficient need the exact local power, so the averaging will decrease the accuracy. To keep the averaging as small, and therefore the accuracy as good as possible the coupler tip should be narrow.

2.2.3 Standing Wave Probe

This subsection deals with the structure and optimisation of the standing wave probe. The standing wave probe consists of a transmission line on which a standing wave arises and five couplers that sample the power of that standing wave at distinct positions. Firstly different coupler settings will be shown so that the optimisation problem could be understood. Then the theoretical basis for the optimisation will be explained.

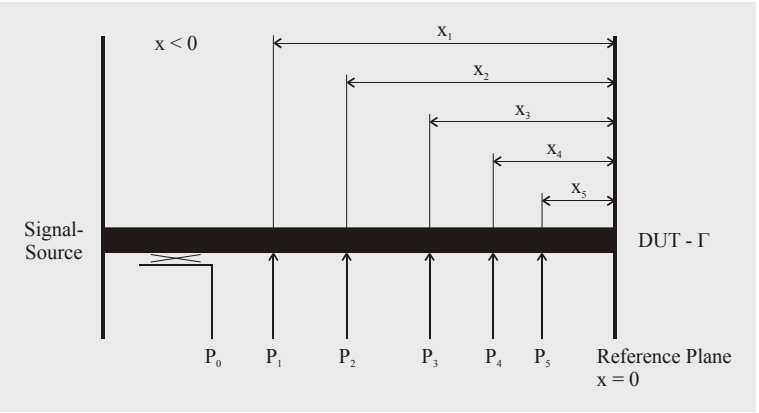

Fig. 2.12 - Basic Structure for the Optimisation

The theory of the optimisation is based on [5]. Firstly the physical layout for the optimisation is explained. Then a simple algorithm for the determination of the reflection coefficient is shown. Based on this algorithm the theory of the optimisation will be explained. For the optimisation an ideal system is assumed, therefore no calibration is used. The differences to the real implementation will be explained where they occur.

First of all the physical layout of the coupler for the optimisation is shown in Fig. 2.12. The positions of the sampling points are measured from the reference plane. Since the reference plane is at *x*-position 0 all *x*-values are negative.

If the power of the incident wave is assumed as P_0 and the powers $P_i(x_i)$ as the powers at the different sampling points x_i, one can find the general equation for the normalized power as equation (2-37). Q_i is a complex coefficient, k_i is a real coefficient.

$$p_i = \frac{P_i(x_i)}{P_0} = k_i \cdot \frac{|Q_i \cdot \Gamma + 1|^2}{|Q_0 \cdot \Gamma + 1|^2} \qquad (2\text{-}37)$$

For the later optimisation and the determination of the reflection coefficient the five single equations can be written as a matrix equation of the form given in equation (2-38).

$$\mathbf{A} \cdot \underline{\mathbf{\Gamma}} = \underline{\mathbf{B}} \qquad (2\text{-}38)$$

In this equation **A** is a coefficient matrix, $\underline{\mathbf{B}}$ is a coefficient vector and $\underline{\mathbf{\Gamma}}$ is a vector that contains the square of the magnitude of the reflection coefficient $|\Gamma|^2$ and the real- Γ_R and imaginary part Γ_I of the reflection coefficient in the following form (2-39):

$$\underline{\mathbf{\Gamma}} = \begin{pmatrix} |\Gamma|^2 \\ \Gamma_R \\ \Gamma_I \end{pmatrix} \qquad (2\text{-}39)$$

As known from theory at least three power measurements are needed to determine the correct reflection coefficient. Now five power measurements are used, which means that a Least Mean Square algorithm can be used to determine $\underline{\mathbf{\Gamma}}$ from (2-38). This LMS-solution will lead to more accurate results of the reflection coefficient because all five powers sampled with the standing wave probe are used. The LMS-solution for $\underline{\mathbf{\Gamma}}$ can be calculated using (2-40). In this equation index *T* stands for the transpose of the matrix and index *–1* stand for the inverse of the matrix.

$$\underline{\mathbf{\Gamma}} = \left(\mathbf{A}^T \cdot \mathbf{A}\right)^{-1} \cdot \mathbf{A}^T \cdot \underline{\mathbf{B}} \qquad (2\text{-}40)$$

Measurement errors of the power meter appear as small perturbations of the coefficients in matrix **A** and vector $\underline{\mathbf{B}}$. A measure for the influeces of these errors is the condition number of matrix **A**. It is defined as equation (2-41).

$$\kappa_2(\mathbf{A}) = \|\mathbf{A}\|_2 \cdot \left\|\left(\mathbf{A}^T \cdot \mathbf{A}\right)^{-1} \cdot \mathbf{A}^T\right\|_2 \qquad (2\text{-}41)$$

In general the condition number of a matrix is a measurement whether a matrix equation is sensitive to perturbations of the coefficients or not. If the condition number is small the distances are well chosen and the measurement is insensitive to perturbations. On the other hand if the condition number is large, small perturbations of the coefficients will lead to large errors in the result. Using this fact one has to minimize the condition number of the coefficient matrix in equation (2-38). But there is still a problem, as will be shown in subsection 3.1.2 both matrix **A** and vector $\underline{\mathbf{B}}$ depend on the power values sampled at different couplers. For the optimisation

matrix **A** should depend only on the probe parameters. To change equation (2-37) to this condition transformation (2-42) is used.

$$\frac{Q_1 \cdot \Gamma + 1}{Q_0 \cdot \Gamma + 1} \equiv \gamma + 1 \qquad (2\text{-}42)$$

With equation (2-42) a new equation for p_i (2-43) can be found with k_i from equation (2-37) and q_i given by equation (2-44).

$$p_i = k_i \cdot |q_i \cdot \gamma + 1|^2 \qquad (2\text{-}43)$$

$$q_i = \frac{Q_i - Q_0}{Q_1 - Q_0} \qquad (2\text{-}44)$$

If a matrix equation (2-45) is formulated with all five equations (2-43) an equation in which the coefficient matrix **C** only depends on the probe parameters (the *x*-positions) is found. The vector $\underline{\boldsymbol{\gamma}}$ consist of $|\gamma|^2$ and the real- γ_R and imaginary part γ_I as in equation (2-46).

$$\mathbf{C} \cdot \underline{\boldsymbol{\gamma}} = \underline{\mathbf{B}} \qquad (2\text{-}45)$$

$$\underline{\boldsymbol{\gamma}} = \begin{pmatrix} |\gamma|^2 \\ \gamma_R \\ \gamma_I \end{pmatrix} \qquad (2\text{-}46)$$

To finish this analysis one can determine the error propagation from $\underline{\boldsymbol{\gamma}}$ to $\underline{\boldsymbol{\Gamma}}$. A small error $\delta\underline{\boldsymbol{\gamma}}$ propagates to $\delta\underline{\boldsymbol{\Gamma}}$ as calculated in (2-47).

$$\delta\underline{\Gamma} = \frac{\partial\underline{\Gamma}}{\partial\underline{\gamma}}\delta\underline{\gamma} = \frac{(Q_0 \cdot \Gamma + 1)^2}{Q_0 - Q_1} \cdot \delta\underline{\gamma} \qquad (2\text{-}47)$$

Since a matrix that just depends on the probe parameters is found one can optimise the condition number of this matrix with respect to the distances between the probes (which is equal to determine the distances to the reference plane).

According to the theory for a three-probe reflectometer the optimum distance between the probes is 120° for every measurement frequency. Since this cannot be fulfilled for every frequency in a broad frequency band this implementation uses five probes that are distributed in such a way that over the whole frequency range the best distribution of the probes is reached. This is when the condition number over the whole frequency range is a minimum. To find the optimum distribution an optimisation function, which sums up the square of the condition number for all frequencies in the application frequency band is used. This optimisation function is given in equation(2-48), where *m* is the frequency index and *M* is the number of frequencies at which the function is optimised.

$$F(d_2, d_3, d_4, d_5) = \frac{1}{M} \cdot \sum_{m=1}^{M} |\kappa_2(C_m)|^2 \qquad (2\text{-}48)$$

As it will be shown in the next chapter this function is optimised in four dimensions, which are the distances between the first and the i^{th} coupler in equation (2-49) where *i* is in range from 2 to 5. The best result of the coupler distribution is reached if equation (2-48) is a minimum.

$$d_i = x_i - x_1 \qquad (2\text{-}49)$$

At the end of this subsection three different non-optimally distributions for the couplers are explained and their condition number is plotted over frequency.

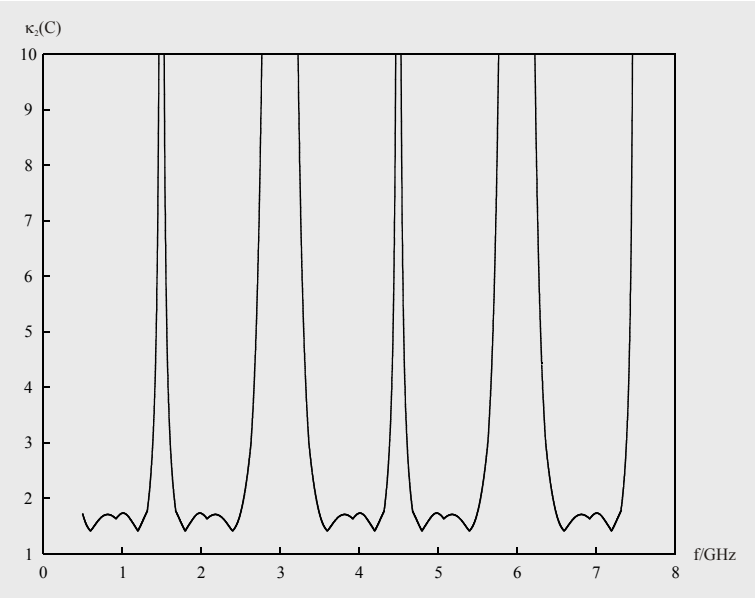

Fig. 2.13 - Condition Number for 3-Coupler Optimisation

The first example is equal to the standing wave probe in subsection 0 which is a optimum for three couplers. As explained in the theory the distance between adjacent couplers for this standing wave probe is $\frac{\lambda_0}{6}$. So the distances are optimised for the use of 3 couplers, but the standing wave probe uses five couplers what causes two couplers to coincide, what means they lead to the same centre points on the unit circle. The optimum frequency for this example is chosen to be 1 GHz what results in a wavelength of λ = 206.6 mm on the used substrate with ε_R = 2.5 (what results in ε_{EFF} = 2.1085). The material is described in subsection 3.2.1. The distance is $\frac{\lambda_0}{6}$ = 34.433 mm. The resulting condition number over frequency is shown in Fig. 2.13. The Figure shows that the condition number for a frequency of 1.5 GHz goes to infinity. This happens when two of the three points in the smith chart have the same angular position. Then there are two possible solutions for the reflection coefficient and no unique result can be calculated. This shows that the condition number can be used as a measure for the accuracy of the solution, or for the case that it goes to infinity to show the frequencies where no solution can be found.

The next example of a standing wave probe has a distance of $\frac{\lambda_0}{10}$ between two adjacent couplers. This is the optimum distance for a standing wave probe that uses five couplers, when none of them coincide for the design frequency. In that case the five centre points are equally distributed around the unit circle. On the material of the former example the distance of $\frac{\lambda_0}{10}$ = 20.660 mm for the design frequency of 1 GHz. The frequency where the centre points coincide in such a way that just two different centre points are left on the unit circle can be calculated to be 2.5 GHz, what can be shown with a calculation that is similar to equation (2-19) too. This problematic frequency can also be seen in Fig. 2.14 where the condition number goes to infinity for this frequency.

From these two examples we can see that the measurement frequency range can be broadened if the number of couplers is increased. But the increase in the frequency range is not proportional to the increased expenditure in introducing new couplers. Another possibility to increase the

measurement frequency range is to use non-equally spaced couplers, what will be analysed in the next example.

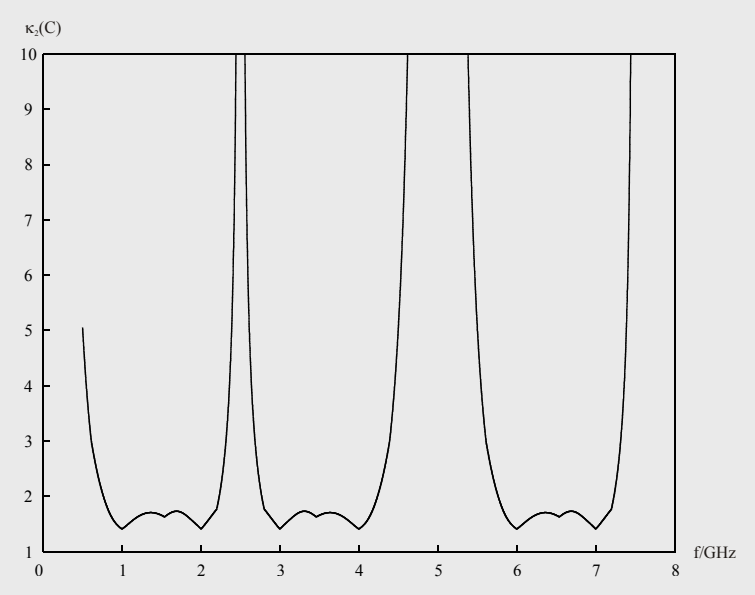

Fig. 2.14 - Condition Number for 5-Coupler Optimisation

The last example for a not optimised standing wave probe uses non equally space probes. The design idea goes back to reference [6]. This article is on a sampled transmission line reflectometer that uses five couplers to measure the reflection coefficient for the fundamental, 2nd and 3rd harmonic frequency. For that reason the standing wave probe is optimised for a three-coupler standing wave probe for the first harmonic frequency. Since the 2nd harmonic frequency has half the wavelength of the fundamental frequency one more coupler must be inserted in the middle of two adjacent couplers to get an equally spaced three coupler standing wave probe for the 2nd harmonic frequency. If one more coupler is inserted between two adjacent couplers for the 2nd harmonic frequency, a three-coupler standing wave probe for the 3rd harmonic frequency is built. So the reflection coefficient for fundamental, 2nd and 3rd harmonic frequency can be determined using five couplers. From another view the measurement for the 3 different harmonics is equal to a broadening of the measurement frequency range that should be reached with the use of the non-equally spaced probes.

If the distance between the nearest positioned couplers is referred to as d_0 this kind of standing wave probe uses the distances: d_0, d_0, $2 \cdot d_0$, $4 \cdot d_0$ between the adjacent couplers. The optimal distance d_0 for the frequency range from 0.5 GHz to 7.5 GHz was found experimentally by comparing the condition numbers. The optimal distances are: 6.665 mm, 6.665 mm, 13.329 mm, 26.658 mm what leads to a condition number of 9.0247 calculated according to equation (2-48). The condition number over frequency is shown Fig. 2.15.

Also for this kind of standing wave probe the frequency where the condition number goes to infinity can be calculated. This frequency depends on the smallest distance between two consecutive probes d_0 and can be calculated to be 7.75 GHz.

After these examples the consequences of the coupler placing to the condition number should be clearer. The optimisation that is carried out will lead to distances between adjacent couplers that have no relation to each other, but altogether the minimum condition number is reached.

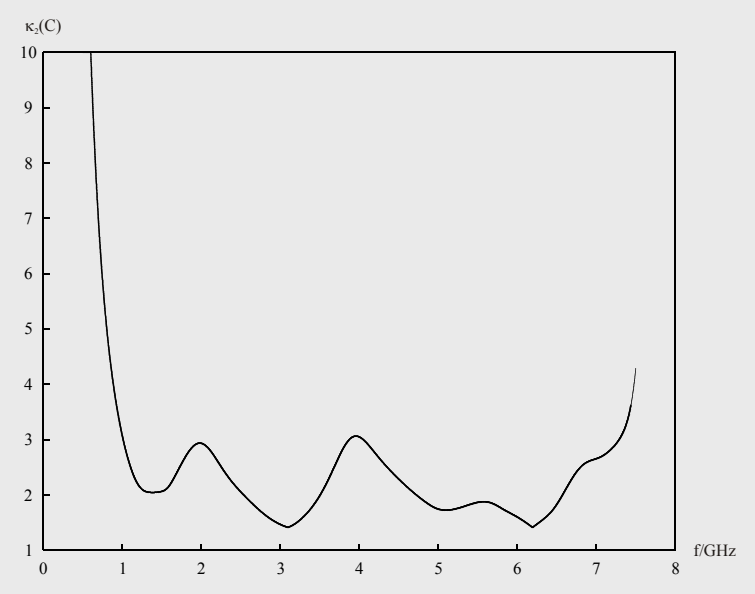

Fig. 2.15 - Condition Number for Distances: d_0-d_0-2·d_0-4·d_0

2.3 Software Theory

This chapter introduces the reader to the theory of the used algorithms for the determination of the reflection coefficient. To counteract imperfections of the implementation of the hardware components the according calibration algorithms are used. They will be discussed in this chapter too.

2.3.1 3-Probe Algorithm

This algorithm is based on [7]. In this article additional information and some more references can be found. As the name says this algorithm uses three probes to determine the reflection coefficient. Additionally one normalization value is used. This normalization value is taken from the directional coupler or from one probe. Since there are five probes but just three are used for the determination the best ones should be chosen for the determination of the reflection coefficient. How this is done and how the reflection coefficient can be determined will be described in the next subsection. After this the accompanying calibration method will be explained.

Determination Algorithm

Using equation (2-12) in subsection 2.1.1 we can write the power at a distinct coupler port as a function of the incident wave power, a constant factor, the real part, the imaginary part and the magnitude of the reflection coefficient. Since the exact values of the coefficients are not known, we have to introduce calibration values $c_{i,1}$ to $c_{i,4}$ into this equation. This leads us to expression (2-50) for the power at one certain port.

$$P_{i,j} = P_{0,j} \cdot \left(c_{i,1} + c_{i,2} \cdot \left| \Gamma_j \right|^2 + c_{i,3} \cdot \Gamma_{j,R} + c_{i,4} \cdot \Gamma_{j,I} \right) \qquad (2\text{-}50)$$

Index i stands for the port number, index j stands for different reflection coefficients Γ_j. The reflection coefficient can be determined from four equations like (2-50) which must be for four different power values. For the explanation of the algorithm it is assumed that the normalisation value is taken from the directional coupler and the other three powers are from those coupler ports that are best placed for a certain frequency. From the theory it is known that it is best to use

those ports of the standing wave probe, that are placed in such a way, that their according positions are most equipartitioned on the unit circle.

The best positioned probes can be derived, by calculating the angular position of every port on the unit circle using equation (2-51). If a triple T(l, m, n) of three ports out of the five possible ports is chosen the angular distance between each two ports can be calculated. The best triple is the one for that angular distances are closest to 120°. This triple can be found if equation (2-52) is solved for all possible combinations of l ≠ m ≠ n each from 1 to 5 and the smallest value can be determined as optimum. The according l-, m- and n-values of this optimum triple are used for further calculations.

$$\varphi_l(x_l) = (2\beta \cdot x_l) mod(360) \tag{2-51}$$

$$\begin{aligned} T(l,m,n) = & \left|\left[(\varphi_l - \varphi_m) mod(180)\right] - 120\right| + \\ & + \left|\left[(\varphi_m - \varphi_n) mod(180)\right] - 120\right| + \\ & + \left|\left[(\varphi_n - \varphi_l) mod(180)\right] - 120\right| \end{aligned} \tag{2-52}$$

Equation (2-53a) derives the power measured at the output of the directional coupler. Actually the power of the directional coupler should be equal to $P_{0,j}$ but due to imperfections of the directional coupler, for example a finite directivity, it has to be calibrated too. Equations (2-53b) to (2-53d) compute the powers measured at the three best-positioned ports.

$$P_{DC,j} = P_{0,j} \cdot \left(c_{1,1} + c_{1,2} \cdot \left|\Gamma_j\right|^2 + c_{1,3} \cdot \Gamma_{j,R} + c_{1,4} \cdot \Gamma_{j,I}\right) \tag{2-53a}$$

$$P_{l,j} = P_{0,j} \cdot \left(c_{2,1} + c_{2,2} \cdot \left|\Gamma_j\right|^2 + c_{2,3} \cdot \Gamma_{j,R} + c_{2,4} \cdot \Gamma_{j,I}\right) \tag{2-53b}$$

$$P_{m,j} = P_{0,j} \cdot \left(c_{3,1} + c_{3,2} \cdot \left|\Gamma_j\right|^2 + c_{3,3} \cdot \Gamma_{j,R} + c_{3,4} \cdot \Gamma_{j,I}\right) \tag{2-53c}$$

$$P_{n,j} = P_{0,j} \cdot \left(c_{4,1} + c_{4,2} \cdot \left|\Gamma_j\right|^2 + c_{4,3} \cdot \Gamma_{j,R} + c_{4,4} \cdot \Gamma_{j,I}\right) \tag{2-53d}$$

Equations (2-53a) to (2-53d) can be written as a vector equation (2-57), using the vectors $\underline{\mathbf{P}}_j$ and $\underline{\mathbf{\Gamma}}_j$ and matrix **C**. If a matrix **X** is defined as an inverse of matrix **C**, $\underline{\mathbf{\Gamma}}_j$ can be calculated.

$$\underline{\mathbf{P}}_j = \begin{pmatrix} P_{DC,j} \\ P_{l,j} \\ P_{m,j} \\ P_{n,j} \end{pmatrix}, \quad \mathbf{C} = \begin{pmatrix} c_{1,1} & c_{1,2} & c_{1,3} & c_{1,4} \\ c_{2,1} & c_{2,2} & c_{2,3} & c_{2,4} \\ c_{3,1} & c_{3,2} & c_{3,3} & c_{3,4} \\ c_{4,1} & c_{4,2} & c_{4,3} & c_{4,4} \end{pmatrix}, \quad \underline{\mathbf{\Gamma}}_j = \begin{pmatrix} 1 \\ \left|\Gamma_j\right|^2 \\ \Gamma_{j,R} \\ \Gamma_{j,I} \end{pmatrix} \tag{2-54), (2-55), (2-56}$$

$$\underline{\mathbf{P}}_j = P_{0,j} \cdot \mathbf{C} \cdot \underline{\mathbf{\Gamma}}_j \tag{2-57}$$

$$\underline{\mathbf{\Gamma}}_j = \frac{1}{P_{0,j}} \cdot \mathbf{C}^{-1} \cdot \underline{\mathbf{P}}_j = \frac{1}{P_{0,j}} \cdot \mathbf{X} \cdot \underline{\mathbf{P}}_j \tag{2-58}$$

The values of $|\Gamma_j|^2$, $\Gamma_{j,R}$ and $\Gamma_{j,I}$ can be calculated using equations (2-59a) to (2-59c), where $\underline{\mathbf{X}}_i$ is a row vector with the elements of the i^{th} row of matrix **X**. In this calculation the formulation $\underline{\mathbf{X}}_1^T \cdot \underline{\mathbf{P}}$ is equal to the power level exciting the device under test.

$$\left|\Gamma_j\right|^2 = \frac{\underline{\mathbf{X}}_2^T \cdot \underline{\mathbf{P}}_j}{\underline{\mathbf{X}}_1^T \cdot \underline{\mathbf{P}}_j} \qquad (2\text{-}59a)$$

$$\Gamma_{j,R} = \frac{\underline{\mathbf{X}}_3^T \cdot \underline{\mathbf{P}}_j}{\underline{\mathbf{X}}_1^T \cdot \underline{\mathbf{P}}_j} \qquad (2\text{-}59b)$$

$$\Gamma_{j,I} = \frac{\underline{\mathbf{X}}_4^T \cdot \underline{\mathbf{P}}_j}{\underline{\mathbf{X}}_1^T \cdot \underline{\mathbf{P}}_j} \qquad (2\text{-}59c)$$

Calibration Algorithm

The calibration procedure is needed to determine the coefficients $c_{1,1}$ to $c_{4,4}$. It starts with equation system (2-53a) to (2-53d). For normalisation purposes the powers of the coupling points are divided by the power measured at the output of the directional coupler. This normalisation is done to eliminate the influence of the incident wave power $P_{0,j}$ and leads to equations (2-60a) to (2-60c).

$$c_{2,1} + c_{2,2} \cdot \left|\Gamma_j\right|^2 + c_{2,3} \cdot \Gamma_{j,R} + c_{2,4} \cdot \Gamma_{j,I} = \frac{P_{l,j}}{P_{DC,j}} \left(c_{1,1} + c_{1,2} \cdot \left|\Gamma_j\right|^2 + c_{1,3} \cdot \Gamma_{j,R} + c_{1,4} \cdot \Gamma_{j,I} \right) \qquad (2\text{-}60a)$$

$$c_{3,1} + c_{3,2} \cdot \left|\Gamma_j\right|^2 + c_{3,3} \cdot \Gamma_{j,R} + c_{3,4} \cdot \Gamma_{j,I} = \frac{P_{m,j}}{P_{DC,j}} \left(c_{1,1} + c_{1,2} \cdot \left|\Gamma_j\right|^2 + c_{1,3} \cdot \Gamma_{j,R} + c_{1,4} \cdot \Gamma_{j,I} \right) \qquad (2\text{-}60b)$$

$$c_{4,1} + c_{4,2} \cdot \left|\Gamma_j\right|^2 + c_{4,3} \cdot \Gamma_{j,R} + c_{4,4} \cdot \Gamma_{j,I} = \frac{P_{n,j}}{P_{DC,j}} \left(c_{1,1} + c_{1,2} \cdot \left|\Gamma_j\right|^2 + c_{1,3} \cdot \Gamma_{j,R} + c_{1,4} \cdot \Gamma_{j,I} \right) \qquad (2\text{-}60c)$$

To determine all coefficients five standards with different reflection coefficients are needed, one 50 Ω-load that will be used in a later step and four other standards that are combined to a reflection coefficient matrix **G** as in (2-61).

$$\mathbf{G} = \begin{pmatrix} 1 & \left|\Gamma_1\right|^2 & \Gamma_{1,R} & \Gamma_{1,I} \\ 1 & \left|\Gamma_2\right|^2 & \Gamma_{2,R} & \Gamma_{2,I} \\ 1 & \left|\Gamma_3\right|^2 & \Gamma_{3,R} & \Gamma_{3,I} \\ 1 & \left|\Gamma_4\right|^2 & \Gamma_{4,R} & \Gamma_{4,I} \end{pmatrix} \qquad (2\text{-}61)$$

If the power vector defined in equation (2-54) is written as a diagonal matrix in equation (2-62) equations (2-60a) to (2-60c) can be commonly written as in (2-63) or in another form as in (2-64a) to (2-64c). In these equations $\underline{\mathbf{C}}_i$ is a column vector with the elements of the i^{th} row of matrix **C**.

$$\mathbf{P}_j = \begin{pmatrix} P_{DC,j} & 0 & 0 & 0 \\ 0 & P_{l,j} & 0 & 0 \\ 0 & 0 & P_{m,j} & 0 \\ 0 & 0 & 0 & P_{n,j} \end{pmatrix} \qquad (2\text{-}62)$$

$$\mathbf{G} \cdot \underline{\mathbf{C}}_2 = \mathbf{P}_2 \cdot \mathbf{P}_1^{-1} \cdot \mathbf{G} \cdot \underline{\mathbf{C}}_1 \qquad (2\text{-}63)$$

$$\underline{\mathbf{C}}_2 = \mathbf{G}^{-1} \cdot \mathbf{P}_2 \cdot \mathbf{P}_1^{-1} \cdot \mathbf{G} \cdot \underline{\mathbf{C}}_1 \qquad (2\text{-}64a)$$

$$\underline{\mathbf{C}}_3 = \mathbf{G}^{-1} \cdot \mathbf{P}_3 \cdot \mathbf{P}_1^{-1} \cdot \mathbf{G} \cdot \underline{\mathbf{C}}_1 \qquad (2\text{-}64b)$$

$$\underline{\mathbf{C}}_4 = \mathbf{G}^{-1} \cdot \mathbf{P}_4 \cdot \mathbf{P}_1^{-1} \cdot \mathbf{G} \cdot \underline{\mathbf{C}}_1 \qquad (2\text{-}64c)$$

After a simple transformation equations (2-64a) to (2-64c) can be written as equations (2-65a) to (2-65c). In this formulation there is always $\underline{\mathbf{C}}_1$ on the left side. With a further transformation it can be shown that a common relation between all equations can be found. With this equation shown in (2-66) every row of matrix **C** can be found by any other row if just the according power- and the reflection coefficient matrix is known and its inverse can be calculated.

$$\underline{\mathbf{C}}_1 = \mathbf{G}^{-1} \cdot \mathbf{P}_1 \cdot \mathbf{P}_2^{-1} \cdot \mathbf{G} \cdot \underline{\mathbf{C}}_2 \qquad (2\text{-}65a)$$

$$\underline{\mathbf{C}}_1 = \mathbf{G}^{-1} \cdot \mathbf{P}_1 \cdot \mathbf{P}_3^{-1} \cdot \mathbf{G} \cdot \underline{\mathbf{C}}_3 \qquad (2\text{-}65b)$$

$$\underline{\mathbf{C}}_1 = \mathbf{G}^{-1} \cdot \mathbf{P}_1 \cdot \mathbf{P}_4^{-1} \cdot \mathbf{G} \cdot \underline{\mathbf{C}}_4 \qquad (2\text{-}65c)$$

$$\underline{\mathbf{C}}_x = \mathbf{G}^{-1} \cdot \mathbf{P}_x \cdot \mathbf{P}_y^{-1} \cdot \mathbf{G} \cdot \underline{\mathbf{C}}_y \qquad (2\text{-}66)$$

If equation (2-66) is multiplied by **G** and $\mathbf{P}_x$ on the left side one can find a vector $\underline{\mathbf{V}}_0$ as given by equation (2-67) that is equal for all values of x from 1 to 4. This vector is built by the inverse incident wave power matrices as shown in (2-68).

$$\mathbf{P}_1^{-1} \cdot \mathbf{G} \cdot \underline{\mathbf{C}}_1 = \mathbf{P}_2^{-1} \cdot \mathbf{G} \cdot \underline{\mathbf{C}}_2 = \mathbf{P}_3^{-1} \cdot \mathbf{G} \cdot \underline{\mathbf{C}}_3 = \mathbf{P}_4^{-1} \cdot \mathbf{G} \cdot \underline{\mathbf{C}}_4 = \underline{\mathbf{V}}_0 \qquad (2\text{-}67)$$

$$\underline{\mathbf{V}}_0^T = \left(\frac{1}{P_{0,1}}, \frac{1}{P_{0,2}}, \frac{1}{P_{0,3}}, \frac{1}{P_{0,4}} \right) \qquad (2\text{-}68)$$

As soon as vector $\underline{\mathbf{V}}_0$ is known matrix **C** can be determined since the power matrices and reflection coefficient matrices are known too. The explicit expression for one row of matrix **C** is given by equation (2-69).

$$\underline{\mathbf{C}}_x = \mathbf{G}^{-1} \cdot \mathbf{P}_x \cdot \underline{\mathbf{V}}_0 \qquad (2\text{-}69)$$

$$\mathbf{P}_0 = \mathbf{P} \cdot Diag\left[\left(\mathbf{G}^{-1} \right)^T \cdot \underline{\mathbf{\Gamma}}_0 \right] \cdot \underline{\mathbf{V}}_0 \qquad (2\text{-}70)$$

$$\mathbf{P} = \begin{pmatrix} P_{DC,1} & P_{DC,2} & P_{DC,3} & P_{DC,4} \\ P_{l,1} & P_{l,2} & P_{l,3} & P_{l,4} \\ P_{m,1} & P_{m,2} & P_{m,3} & P_{m,4} \\ P_{n,1} & P_{n,2} & P_{n,3} & P_{n,4} \end{pmatrix} \qquad (2\text{-}71)$$

$$\underline{\mathbf{V}}_0 = \left\{ Diag\left[\left(\mathbf{G}^{-1} \right)^T \cdot \underline{\mathbf{\Gamma}}_0 \right] \right\}^{-1} \cdot \mathbf{P}^{-1} \cdot \mathbf{P}_0 \qquad (2\text{-}72)$$

With some simple matrix manipulations it can be that shown the power matrix for using a 50 Ω-load as termination can be found from the other power measurements as given by equation (2-70). In this equation $\mathbf{P}_0$ stands for the power value when a 50 Ω-load is connected as termination. $\underline{\mathbf{\Gamma}}_0$ is the accompanying gamma vector that is valid for the load. With this equation

the power matrix can now be defined as shown in (2-71). From equation (2-70) vector $\underline{\mathbf{V}}_0$ can be calculated with equation (2-72). The practical used calibration standards were a short, an open, a load and short and open plus 3 dB attenuator.

2.3.2 Least-Mean-Square Algorithm

The Least Mean Square Algorithm uses all five power measurements that are available from the standing wave probe. Additionally the power measurement of the incident wave that is available at the directional coupler will be used for normalisation purposes. The theory for the determination is based on [5]. The accompanying calibration method is based on [8].

Determination Algorithm

The determination algorithm is already shown in subsection 2.2.3 but without the calibration coefficients. For the determination of the reflection coefficient the basic equation (2-12) from subsection 2.1.1 that describes the power of the standing wave on a certain position is used. If the powers measured at the output of the standing wave probe are normalised to the power measured at the output of the directional coupler and calibration coefficients are introduced, equation (2-73) can be written for the power ratio p_i ($i = 1\ldots5$).

$$p_i = \frac{P_i}{P_{DC}} = q_i \cdot \left| \frac{1 + A_i \cdot \Gamma_j}{1 + A_0 \cdot \Gamma_j} \right|^2 \qquad (2\text{-}73)$$

In this equation q_i ($i = 1\ldots5$) is a scalar calibration coefficient that is responsible for the different coupling factors. The calibration coefficients A_i are complex and defined as $A_i = a_i + j \cdot b_i$ ($i = 0\ldots5$). If both, the calibration coefficients and the reflection coefficient are substituted by their real and imaginary part one can formulate equation (2-74):

$$p_i = q_i \cdot \frac{1 + 2 \cdot a_i \cdot \Gamma_{j,R} + 2 \cdot b_i \cdot \Gamma_{j,I} + a_i^2 \cdot \left|\Gamma_j\right|^2 + b_i^2 \cdot \left|\Gamma_j\right|^2}{1 + 2 \cdot a_0 \cdot \Gamma_{j,R} + 2 \cdot b_0 \cdot \Gamma_{j,I} + a_0^2 \cdot \left|\Gamma_j\right|^2 + b_0^2 \cdot \left|\Gamma_j\right|^2} \qquad (2\text{-}74)$$

With the next two steps shown in equations (2-75) and (2-76) equation (2-74) is transformed in such a way that the left side of the equation is independent of the reflection coefficient. The terms on the right side depend on the real part, imaginary part and the squared magnitude of the reflection coefficient, respectively.

$$\frac{p_i}{q_i} \cdot \left(1 + 2 \cdot a_0 \cdot \Gamma_{j,R} + 2 \cdot b_0 \cdot \Gamma_{j,I} + a_0^2 \cdot \left|\Gamma_j\right|^2 + b_0^2 \cdot \left|\Gamma_j\right|^2\right) = 1 + 2 \cdot a_i \cdot \Gamma_{j,R} + 2 \cdot b_i \cdot \Gamma_{j,I} + a_i^2 \cdot \left|\Gamma_j\right|^2 + b_i^2 \cdot \left|\Gamma_j\right|^2 \qquad (2\text{-}75)$$

$$\frac{p_i}{q_i} - 1 = 2 \cdot \left(a_i - a_0 \cdot \frac{p_i}{q_i}\right) \cdot \Gamma_{j,R} + 2 \cdot \left(-b_i + b_0 \cdot \frac{p_i}{q_i}\right) \cdot \Gamma_{j,I} + \left(a_i^2 + b_i^2 - a_0^2 \cdot \frac{p_i}{q_i} - b_0^2 \cdot \frac{p_i}{q_i}\right) \cdot \left|\Gamma_j\right|^2 \qquad (2\text{-}76)$$

Using the matrix and the vectors defined in equations (2-77) to (2-79) one can formulate a matrix equation (2-80) for the power ratios of all five coupler ports.

$$\underline{\mathbf{B}} = \begin{pmatrix} \frac{p_1}{q_1} - 1 \\ \frac{p_2}{q_2} - 1 \\ \frac{p_3}{q_3} - 1 \\ \frac{p_4}{q_4} - 1 \\ \frac{p_5}{q_5} - 1 \end{pmatrix}, \mathbf{A} = \begin{pmatrix} a_1 - a_0 \cdot \frac{p_1}{q_1} & -b_1 + b_0 \cdot \frac{p_1}{q_1} & a_1^2 + b_1^2 - a_0^2 \cdot \frac{p_1}{q_1} - b_0^2 \cdot \frac{p_1}{q_1} \\ a_2 - a_0 \cdot \frac{p_2}{q_2} & -b_2 + b_0 \cdot \frac{p_2}{q_2} & a_2^2 + b_2^2 - a_0^2 \cdot \frac{p_2}{q_2} - b_0^2 \cdot \frac{p_2}{q_2} \\ a_3 - a_0 \cdot \frac{p_3}{q_3} & -b_3 + b_0 \cdot \frac{p_3}{q_3} & a_3^2 + b_3^2 - a_0^2 \cdot \frac{p_3}{q_3} - b_0^2 \cdot \frac{p_3}{q_3} \\ a_4 - a_0 \cdot \frac{p_4}{q_4} & -b_4 + b_0 \cdot \frac{p_4}{q_4} & a_4^2 + b_4^2 - a_0^2 \cdot \frac{p_4}{q_4} - b_0^2 \cdot \frac{p_4}{q_4} \\ a_5 - a_0 \cdot \frac{p_5}{q_5} & -b_5 + b_0 \cdot \frac{p_5}{q_5} & a_5^2 + b_5^2 - a_0^2 \cdot \frac{p_5}{q_5} - b_0^2 \cdot \frac{p_5}{q_5} \end{pmatrix} \quad (2\text{-}77), (2\text{-}78)$$

$$\underline{\mathbf{\Gamma}}_j = \begin{pmatrix} \Gamma_{j,R} \\ \Gamma_{j,I} \\ |\Gamma|^2 \end{pmatrix} \quad (2\text{-}79)$$

$$\underline{\mathbf{B}} = \mathbf{A}^T \cdot \underline{\mathbf{\Gamma}}_j \quad (2\text{-}80)$$

Since this equation system is overdetermined a Least Mean Square solution is applied. According to reference [5] this LMS solution can be determined with equation (2-81).

$$\underline{\mathbf{\Gamma}}_j = \left(\mathbf{A}^T \cdot \mathbf{A}\right)^{-1} \cdot \mathbf{A}^T \cdot \underline{\mathbf{B}} \quad (2\text{-}81)$$

Calibration Algorithm

This calibration algorithm bases on [8]. As the title of the paper says four different open/short circuits are used, so the magnitude of all four standards is 1 and just the phase is different. Additionally one 50 Ω-load termination is used but this must not be very accurate since it is not used as a standard but to determine the sign of a square root. This will be recalled on the appropriate position.

What has to be determined by this calibration procedure are 5 scalar q_i-values and 6 complex A_i-values of equation (2-73).

If all four standards have a magnitude of 1 the reflection coefficient can be written as in equation (2-82) where φ_j stands for the angle of standard j. In the further calibration only this angle will be important, because the magnitude is supposed 1.

$$\Gamma_j = \left|\Gamma_j\right| \cdot e^{j\varphi_j} = e^{j\varphi_j} \quad (2\text{-}82)$$

Accompanying with the four different reflection coefficient standards four times six powers (five at the coupler port and one at the directional coupler for normalisation) are measured. So twenty power ratios can be calculated. How these power ratios are calculated is shown in equation (2-83). In this equation the index i stands for the number of the coupler port, the index j for the accompanying reflection coefficient. The index DC stands for the power measured at the output of the directional coupler that is used for normalisation purposes.

$$p_{i,j} = \frac{P_{i,j}}{P_{DC,j}} = q_i \cdot \left|\frac{1 + A_i \cdot \Gamma_j}{1 + A_0 \cdot \Gamma_j}\right|^2 \quad (2\text{-}83)$$

$$A_i = \alpha_i \cdot e^{j\phi_i} = a_i + j \cdot b_i \qquad (2\text{-}84)$$

As explained earlier q_i is a scalar calibration value, A_i is a complex one, where α_i is the magnitude and ϕ_i is the angle. The according real and imaginary parts are a_i and b_i, respectively. The first step in the calculation is the determination of A_0. With the use of equations (2-88) and (2-89) equation (2-87) can be evaluated. In equation (2-88) φ_i is the angle of reflection coefficient standard i. For the used constellation the values for the indices j and k can be chosen between 1 and 4 where j must be unequal to k. For all possible combinations the value of $K_{k,j}$ must be the same. In the next steps the equations (2-85) and (2-86) are evaluated to determine A_0.

$$\alpha_0 = K_{k,j} - \sqrt{K_{k,j}^{\,2} - 1} \qquad (2\text{-}85)$$

$$a_0 = \frac{E_j \cdot H_k - E_k \cdot H_j}{G_k \cdot H_j - G_j \cdot H_k} \cdot \frac{1 + \alpha_0^{\,2}}{2} \qquad (2\text{-}86a)$$

$$b_0 = \frac{E_j \cdot G_k - E_k \cdot G_j}{G_k \cdot H_j - G_j \cdot H_k} \cdot \frac{1 + \alpha_0^{\,2}}{2} \qquad (2\text{-}86b)$$

$$K_{k,j} = \frac{\left| G_k \cdot H_j - G_k \cdot H_j \right|}{\sqrt{\left(E_k \cdot H_j - E_j \cdot H_k\right)^2 + \left(E_j \cdot G_k - E_k \cdot G_j\right)^2}} \qquad (2\text{-}87)$$

$$G_k = \sum_{i=1}^{4} p_{k,i} \cdot \beta_i \cdot \cos\varphi_i \qquad (2\text{-}88a)$$

$$H_k = \sum_{i=1}^{4} p_{k,i} \cdot \beta_i \cdot \sin\varphi_i \qquad (2\text{-}88b)$$

$$E_k = \sum_{i=1}^{4} p_{k,i} \cdot \beta_i \qquad (2\text{-}88c)$$

$$\beta_1 = \sin(\varphi_2 - \varphi_3) + \sin(\varphi_3 - \varphi_4) + \sin(\varphi_4 - \varphi_2) \qquad (2\text{-}89a)$$

$$\beta_2 = \sin(\varphi_3 - \varphi_1) + \sin(\varphi_1 - \varphi_4) + \sin(\varphi_4 - \varphi_3) \qquad (2\text{-}89b)$$

$$\beta_3 = \sin(\varphi_1 - \varphi_2) + \sin(\varphi_2 - \varphi_4) + \sin(\varphi_4 - \varphi_1) \qquad (2\text{-}89c)$$

$$\beta_4 = \sin(\varphi_3 - \varphi_2) + \sin(\varphi_1 - \varphi_3) + \sin(\varphi_2 - \varphi_1) \qquad (2\text{-}89d)$$

Now the rest of the calibration values have to be determined. This can be easily done by evaluation of equations (2-90) and (2-91) with use of equation (2-92). In equation (2-92) ϕ_0 stands for the angle of the complex calibration coefficient A_0.

$$q_i = \xi_i \pm \sqrt{\xi_i^{\,2} - \varsigma_i^{\,2} - \eta_i^{\,2}} \qquad (2\text{-}90)$$

$$a_i = \frac{\zeta_i}{q_i} \qquad (2\text{-}91a)$$

$$b_i = \frac{\eta_i}{q_i} \qquad (2\text{-}91b)$$

$$\begin{aligned}\xi_i = \frac{1}{\beta_4}\cdot\Bigg\{&\frac{1+\alpha_0{}^2}{2}\cdot\left[p_{i,1}\cdot sin(\varphi_3-\varphi_2)+p_{i,2}\cdot sin(\varphi_1-\varphi_3)+p_{i,3}\cdot sin(\varphi_2-\varphi_1)\right]+\\&+\alpha_0\cdot\left[p_{i,1}\cdot cos(\phi_0+\varphi_1)\cdot sin(\varphi_3-\varphi_2)+p_{i,2}\cdot cos(\phi_0+\varphi_2)\cdot sin(\varphi_1-\varphi_3)+\right.\\&\left.+p_{i,3}\cdot cos(\phi_0+\varphi_3)\cdot sin(\varphi_2-\varphi_1)\right]\Bigg\}\end{aligned} \qquad (2\text{-}92a)$$

$$\begin{aligned}\zeta_i = \frac{1}{\beta_4}\cdot\Bigg\{&\frac{1+\alpha_0{}^2}{2}\cdot\left[p_{i,1}\cdot(sin\varphi_2-sin\varphi_3)+p_{i,2}\cdot(sin\varphi_3-sin\varphi_1)+p_{i,3}\cdot(sin\varphi_1-sin\varphi_2)\right]+\\&+\alpha_0\cdot\left[p_{i,1}\cdot cos(\phi_0+\varphi_1)\cdot(sin\varphi_2-sin\varphi_3)+p_{i,2}\cdot cos(\phi_0+\varphi_2)\cdot(sin\varphi_3-sin\varphi_1)+\right.\\&\left.+p_{i,3}\cdot cos(\phi_0+\varphi_3)\cdot(sin\varphi_1-sin\varphi_2)\right]\Bigg\}\end{aligned} \qquad (2\text{-}92b)$$

$$\begin{aligned}\eta_i = \frac{1}{\beta_4}\cdot\Bigg\{&\frac{1+\alpha_0{}^2}{2}\cdot\left[p_{i,1}\cdot(cos\varphi_2-cos\varphi_3)+p_{i,2}\cdot(cos\varphi_3-cos\varphi_1)+p_{i,3}\cdot(cos\varphi_1-cos\varphi_2)\right]+\\&+\alpha_0\cdot\left[p_{i,1}\cdot cos(\phi_0+\varphi_1)\cdot(cos\varphi_2-cos\varphi_3)+p_{i,2}\cdot cos(\phi_0+\varphi_2)\cdot(cos\varphi_3-cos\varphi_1)+\right.\\&\left.+p_{i,3}\cdot cos(\phi_0+\varphi_3)\cdot(cos\varphi_1-cos\varphi_2)\right]\Bigg\}\end{aligned} \qquad (2\text{-}92c)$$

Using the derived calibration coefficients the reflection coefficient can be determined. The practical implementation of the algorithms is explained in chapter 4.

3 Hardware Design

The contents of this chapter will concentrate on the development of the directional coupler and the standing wave probe.

Based on the theory from subsection 2.2.1 the development steps of the directional coupler and the standing wave probe will be explained. In a first step the directional coupler and the standing wave probe were built up separately for easier testing. In a further implementation step they should be put together to decrease the insertion loss that arises from the connectors between them.

3.1 Directional Coupler

The directional coupler is used to measure the incident wave power in front of the standing wave probe. As all other components it is built for a nominal impedance of 50 Ω.

First attempts to design the directional coupler based on an optimisation of an intuitively created structure. According to some basic facts on directional couplers this intuitive structure was created with many parameters to optimise, for example the length, the line widths and the distance of the lines in different segments of the coupler. The parameters of this structure were optimised. To find an optimum many different structures and techniques (microstrip and stripline) with and without compensation capacitors, that should compensate different velocities of propagation in the substrate and in the air, were tested and optimised. But finally it showed that no really good results were made with this design attempts.

So another method, basing on coupled line theory, was chosen. The theory that is necessary for developing such a directional coupler is explained in subsection 2.2.1.

3.1.1 Material

To keep the costs small a simple photolithographic production process was chosen. This process is constrained to the following dimensions:

- Minimum distance between two adjacent structures: 140µm
- Minimum line width: 200µm

Because of its uncritical properties and easy availability a RF-laminate of Taconic called TLX-9 was chosen. It is a PTFE/woven glass substrate copper cladded on both sides. The most important properties of this substrate are given in table 3.1. The complete datasheet is added as Appendix D.

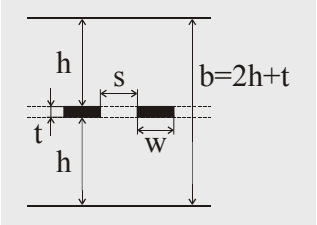

Fig. 3.1 - Stripline Configuration

Substrate Height (h)	762 µm
Copper Height (t)	35µm
Rel. Dielectric Constant (ε_R)	2.50
Loss Tangent ($tan(\delta)$)	0.0019

Tab. 3.1 - Material Characteristics

The low dielectric constant was chosen to make the implementation less sensitive to production inaccuracies. As explained former the trials with microstrip technology did not show good

results. So stripline technology was chosen. At stripline technology the transmission line lies within two substrates that are characterised above. The physical structure of the stripline configuration is shown in Fig. 3.1. In the production process the copper structure is built on one substrate, the other substrate has no copper on one side. Finally the two substrates are bonded together with a bonding film inside. The bonding film has the same dielectric constant as the substrate and a thickness of 35 µm. The bonding process will be explained later.

3.1.2 Implementation

The implementation of the directional coupler is based on the theory of coupled lines and development procedure for directional couplers that is explained in subsection 2.2.1.

Characterisation

First of all the main characteristics of the directional coupler had to be established. Since the application frequency range of the reflectometer should be from 800 MHz to 6.5 GHz and allowing for an appropriate offset the frequency range of the directional coupler was defined to be from f_L = 500 MHz to f_U = 7.5 GHz. Using equations (2-29) and (2-30) the centre frequency and the bandwidth ratio were calculated to be f_0 = 4 GHz and B = 15. The coupling C of the directional coupler should be 20 dB to keep the insertion loss low. From this the value of R = 0.1 was evaluated. Since a calibration is applied to the measurement problem the ripple factor δ does not matter very much, so values up to 1 dB can be accepted. Using these design parameters I looked up the values of the normalized even-mode impedances in table 6.1 of reference [4] which is added as Appendix C. The part of the table that is important for my directional coupler is shown in the next subsection where the whole development process is described.

Simulation and Implementation

The normalised even-mode impedances for a coupling of 20 dB for different ripple factors and bandwidth ratios are shown in Tab. 3.2. Additionally it can be found in the table that N = 9 sections are used for the directional coupler.

δ	Z_{OE1}	Z_{OE2}	Z_{OE3}	Z_{OE4}	Z_{OE5}	B
0.2	1.00555	1.01529	1.03447	1.07471	1.21931	9.061
0.4	1.00886	1.02054	1.04153	1.08328	1.22965	11.571
0.6	1.01187	1.02485	1.04700	1.08974	1.23478	13.697
0.8	1.01474	1.02871	1.05175	1.09527	1.24426	15.674
1.0	1.01753	1.03232	1.05608	1.10028	1.25049	17.588

Tab. 3.2 - Normalized Even-Mode Impedances for 20 dB Coupling

Using equation (2-31) the minimum number of elements could be calculated to be n = 5. With this the constraints for u were determined as in equation (3-1) what results in a length of $20 \cdot \pi$.

$$-10 \cdot \pi \le u \le 10 \cdot \pi \qquad (3\text{-}1)$$

The weighting factors were calculated from the even-mode impedances using equation (2-32). Since the bandwidth ratio is 14 the values for δ = 0.8 or B = 15.674 were used. These values were chosen, since δ is not important and the according bandwidth ratio is larger than the demanded one. With this choice the required properties should be met. The weighting factors and the according u-ranges are given in Tab. 3.3.

u-Range	$w_i(u)$
$-2 \cdot \pi \leq u \leq 0$	1.13603
$-4 \cdot \pi \leq u \leq -2 \cdot \pi$	1.04138
$-6 \cdot \pi \leq u \leq -4 \cdot \pi$	1.02240
$-8 \cdot \pi \leq u \leq -6 \cdot \pi$	1.01377
$-10 \cdot \pi \leq u \leq -8 \cdot \pi$	1.01474

Tab. 3.3 - Weighting Factors

How the integral (2-33) was evaluated is shown in equation (3-2). According to the weighting factors the constraints of the ranges were chosen. In equation (3-2) the value for $u = -\pi$ is calculated. After a simple transformation the value for $Z_{0E}|_{u=-\pi}$ could be derived. From that the value of $Z_{0O}|_{u=-\pi}$ was determined using equation (2-20).

For my implementation I chose 80 elements over the whole length of the directional coupler. So the odd- and even-mode impedances had to be calculated on 41 different postions, since the directional coupler is symmetrical with respect to its vertical axis.

$$\frac{1}{2} \cdot ln \frac{Z_{0E}\big|_{u=-\pi}}{Z_0} = -\frac{R}{\pi} \cdot \left[w_5 \cdot \int_{-10\pi}^{-8\pi} \frac{sin^2\left(\frac{u}{2}\right)}{\frac{u}{2}} \cdot du + w_4 \cdot \int_{-8\pi}^{-6\pi} \frac{sin^2\left(\frac{u}{2}\right)}{\frac{u}{2}} \cdot du + w_3 \cdot \int_{-6\pi}^{-4\pi} \frac{sin^2\left(\frac{u}{2}\right)}{\frac{u}{2}} \cdot du + w_2 \cdot \int_{-4\pi}^{-2\pi} \frac{sin^2\left(\frac{u}{2}\right)}{\frac{u}{2}} \cdot du + w_1 \cdot \int_{-2\pi}^{-\pi} \frac{sin^2\left(\frac{u}{2}\right)}{\frac{u}{2}} \cdot du \right] \quad (3\text{-}2)$$

The number of 80 elements was found empirically. I also tried implementations with 60 and 100 elements. The implementation with 80 elements showed still improvements of the simulation accuracy to the implementation with 60 elements. The implementation with 100 elements did not increase the accuracy any more. So 80 elements were a good trade off between exact results and economic implementation.

The line widths and the distances according to the calculated odd- and even impedances were calculated as described in subsection 2.2.1. What is still left is the physical length d of the directional coupler which can be determined using equation (3-3).

$$d = \frac{n \cdot \pi}{\beta_0} = \frac{n \cdot c_0}{2 \cdot f_0 \cdot \sqrt{\varepsilon_R}} \quad (3\text{-}3)$$

The length of one element was calculated by dividing the whole length d by the number of elements. The layout of the implementation of this first directional coupler is shown in Fig. 3.2. The according simulation results are shown in Fig. 3.3.

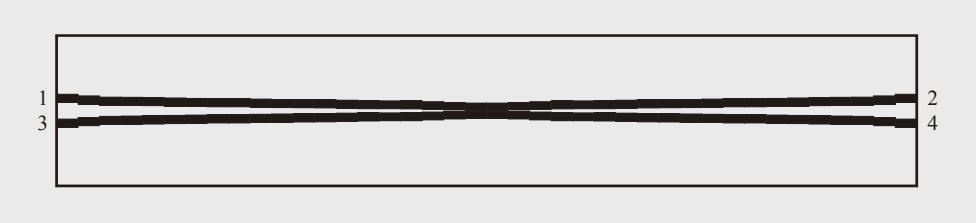

Fig. 3.2 - Layout: First Directional Coupler

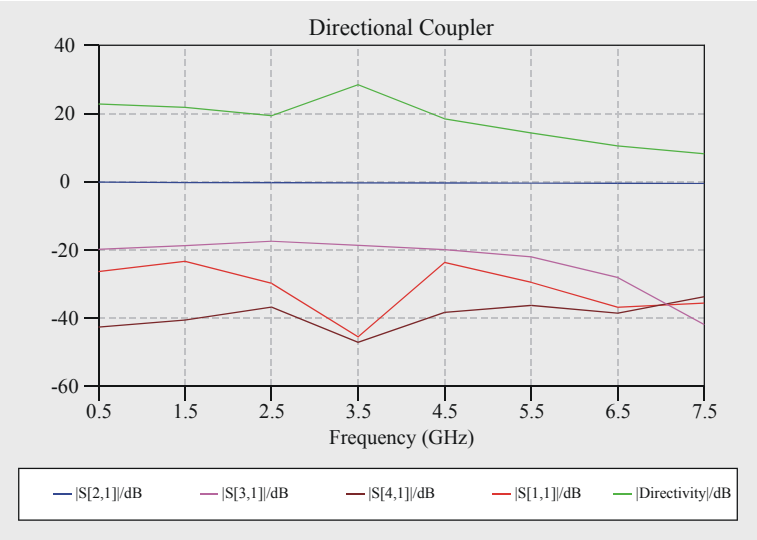

Fig. 3.3 - Simulated Characteristic: First Coupler

The simulations were made for optimal material, what means that the substrate is lossless and the conductors are perfect and infinitely thin. Since the directivity should have been at least 10 dB this implementation was not sufficient. Secondly the coupling is not close to -20 dB for higher frequencies. For that two reasons further attempts were made. The best implementation uses a lower frequency limit of f_L = 0.8 GHz and an increased bandwidth ratio of B = 17.588. For that reason the centre frequency increases and physical length of the coupler decreases. With these new parameters the development process was repeated. The new odd- and even-mode impedances with according u and x values are shown in Tab. 3.4. In the last two columns the physical dimensions for perfect conductor in the according segment are listed.

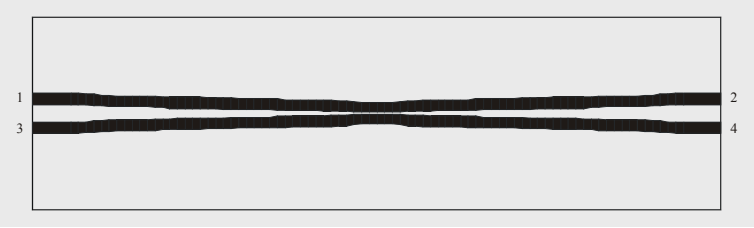

Fig. 3.4 - Layout: Second Directional Coupler

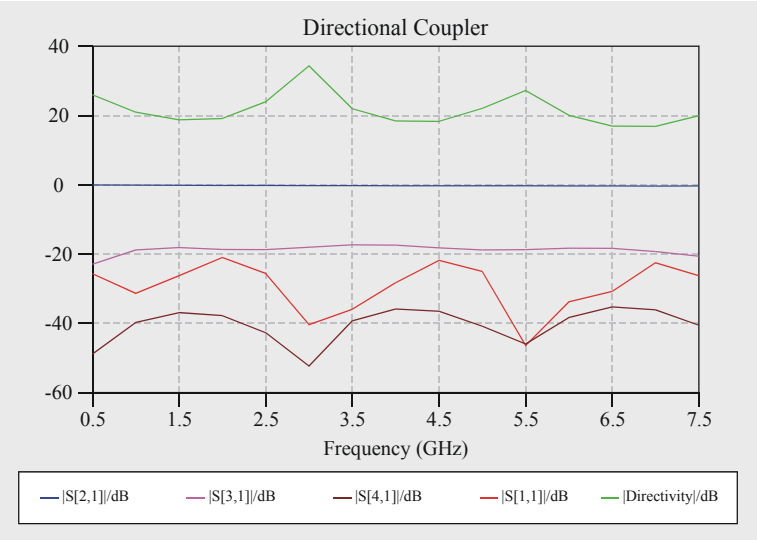

Fig. 3.5 - Simulated Characteristics: Second Coupler

Since the lower frequency limit is f_L = 0.8 GHz and the bandwidth ratio B=17.588 the upper frequency limit calculates to f_U = 14.070 GHz. The centre frequency follows to be f_0 = 7.4352 GHz. Therefore the overall length is d = 64 mm. Since 80 Elements were used every element has a length of 0.8 mm. The simulation results for this structure on optimal material shows are depicted in Fig. 3.5 with the according layout in Fig. 3.4.

U	x / mm	Z_{0E} / Ω	Z_{0O} / Ω	w / mm	s / mm
-31.4159	-32.00	50.0000	50.0000	1.15	Inf
-30.6305	-31.20	50.0099	49.9901	1.15	3.50
-29.8451	-30.40	50.0738	49.9263	1.15	2.52
-29.0597	-29.60	50.2176	49.7834	1.15	2.00
-28.2743	-28.80	50.4225	49.5810	1.15	1.68
-27.4889	-28.00	50.6340	49.3739	1.14	1.48
-26.7035	-27.20	50.7916	49.2207	1.14	1.38
-25.9181	-26.40	50.8658	49.1489	1.14	1.32
-25.1327	-25.60	50.8779	49.1372	1.14	1.32
-24.3473	-24.80	50.8861	49.1293	1.14	1.32
-23.5619	-24.00	50.9392	49.0781	1.14	1.30
-22.7765	-23.20	51.0592	48.9627	1.14	1.24
-21.9911	-22.40	51.2316	48.7980	1.14	1.16
-21.2058	-21.60	51.4106	48.6281	1.14	1.10
-20.4204	-20.80	51.5451	48.5012	1.14	1.06
-19.6350	-20.00	51.6090	48.4412	1.14	1.04
-18.8496	-19.20	51.6195	48.4314	1.14	1.04
-18.0642	-18.40	51.6320	48.4195	1.14	1.02
-17.2788	-17.60	51.7143	48.3425	1.14	1.00
-16.4934	-16.80	51.9029	48.1668	1.14	0.96
-15.7080	-16.00	52.1776	47.9133	1.14	0.90
-14.9226	-15.20	52.4675	47.6485	1.14	0.84
-14.1372	-14.40	52.6891	47.4482	1.14	0.80
-13.3518	-13.60	52.7960	47.3521	1.14	0.78
-12.5664	-12.80	52.8139	47.3360	1.14	0.78
-11.7810	-12.00	52.8351	47.3170	1.14	0.76
-10.9956	-11.20	52.9768	47.1904	1.14	0.74
-10.2102	-10.40	53.3104	46.8951	1.14	0.70
-9.4248	-9.60	53.8120	46.4580	1.13	0.64
-8.6394	-8.80	54.3614	45.9885	1.13	0.58
-7.8540	-8.00	54.7988	45.6214	1.12	0.54
-7.0686	-7.20	55.0197	45.4383	1.12	0.52
-6.2832	-6.40	55.0583	45.4064	1.12	0.52
-5.4978	-5.60	55.1068	45.3665	1.12	0.50
-4.7124	-4.80	55.4537	45.0827	1.12	0.48
-3.9270	-4.00	56.3561	44.3608	1.11	0.42
-3.1416	-3.20	57.9106	43.1700	1.09	0.34
-2.3562	-2.40	59.9642	41.6915	1.07	0.26
-1.5708	-1.60	62.0996	40.2579	1.04	0.18
-0.7854	-0.80	63.7360	39.2243	1.02	0.16
0	0.0	64.3519	38.8489	1.01	0.14

Tab. 3.4 - Physical Parameters of the Final Coupler

For the simulation of the directional coupler on the material chosen for the implementation the gap between the two coupler parts and the line width were adapted to the material parameters. These adaptions were found by an empirical process, which compared the parameters on optimal material to the parameters on the used material at different positions. The used adaptions were an increase of the gap width of about 40 µm and a reduction of the line width of about 60 µm. Due to the small distance between the two coupler parts at the connectors the layout had to be adapted, for better mechanical handling. Therefore the ports 3 and 4 were placed at the frontside of the layout. Fig. 3.6 shows the final layout in scale 1:2. It consists of two parts the one on the top that contains the copper structure and the one on the bottom that is the cover for the stripline implementation. A photography of the final prints is shown in Fig. 3.7. As the distance in the middle of the coupler is just 140 µm a detail photo is added in Fig. 3.8.

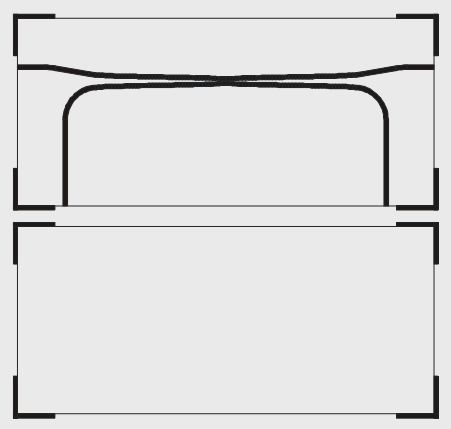

Fig. 3.6 - Layout of the Final Coupler

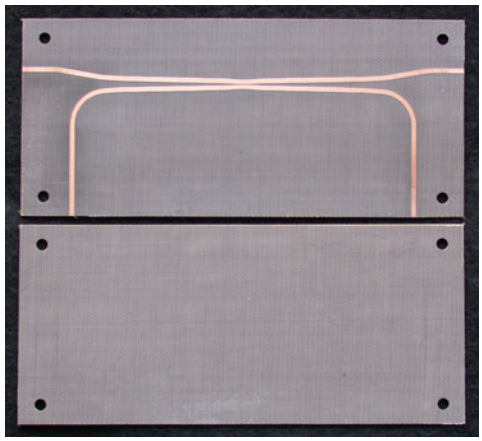

Fig. 3.7 - Final Prints of the Directional Coupler

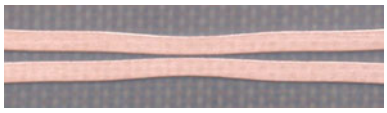

Fig. 3.8 - Detail of the Directional Coupler

Assembling

Because the substrate thickness is less than 1 mm a brass carrier was used to increase the stability and as a fixture for the connectors. A photography of one of the brass carriers with one half of the layout of an older version of the directional and the applied connectors is shown in Fig. 3.9. A detailed description how the connectors are applied is given in subsection 3.2.5. The mechanical drawings of the used brass carriers are added in Appendix B.

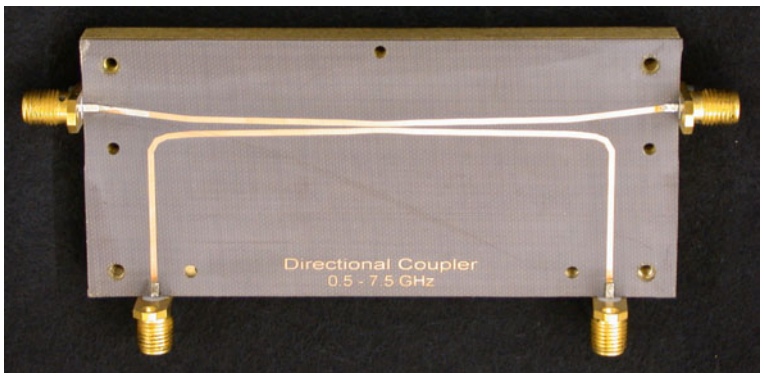

Fig. 3.9 - Directional Coupler Before Bonding

After the connectors were applied the bonding film and the upper half of the substrate were positioned. Finally the upper brass carrier was applied. To bond both parts of the substrate the brass carrier was externally heated up to 120 °C. Best results were reached if the bonding film reached a temperature of 100 °C. This temperature was measured with a very small thermocouple between the substrates. Important is that the connectors are not fixed by screws during the heating process, because in that case the connectors could break inside the substrate due to thermal expansion.

When the substrate was finally bonded the brass carriers and the connectors were fixed by screws. A photography of the readily assembled directional coupler is shown in Fig. 3.10. In this photography the ports are numbered according to simulation and measurement, respectively.

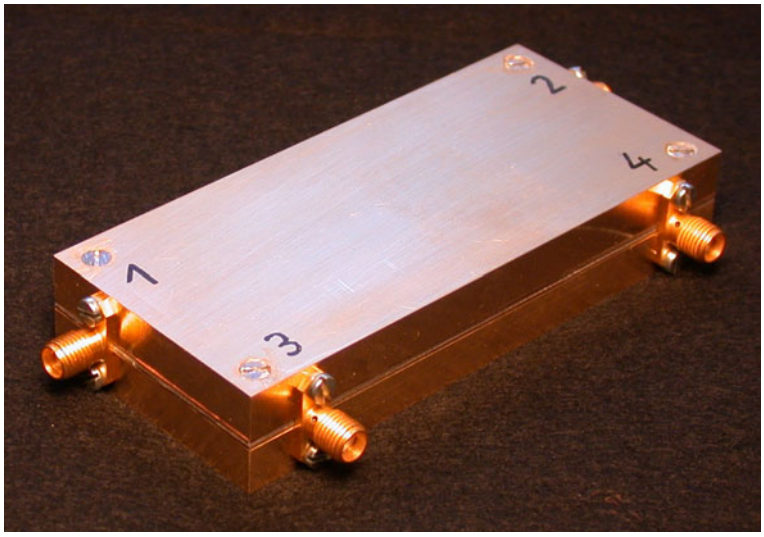

Fig. 3.10 - Assembled Directional Coupler

3.1.3 Measurements

For all measurements a HP 8510 C VNA was used. The calibration was done using a commercial SOLT calibration kit to eliminate the influences of the connectors and the measurement system (cables). For a SOLT calibration four different standards are used: through connection, short, open and load.

After that calibration the S-parameters were measured between any two ports of the directional coupler. The other ports were terminated with a standard 50 Ω-load. The measured data were linked together to one four-port file that could be read by Microwave Office®. This link of data was done using the SXP-FileConverter tool described in Appendix A.

The measured data were analysed with Microwave Office® and are shown in Fig. 3.11 to Loss Fig. 3.13. Fig. 3.11 shows the coupling from port one to the coupled port 3 ($|S_{31}|$) and the isolated port 4 ($|S_{41}|$). As a figure of merit the directivity is defined as $|Directivity|_{[dB]} = |S_{31}|_{[dB]} - |S_{41}|_{[dB]}$.

The directivity is the relation between the power from the coupled port to the power of the isolated port. As one can see the coupling to the coupled port is very flat over the whole frequency range, what is very good. The directivity is good for frequencies up to 5.5 GHz. Since the directivity is still larger then 8 dB in the whole frequency range and the coupling is very good this version of the coupler can be used in the reflectometer.

Fig. 3.12 shows the insertion loss of the directional coupler that meets the requirements for this application. Also the reflection coefficients shown in Fig. 3.13 are sufficient.

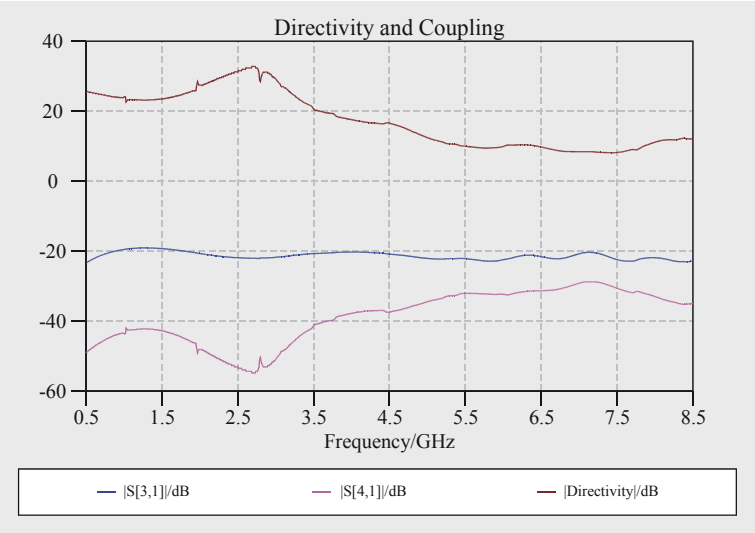

Fig. 3.11 - Directional Coupler: Directivity and Coupling (S_{31})

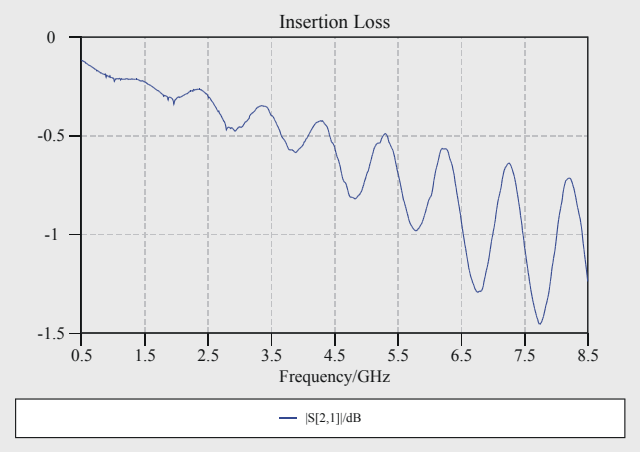

Fig. 3.12 - Directional Coupler: Insertion Loss

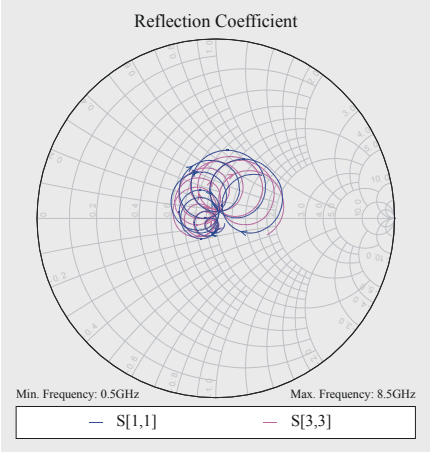

Fig. 3.13 - Direct. Coupler: Refl. Coeff.

3.2 Standing Wave Probe

The Standing Wave Probe was used to sample the power of the standing wave pattern on five different positions. For that reason five couplers were placed at certain positions. Following from this the main tasks of the development were the design of a single coupler and the determination of the positions of these couplers.

3.2.1 Material and Production Process

For the reasons of low cost and simple production process the same material as for the directional coupler was chosen. Since the same production process was used the directional coupler and the standing wave probe could be produced cost efficiently in one step on one substrate.

The difference is that the standing wave probe is built in microstrip technology instead of stripline technology so there is just one substrate and no bonding process. Microstrip technology is used because resistors have to be mounted on the substrate what is impossible using stripline technology.

The low dielectric constant was chosen because it improves the accuracy of the implementation. Since the wavelength of the standing wave pattern on the transmission line depends on the

dielectric constant (the smaller the dielectric constant the longer the wavelength) the wavelength can be increased at the same manufactural accuracy because the production process parameters are not influenced by the dielectric constant. For that reason a coupler can have smaller physical dimensions compared to the wavelength and so the sampling area is more locally then with a higher dielectric constant.

3.2.2 Coupler

The basic requirements for the coupler were an insertion loss that is as low as possible and a defined flat coupling over the whole frequency range. If the coupling is not flat over the whole frequency range the measurement range of the power meter is used to compensate these differences of coupling, what leads to more inaccurate measurements.

Resistor Model

As it will be shown later resistors were used for the implementation of the coupler. Before these resistors could be modelled for the development of the coupler they had to be measured. For that reason a test structure was made on the substrate that was used for the standing wave probe. This substrate is described in subsection 3.2.1. To measure the resistor I used a transmission line with a gap in the middle. On both sides of this gap were solder pads for the SMD resistors. The solder pads had a width of 0.7 mm and a length of 1 mm. The gap had a length of 0.4 mm. After the solder pads tapers widened the transmission line to 2.167 mm, which is the line width for 50 Ω on this substrate. The layout of the resistor measurement print is shown in Fig. 3.14.

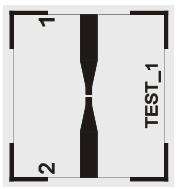

Fig. 3.14 – Layout Resistor Meas.

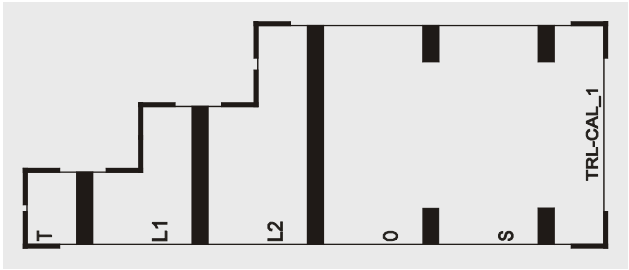

Fig. 3.15 - Layout Calibration Kit

For the measurement the reference planes were chosen 5 mm inside the print on each side. This was done to calibrate the influence of the transition from the microstrip transmission line to the coaxial connector of the test fixture.

To get the characteristics of the resistor the transmission lines and the connector influences had to be eliminated by a proper calibration procedure. This was done by a TRL calibration with a special calibration kit that is shown in Fig. 3.15. For that kind of calibration three different standards are used: most left the through connection T, on the right side the reflect standards (short and open) and in the middle the two different lines. The through connection should be a direct connection between the two ports of the VNA. Since the reference planes for the measurement of the resistor were chosen 5 mm inside the measurement print the through connection had a length of 10 mm. For the same reason the open and short were chosen 5 mm inside the board and the lines were extended 5 mm on each side. The short was realised by a transmission line with a copper conductor at the end that is connected to ground through a proper hole.

According to the manual of the VNA the lines must have a length of 20° to 160°. This is not possible for the whole measurement frequency range from 0.5 GHz to 10 GHz with one line, so two lines had to be used. Those lengths were calculated to be 9.1 mm and 20.3 mm. The calculation was done according to the manual of the HP 8510 C VNA.

The resistors were measured using a HP 8510 C VNA. It was calibrated using the calibration kit described above. For the measurements different resistors were soldered to the measurement print. The data was stored and analysed to find the proper resistor models.

First of all the empty measurement print was modelled and compared to the according measurement. After these parameters were determined the resistor model was switched in parallel. The used model for the SMD chip resistors and the connection pads is shown in Fig. 3.16. Fig. 3.17 shows a comparison of the measured and simulated S_{12} curves for magnitude and phase of a 680 Ω resistor.

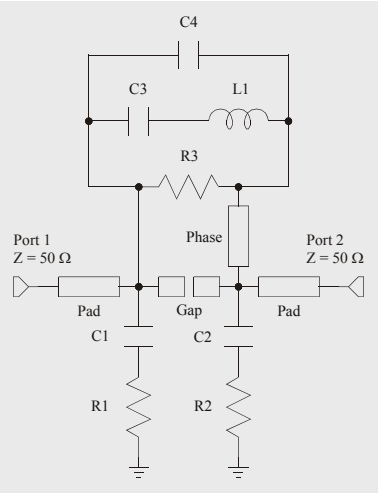

Fig. 3.16 - Resistor Model

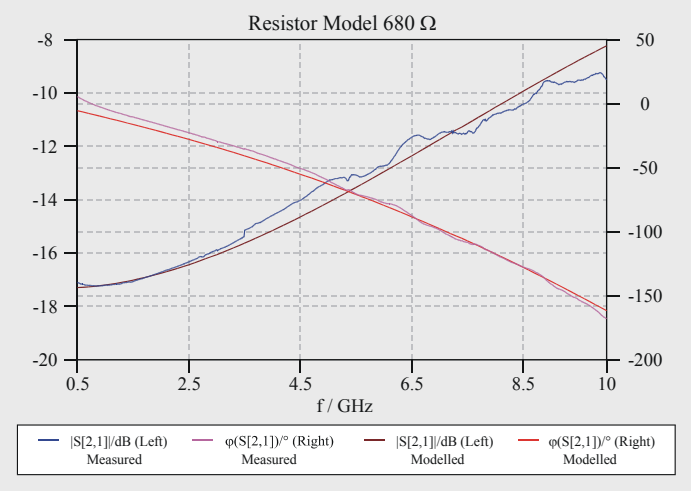

Fig. 3.17 - Resistor Measured and Modelled

Nom. Value	$R_1=R_2$/Ω	R3/Ω	$C_1=C_2$/pF	C3/pF	C4/pF	L1/nH	Phase
330 Ω	10000	314.2	0.016	0.004	0.035	6.60	4.6 ° @ 5 GHz
680 Ω	10000	630.7	0.050	0.011	0.024	2.76	8° @ 5 GHz

Tab. 3.5 - Typical Values for the Resistor Model

Typical values for the resistor model are shown in Tab. 3.5. With similar models resistor values from 150 Ω to 1500 Ω were modelled to fit the measurements.

Implementation and Simulation

From the considerations that were made on the theory of the coupler, which is explained in subsection 2.2.1, a start layout was created and by means of optimisation the final structure was developed.

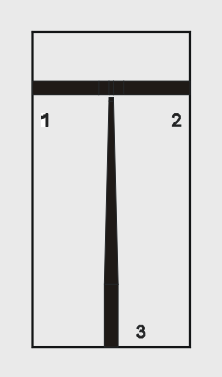

Fig. 3.18 - Layout: First Coupler

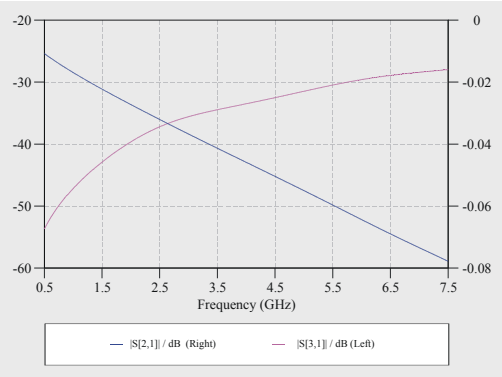

Fig. 3.19 - Simulated Characteristics: First Coupler

The coupling should have been about –25 dB over the whole frequency range from 0.5 to 7.5 GHz. This value was chosen to keep the insertion loss small. On the other hand this value was in the same range as the coupling of the directional coupler, which was good for the measurement range of the power meter. The frequency range was chosen for the same reasons as the frequency range of the directional coupler was chosen.

The main line on which the standing wave pattern arises should be a 50 Ω line. For the given material parameters the width of a 50 Ω line is 2.167 mm. The basic structure for the optimisation of the coupler consists of a transmission line and a probe tip that was capacitively coupled to this line. The distance between the transmission line and the probe tip is d = 0.2 mm. The width of the probe tip c = 0.7 mm. The layout of this coupler structure is shown in Fig. 3.18 in original size.

The simulated S-parameters of the start layout are shown in Fig. 3.19. With respect to the coupling (S_{31}) there are two points to criticise in this design. Firstly the coupling is much lower than the demanded - 25 dB over the whole frequency range. Secondly the coupling varies about 30 dB over frequency. To overcome these disadvantages various widths of the coupler tip d and distances between coupler tip and transmission line c were evaluated but no satisfying results were reached. Some examples and constraints should be pointed out here. If the distance between coupler tip and transmission line is lowered to the technological limit of 140 µm a coupling of - 26 dB is reached. So the only possibility to increase the coupling is an increase of the width of the coupler tip. But if this is done the coupler detects the varying power of the standing wave pattern of about 1 mm. If a frequency of 7.5 GHz is used half of the wavelength on the transmission line is 20 mm. What follows is that such a wide coupler tip would average the power over an angle of 9°. This has direct consequences to the accuracy of the measurement result. Because of that the coupler tip cannot be widened any more. Also if the problem with the low coupling could have been solved this would not decrease the wide dynamic range of the coupling. So another possibility was investigated.

This possibility was to use resistive coupling in parallel to the capacitive coupling that means that a resistor was mounted over the gap between transmission line and coupler tip. For the simulation several 0402 SMD chip resistors were measured and modelled as described in the former subsection. Those resistor models were used for further simulations. The resistance value in the following coupler simulation is 1000 Ω. The characteristics of this kind of coupler are shown in Fig. 3.21. The accompanying model of the coupler is depicted in Fig. 3.20.

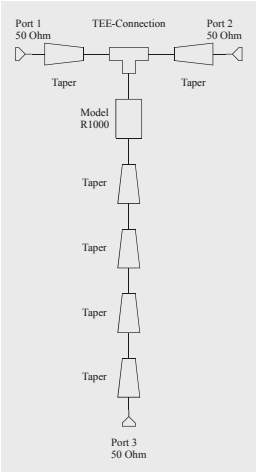

Fig. 3.20 - Coup. w. Res. - Model

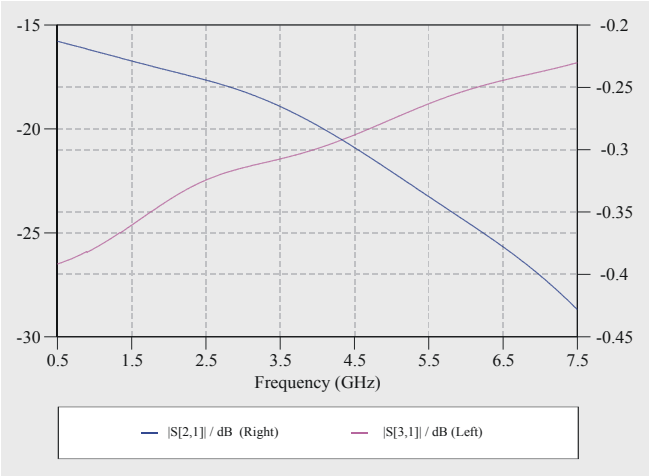

Fig. 3.21 - Coupler with Resistor - Simulated Characteristic

In this simulation there is still a wide range of coupling. This is a consequence of the capacitive coupling between the solder pads of the SMD chip resistor. To lower this capacity two resistors were connected in series, because then the capacity of the solder pads is divided in half.

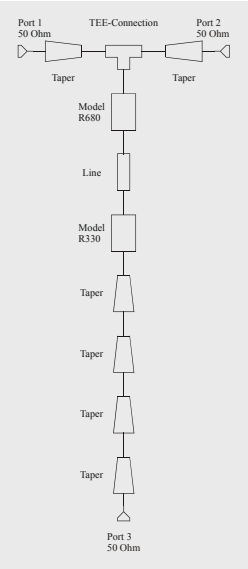

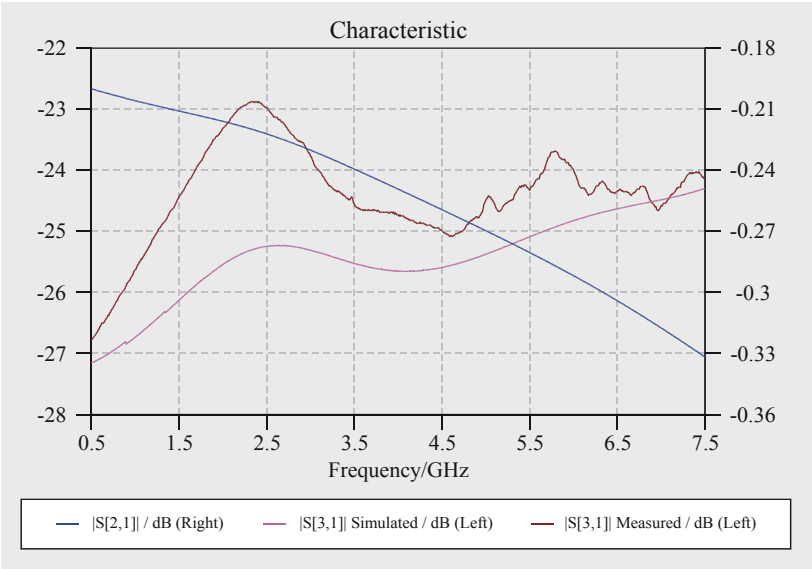

Fig. 3.22 - F. Coupler - Model

Fig. 3.23 - Final Coupler - Characteristics

The resistance values of the two resistors were chosen from the range of 150 Ω to 1500 Ω basing on the models. The combination of 680 Ω and 330 Ω showed an optimum for the key features of the coupler that are the insertion loss and the coupling. To reach these good results the 680 Ω resistor must be placed near the transmission line and the 330 Ω resistor near port 3.

The impedance transformer at port 3 was built of four tapered lines with the same length. It transforms the impedance according to a line width of 0.7 mm to 50 Ω at port 3. The different line widths along the impedance transformer were optimised for low insertion loss and small reflection coefficient at port 3.

Finally the width of the transmission line was optimised at the position where the coupler is connected. For this the width of the transmission line was decreased so that the impedance of the transmission line rises. Together with the impedance reduction due to coupling the main line impedance lowers to the nominal value of 50 Ω that is the optimum.

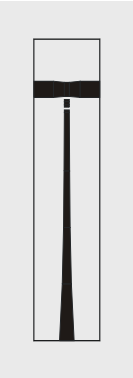

Fig. 3.24 - Layout Coupler

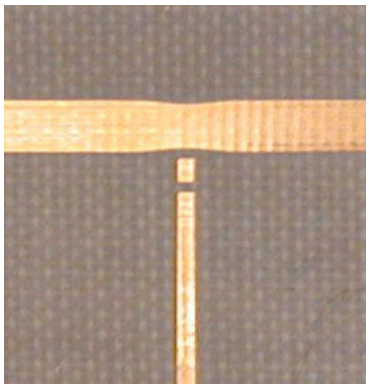

Fig. 3.25 - Coupler without Resistor

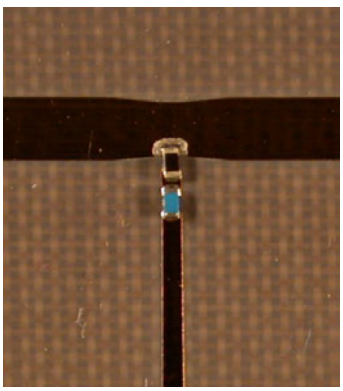

Fig. 3.26 - Coupler with Resistor

Fig. 3.23 shows the characteristics of the final implemented coupler. What is very good is the coupling. It is in the range of about –25 dB over the whole frequency range and the coupling span is less than 4 dB. The insertion loss is less than 0.3 dB in the application frequency range of the reflectometer. This relatively large value will be explained together with the simulations of the standing wave probe and is accepted because it leads to a the very flat coupling. Fig. 3.22 shows the accompanying coupler model.

Fig. 3.24, Fig. 3.25 and Fig. 3.26 show different states of the production process of the coupler. Most left the layout, in the middle the copper structure of the coupler and most right the final coupler with mounted resistors (black resistor 680 Ω, blue resistor 330Ω).

Measurements

Since five couplers were fitted together to the standing wave probe just a few test measurements were made to prove the simulation. Those measurements showed that the simulated coupling had the same frequency behaviour as the measured one, but its value is up to 2 dB lower than the measured coupling. The comparison of measured and simulated coupling is shown in Fig. 3.23. Detailed measurements of the whole standing wave probe are shown in subsection 3.2.6.

3.2.3 Distance Optimisation

This chapter deals with the optimisation and development of the standing wave probe. The standing wave probe consists of a transmission line on which the standing wave arises and five couplers that sample the local power of the standing wave pattern on distinct positions. To get an optimum result over frequency these positions have to be optimised.

Optimisation

For the optimisation of the sampling positions the elements of the matrices and the vectors of subsection 2.2.3 had to be determined. The optimisation starts with equation (3-4) for the local power of the standing wave at a certain position. This equation is equal to equation (2-12) in subsection 2.1.1.

$$\frac{P(x)}{P_0} = \left|1 + \Gamma \cdot e^{+j2\beta \cdot x}\right|^2 \qquad (3\text{-}4)$$

Since the reflection coefficient vector for the optimisation should consist of $|\Gamma|^2$, Γ_R and Γ_I equation (3-4) has to be transformed to these parameters. This was done with a simple transformation as shown with equations (3-5) and (3-6). Equation (3-6) contains the sine- and cosine-function instead of the exponential terms.

$$\frac{P(x)}{P_0} = 1 + \left|\Gamma\right|^2 + \Gamma_R \cdot \left(e^{j2\beta x} + e^{-j2\beta x}\right) + j \cdot \Gamma_I \cdot \left(e^{j2\beta x} - e^{-j2\beta x}\right) \qquad (3\text{-}5)$$

$$\frac{P(x)}{P_0} = 1 + \left|\Gamma\right|^2 + 2 \cdot \Gamma_R \cdot cos(2\beta \cdot x) - 2 \cdot \Gamma_I \cdot sin(2\beta \cdot x) \qquad (3\text{-}6)$$

To distinguish between the powers at the different sampling points the index *i*, that goes from 1 to 5, was introduced. For matching with equation (2-38) the constant term on the right side was moved to the left side. The new equation with indices is shown in (3-7)

$$\frac{P_i(x_i)}{P_0} - 1 = \left|\Gamma\right|^2 + 2 \cdot \Gamma_R \cdot cos(2\beta \cdot x_i) - 2 \cdot \Gamma_I \cdot sin(2\beta \cdot x_i) \qquad (3\text{-}7)$$

For the optimisation of the standing wave probe I made some simplifications. Those simplifications are:

- the directional coupler is assumed to be lossless
- the junctions are assumed to be lossless

- all probes are assumed to be identical and symmetrical with respect to their longitudinal axis
- the main line is assumed to be perfectly matched

These simplifications should be explained a little more. The lossless directional coupler should have no insertion loss and it should have infinite directivity. The lossless junctions should have no insertion loss and therefore should not take away any power from the main line. That the probes are identical means that all five probes have the same shape and characteristics and the symmetry means that they do not distinguish between incident- and reflected wave. The perfect matching of the main line means that the impedance along the transmission line is constant what means that no reflections occur on the transmission line except at the reference plane.

Due to these simplifications the power that is measured at the output of the directional coupler is equal to the incident wave power P_0 in equation (3-4). So equation (3-4) is equal to equation (2-37) if the coefficients are set as follows (3-8).

$$\begin{aligned} k_i &= 1 \\ Q_0 &= 0 \\ Q_i &= e^{+j2\beta \cdot x_i} \end{aligned} \qquad (3\text{-}8)$$

Using this form vectors $\underline{\mathbf{\Gamma}}$ (3-10) and $\underline{\mathbf{B}}$ (3-11) and matrix **A** (3-9 **)** could be defined and so equation (2-38) was complete.

$$\mathbf{A} = \begin{pmatrix} 1 & 2\cdot cos(2\beta\cdot x_1) & -2\cdot sin(2\beta\cdot x_1) \\ 1 & 2\cdot cos(2\beta\cdot x_2) & -2\cdot sin(2\beta\cdot x_2) \\ 1 & 2\cdot cos(2\beta\cdot x_3) & -2\cdot sin(2\beta\cdot x_3) \\ 1 & 2\cdot cos(2\beta\cdot x_4) & -2\cdot sin(2\beta\cdot x_4) \\ 1 & 2\cdot cos(2\beta\cdot x_5) & -2\cdot sin(2\beta\cdot x_5) \end{pmatrix}, \qquad \underline{\mathbf{\Gamma}} = \begin{pmatrix} |\Gamma|^2 \\ \Gamma_R \\ \Gamma_I \end{pmatrix} \qquad (3\text{-}9), (3\text{-}10)$$

$$\underline{\mathbf{B}} = \begin{pmatrix} \frac{P_1(x_1)}{P_0} - 1 \\ \frac{P_2(x_2)}{P_0} - 1 \\ \frac{P_3(x_3)}{P_0} - 1 \\ \frac{P_4(x_4)}{P_0} - 1 \\ \frac{P_5(x_5)}{P_0} - 1 \end{pmatrix} \qquad (3\text{-}11)$$

In the theory equation (2-37) could not be optimised, because matrix **A** depends on the measured powers and the coupler parameters. Due to the simplifications introduced at the beginning of this chapter matrix **A** just depends on the coupler parameters, but another problem arises. In matrix (3-9 **)** the coupler parameters are related to the distances to the reference plane and not to distances between the first and each other as in equation (2-49). One can solve this problem, if a substitution as in equations (2-42), (2-43) and (2-44) is applied. Because Q_0 equals 0 and k_i equals 1, these equations simplify to equations (3-12), (3-13) and (3-14), respectively.

$$Q_1 \cdot \Gamma \equiv \gamma + 1 \qquad (3\text{-}12)$$

$$p_i = \left| q_i \cdot \gamma + 1 \right|^2 \qquad (3\text{-}13)$$

$$q_i = \frac{Q_i}{Q_1} = \frac{e^{+j2\beta \cdot x_i}}{e^{+j2\beta \cdot x_1}} = e^{+j2\beta \cdot (x_i - x_1)} = e^{+j2\beta \cdot d_i} \qquad (3\text{-}14)$$

If the same procedure as in the determination of matrix **A** is used matrix **C** could be found in equation (2-45) with the elements given in matrix (3-15).

$$\mathbf{C} = \begin{pmatrix} 1 & 2 & 0 \\ 1 & 2 \cdot cos(2\beta \cdot d_2) & -2 \cdot sin(2\beta \cdot d_2) \\ 1 & 2 \cdot cos(2\beta \cdot d_3) & -2 \cdot sin(2\beta \cdot d_3) \\ 1 & 2 \cdot cos(2\beta \cdot d_4) & -2 \cdot sin(2\beta \cdot d_4) \\ 1 & 2 \cdot cos(2\beta \cdot d_5) & -2 \cdot sin(2\beta \cdot d_5) \end{pmatrix} \qquad (3\text{-}15)$$

As explained in the theory the optimisation criterion is based on the condition number of matrix **C**, which is calculated with equation (2-41).

The overall condition number with respect to the four distances, which is used for the optimisation is calculated with equation (2-48). It is the sum of the squares of the condition numbers of matrix **C** over the whole frequency range for which the standing wave probe has to be optimised. To get a mean value this sum is divided by the number of frequency points. This value should be as low as possible for a well-conditioned standing wave probe.

My standing wave probe was designed for a frequency range from 0.5 GHz up to 7.5 GHz. The optimisation according to equation (2-48) was made on 71 frequency points (*M*) which are equally spaced in this range, what results in a distance of 100 MHz between two adjacent frequency points.

Because equation (2-48) has to be minimized for a well-designed standing wave probe I chose the MatLab® function ‘fmincon’ that is able to minimize a function according to constrained scalar parameters. Those parameters were the four distances d_2 to d_5 as defined before. A detailed description of this function is given in Appendix A. Also the parameters and the additional m-files that were used for the optimisation can be found there.

The start values for the optimisation were chosen according to the last example on page 22 because this structure led to good results. The constraint for the minimum distance between two adjacent probes was chosen to be 6.9 mm ($\frac{10}{\sqrt{\varepsilon_{eff}}}$) because of manufacturing reasons. The constraint for the overall length was chosen to be 103.3 mm ($\frac{150}{\sqrt{\varepsilon_{eff}}}$) because simulations showed that a larger length does not lead to a smaller condition number. Additionally the reflectometer should be as small as possible.

To find the best results from optimisation a randomly chosen offset was added to every start value. After many optimisations the distances of 16.323 mm, 11.766 mm, 10.080 mm and 39.430 mm led to the best results. The condition number determined with (2-48) is 4.9744 what is the best result I could find. The condition number over frequency for the final implemented probe is shown in Fig. 3.27.

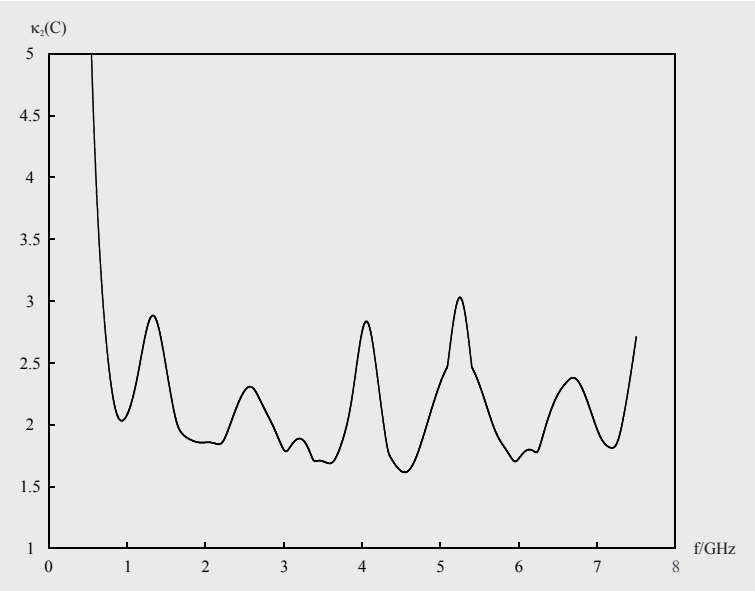

Fig. 3.27 - Condition Number for Optimal Distances

3.2.4 Simulations

For the simulations Microwave Office® was used. For simplification the simulations are divided into 3 parts:

- the Resistor
- the Coupler
- the Standing Wave Probe

The resistor and coupler simulations were already shown in subsection 3.2.2. The simulations of the whole standing wave probe are based on the schematic in Fig. 3.28.

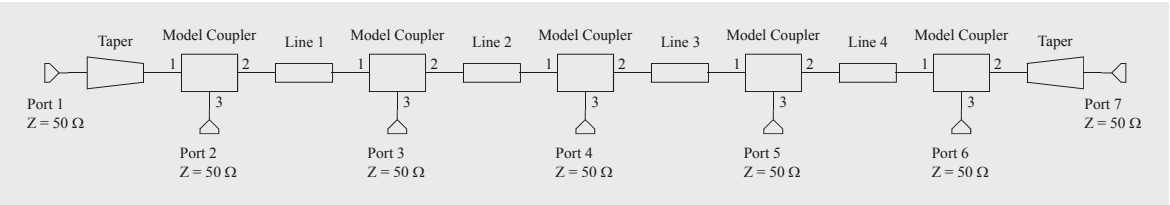

Fig. 3.28 - Schematic Standing Wave Probe

The results of these simulations are shown in Fig. 3.29. Principally the coupling of each port is equal to the coupling determined for a single coupler. What is good is that the couplings of all five couplers lie within less than 4 dB over the whole frequency range. Because of that the whole dynamic range of the power meter can be spent on the power measurement and has not to be used to compensate the differences of the coupling of the standing wave probe.

The last graph Fig. 3.30 shows the simulated reflection coefficients on the different ports of the reflectometer. The reflection coefficients of the ports at the transmission line S_{11} and S_{77} are less than –20 dB. As an example for a coupler port the reflection coefficient of port 3 S_{33} is chosen. It lies in a range of –1 dB to –3 dB. This looks very bad, but it can be explained easily. The coupling is done via a series resistor with about 1000 Ω that is connected to 110 Ω line at the resistor end of the coupler that is transformed to 50 Ω at the coupling port. This structure works as a voltage divider. The power at the sampling point is divided between the 1000 Ω resistor and the 50 Ω input impedance of the power meter. The part of power meter is used for the measurement. The part of the 1000 Ω resistor is lost as heating of the resistor what leads to the large insertion loss. The large reflection coefficient arises because the coupling port is terminated

with 1000 Ω resistor connected to a 110 Ω line. This structure must lead to such a large reflection coefficient but nevertheless this solution was chosen, because the high reflection coefficient does not matter since the ports of the coupler are just output ports that are terminated with a very good load of the power meter. This means no reflected wave should occur. If there is a reflected wave it is attenuated with about 25 dB when it goes back to the main line. So a signal that comes from the main line to a sampling port and is reflected back to the main line is attenuated with at least 50 dB. For that reason its influence to the standing wave on the main line can be ignored.

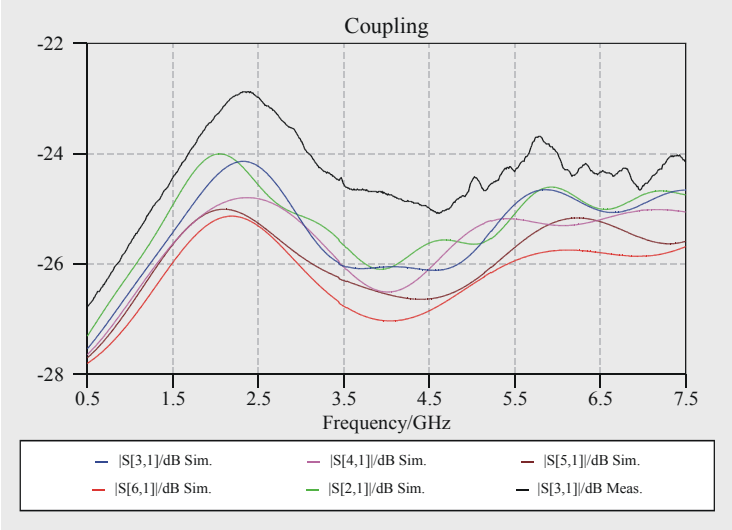

Fig. 3.29 - Simulated Characteristics of the Standing Wave Probe

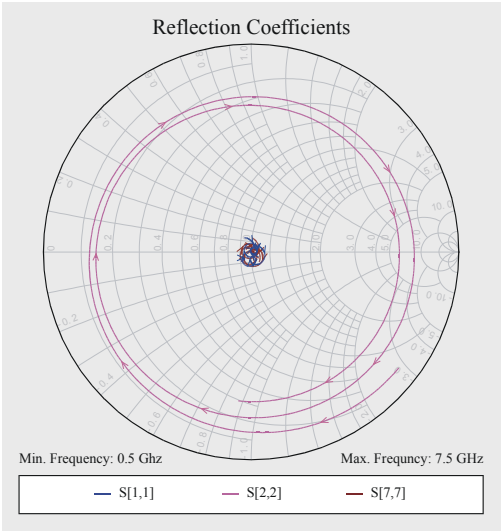

Fig. 3.30 - Reflection Standing Wave Probe

3.2.5 Implementation and Assembling

The implementation of the standing wave probe uses the coupler developed in subsection 3.2.2. Five of these couplers were positioned with the distances determined in the last subsection. The size of the standing wave probe board is 100 mm x 45 mm. The main line has an impedance of 50 Ω, what results in a line width of 2.167 mm on this substrate. The layout of the coupler is shown in Fig. 3.31 in original size.

To prevent oxidation of the copper lines the print was gold plated what was done in two steps. First the copper had to be nickel plated to prevent the diffusion of gold into the copper. In the

second step the gold plating was performed. This plating process was done using a simple electrolytic plating kit. The voltage and current for the plating process were chosen according to the description of this kit. Good results were reached with a voltage of about 4 V and a current of about 30 mA.

Fig. 3.31 - Layout of the Standing Wave Probe

The last step in the print assembling was the soldering of the resistors. For that reason the resistor were attached to the print by a soldering paste under the microscope. The readily assembled print was put into a reflow oven for a preheat phase of 90 s. During this time the print was heated up to 110 °C. In the following soldering phase the print was heated up to 220 °C for another 90 s.

Photos of the different production steps are shown in Fig. 3.32 to Fig. 3.35. The different colours of the substrates appear due to different photography conditions. In Fig. 3.35 the black resistor has a resistance of 680 Ω and the blue one 330 Ω.

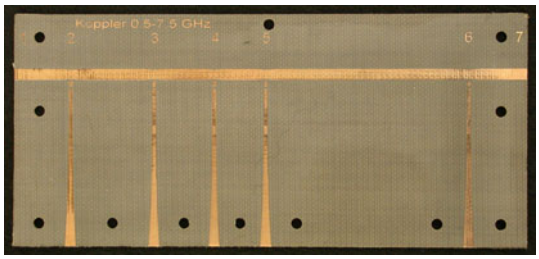

Fig. 3.32 - Standing Wave Probe - Copper

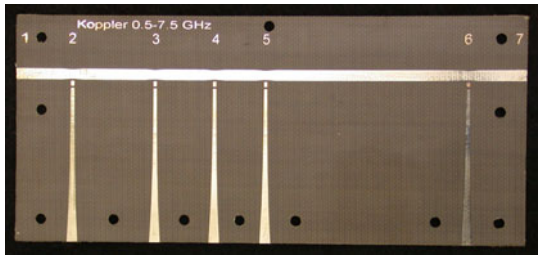

Fig. 3.33 - Standing Wave Probe - Nickel Plated

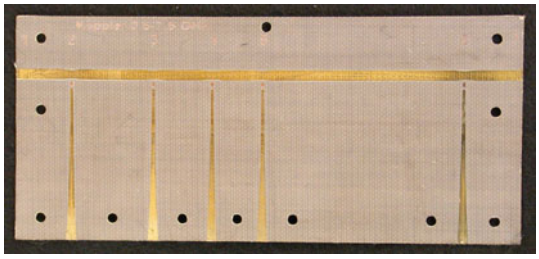

Fig. 3.34 - Standing Wave Probe - Gold Plated

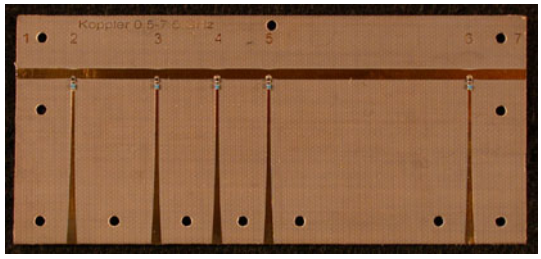

Fig. 3.35 - Standing Wave Probe with Resistors

After all the print work was done the connectors had to be assembled. For that reason and for reasons of stability the print was mounted on a brass carrier plate. The size of the plate is 100 mm x 45 mm with a thickness of 8 mm (a detailed mechanical drawing of this carrier is added in Appendix C). The print was mounted on the carrier with plastic screws. Next to every

connector two screws had to be placed to guarantee a good ground contact. The plastic screws were chosen because there was not much space between the coupler lines and the screw head and metal screws could have influenced the RF performance by an additional ground signal closeby.

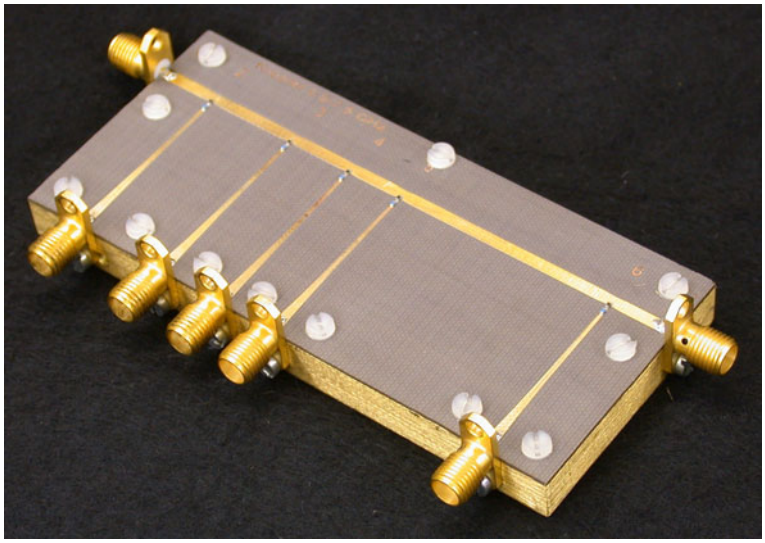

Fig. 3.36 - Standing Wave Probe Readily Assembled

The next step was the assembling of the seven connectors. As connectors SMA connectors were chosen because they fit best to the available measurement equipment that is based on SMA connectors. Detailed views of the connectors and the assembling from the front- and backside are shown in Fig. 3.37 and Fig. 3.38, respectively. As it can be seen the connectors were fixed by one screw to the brass carrier to guarantee mechanical stability and a good ground contact. To the transmission line they were connected by soldering. A photography of the readily assembled standing wave probe can be seen in Fig. 3.36.

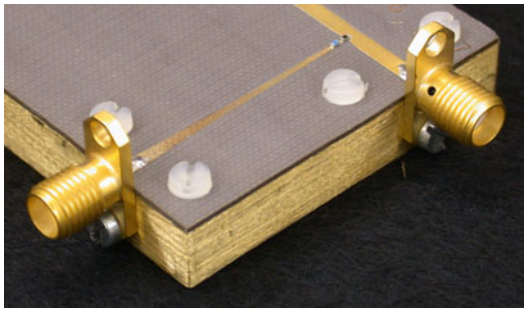

Fig. 3.37 - Detail Connector Frontside

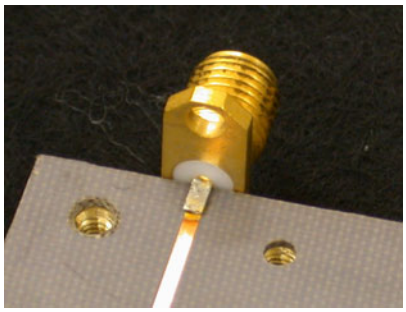

Fig. 3.38 - Detail Connector Backside

3.2.6 Measurements

For the measurements of the standing wave probe a HP 8510C 2-port network analyser was used. The S-parameters for every two ports were measured, while according to the definition of the S-parameters the other ports were terminated with standard loads. The so measured two port S-parameter files were linked together to a seven-port S-parameter file by the use of the SXP-FileConverter tool that is described in Appendix A. This seven port file could be read in Microwave Office® with which the following curves were plotted.

Fig. 3.39 shows the measured coupling between port 1 and every coupling port. The measurement and simulation were split for better clearness. These measurements show good

agreement to the simulation results (Fig. 3.29) except for a 2 dB offset which is mainly caused by simulation inaccuracies of the resistor contact area on the transmission line.

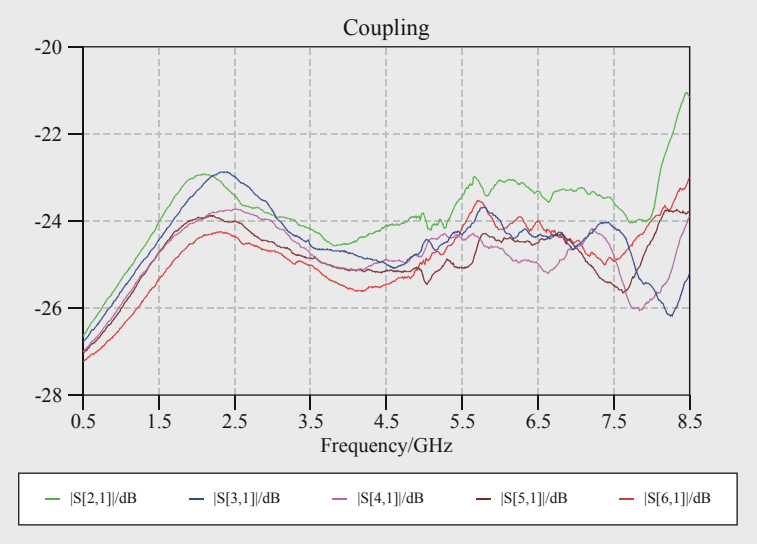

Fig. 3.39 - Coupler: Measured Coupling

The insertion loss of the coupler is shown in Fig. 3.40. The large values of more than 1 dB can be explained by the loss in the resistors. As I explained before the resistive coupling was necessary because of the flat coupling of about 4 dB over the whole application frequency range.

The reflection coefficients of both transmission line ports and one coupler port are shown in Fig. 3.41. The reflection coefficient of the transmission line port is small. The reflection coefficients of the coupler ports are quite high, but this was explained before.

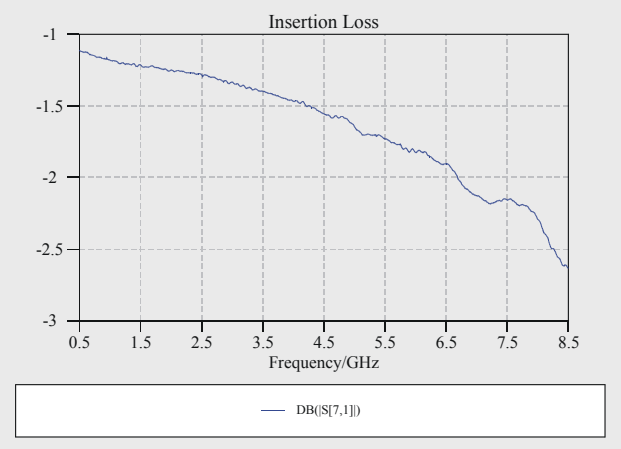

Fig. 3.40 - Coupler: Measured Insertion Loss

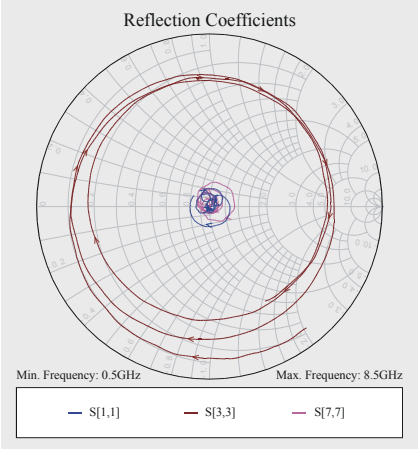

Fig. 3.41 - Coupler: Measured Refl. Coeff.

4 Software Design

This chapter gives an overview on the used software tools, the implementation of the algorithms and the simulations that were carried out.

4.1 Test of the Algorithms

In this subchapter the implementation of the algorithms is described. In a second part the implemented algorithms are tested with simulated input data. These input data are the simulated power values at the different ports of the standing wave probe and the directional coupler. The output data are the determined reflection coefficients. According to the results of these test the better useable algorithm for the reflectometer is chosen.

All algorithms were implemented using Microsoft Visual Basic®. The simulations of the S-parameters were done using Microwave Office®.

4.1.1 Determination of the Test Values

The tests of the algorithms were used to find out if the 3-Probe-Algorithm or the LMS-Algorithm is more sensitive to measurement errors. For that reason the power values at the ports of the standing wave probe and the directional coupler had to be determined and passed to the algorithms by input files.

Since power values at the ports of the directional coupler and the standing wave probe simulated with Microwave Office® cannot be saved in a file a workaround based on S-parameters was made.

Because the magnitude of a S-parameter is the square root of the ratio of the power magnitude at port x to the power magnitude at port y the simulated S-parameter can be used to determine the output power values. Supposing that all output ports (except the port for the device under test) are perfectly matched the output power at a certain port can be calculated by multiplying the input power with the square of the magnitude of the according S-parameter. Since all algorithms presented in chapter 2 use only power ratios the input power can be chosen arbitrarily. Out of convenience it was chosen to be one and therefore the output power values are equivalent to the square of the magnitude of the according S-parameter. The calculation of the power values from the simulated S-parameters is done after reading the input data at the beginning of each program part.

For test purposes the S-parameters were calculated for two different scenarios: for the simulated components and for the measured components. The first scenario was just for the principal test of the algorithms. The tests for the error sensitivity of the reflection coefficient to the errors of the measured power values or to the errors of the calibration coefficients are based on the measured component data. Therefore, the S-parameters of the directional coupler and the standing wave probe were measured with an HP 8510 C network analyser and linked together with the SXP-Fileconverter tool. Based on these S-parameter files the S-parameters of the whole reflectometer hardware were calculated using Microwave Office®.

4.1.2 Implementation of the Algorithms

This subsection deals with the implementation of the most important parts of the 3-Probe-Algorithm and the LMS-Algorithm. Firstly common facts that are valid for both algorithms are explained. Secondly the individual problems of each algorithm are described.

Common Facts on the Algorithms

The most important fact is that both algorithms are divided into two parts: the first part, which is responsible for the determination of the calibration coefficients and the second part that uses these calibration values to determine the reflection coefficient.

The part for determining the calibration coefficients uses the power values for the different calibration standards and reference values of the standards as input data. The output values are the calibration coefficients.

The part for determining the reflection coefficient uses the calibration coefficients and the measured power values for the certain reflection coefficient as input. The output values are the determined reflection coefficients for the specified frequencies.

Every program part has a possibility to select between simulated and measured input data. This selection is controlled by a switch in the dialog window of each program. If the simulated data are chosen as input data the power values are calculated from the s-parameters. The reference values for the determination of the calibration values are set by global variables in that case. If measured data are chosen as input data the measured power values are read from an input file. In that case the reference values for the determination of the calibration coefficients are read from an additional input file.

The number of frequencies has to be entered when running the program files. The frequencies are defined in the input files, either with the simulated S-parameter file or with the measured power file. These frequencies are used in all program parts. The defined number of frequencies has to correspond to the number of frequencies in the files.

3-Probe-Algorithm

The 3-probe-algorithm used the power values of the 3 best-positioned probes. These probes were the ones that were most equipartitioned on the unit circle. The according power values were normalized by the power value of the directional coupler.

Calibration Coefficient Determination

The functional diagram of the calibration coefficient determination algorithm is shown in Fig. 4.1. The two different input sources that are either measured or simulated data are selected at the begin of the algorithm. The following mathematical operations of the algorithm are the same for both sources.

The determination of the calibration coefficients starts with the reading of the input values of the five different calibration standards that are stored in five different files. If measured data are used it is read directly into the power table. In the case of simulated data the power values have to be determined from S-parameters as described in subsection 4.1.1. The determined power values are written to a power table. From that step on there is no difference between simulated and measured power values in the further program.

The next step is to evaluate the reference reflection coefficients for the five different standards. For the case of measured data the reference values are read from s1p-files measured with an HP 8510 C network analyser. For the case of simulated data the reference values are given by global constants.

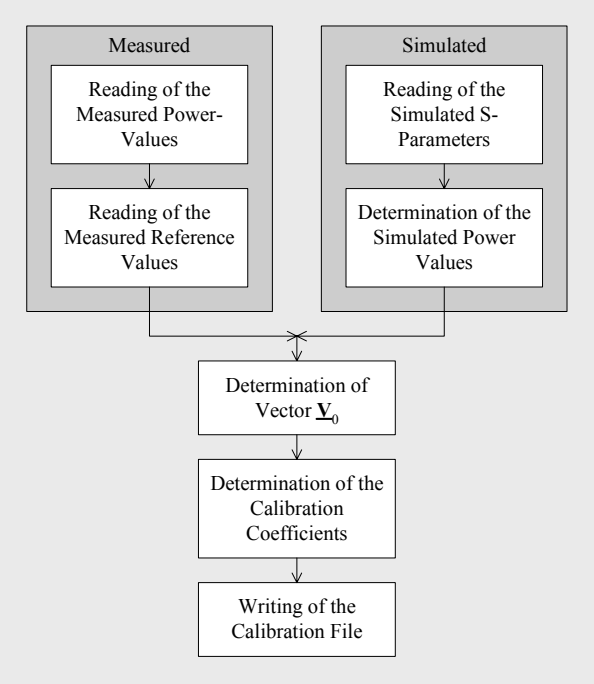

Fig. 4.1 - Functional Diagram of the 3-Probe Calibration Coefficient Determination

The first step of this algorithm is the determination of the three best-positioned probes. For that reason the distances of all five probes to the reference plane have to be known by global constants. From these physical positions the angular positions are calculated. The angular positions change with the frequency as shown in equation (2-51). The triple of the best three probes is chosen according to equation (2-52).

From the power values of the three best-positioned probes and the normalisation value from the directional coupler the calibration values for every frequency are derived. This evaluation starts with equation (2-72) where vector $\underline{\mathbf{V}}_0$ is determined. In a second step the calibration values are determined using equation (2-69). The matrix inversion used in equation (2-72) is done with a gaussian elimination algorithm. Since it is assumed to be a mathematical standard procedure this algorithm is not explained within this thesis.

The last step of the algorithm is to write the calibration coefficients to a file with the format shown in Tab. 4.1. For every frequency there is an array of 32 values in 8 columns. The first four columns contain the coefficients of the calibration matrix **C**. The columns five to seven contain the number of the three best-positioned probes. These values are the same for all rows at the same frequency. The last column shows the number of the normalisation port. This was introduced to be able to change the normalisation port to another port, than the output of the directional coupler. In the file there is such an array for every different frequency.

c_{11} @ f_1	c_{12} @ f_1	C_{13} @ f_1	c_{14} @ f_1	P_1 @ f_1	P_2 @ f_1	P_3 @ f_1	Norm. Port @ f_1
c_{21} @ f_1	c_{22} @ f_1	C_{23} @ f_1	c_{24} @ f_1	P_1 @ f_1	P_2 @ f_1	P_3 @ f_1	Norm. Port @ f_1
c_{31} @ f_1	c_{32} @ f_1	C_{33} @ f_1	c_{34} @ f_1	P_1 @ f_1	P_2 @ f_1	P_3 @ f_1	Norm. Port @ f_1
c_{41} @ f_1	c_{42} @ f_1	C_{43} @ f_1	c_{44} @ f_1	P_1 @ f_1	P_2 @ f_1	P_3 @ f_1	Norm. Port @ f_1
c_{11} @ f_2	c_{12} @ f_2	C_{13} @ f_2	c_{14} @ f_2	P_1 @ f_2	P_2 @ f_2	P_3 @ f_2	Norm. Port @ f_2
c_{21} @ f_2	c_{22} @ f_2	C_{23} @ f_2	c_{24} @ f_2	P_1 @ f_2	P_2 @ f_2	P_3 @ f_2	Norm. Port @ f_2
c_{31} @ f_2	c_{32} @ f_2	C_{33} @ f_2	c_{34} @ f_2	P_1 @ f_2	P_2 @ f_2	P_3 @ f_2	Norm. Port @ f_2
…	…	…	…	…	…	…	…

Tab. 4.1 - Format of the Calibration Coefficient File of the 3-Probe Algorithm

The saved calibration coefficient file is used in the second part of the algorithm: the determination of the reflection coefficient that is described next.

Reflection Coefficient Determination

The functional diagram of the reflection coefficient determination part of the 3-probe-algorithm is shown in Fig. 4.2.

At the beginning of the reflection coefficient part the measured power values are read and written to a data field for the case of measured data. For the case of simulated data the simulated power values are calculated from the simulated s-parameters. This is done as described in subsection 4.1.1. The next step is to read the pre-calculated calibration values from the calibration file. The according file format is described in the former subsection.

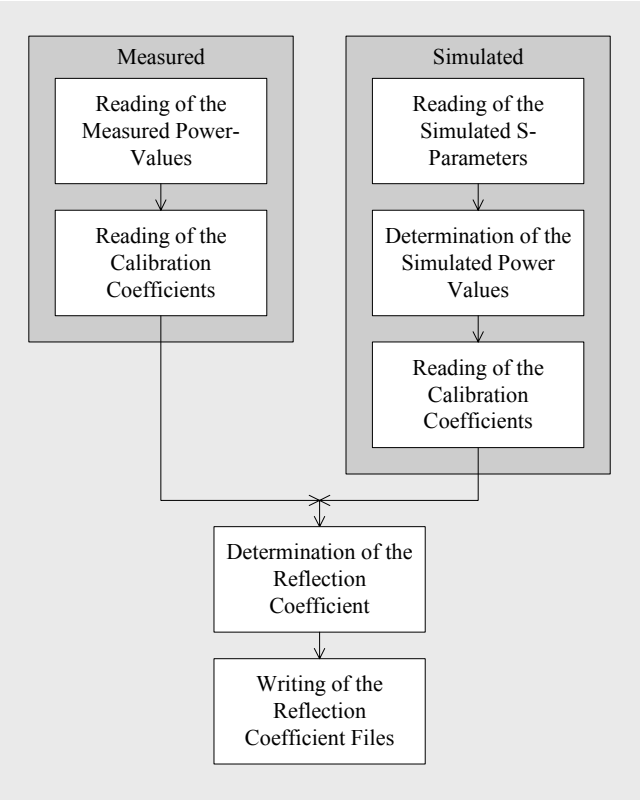

Fig. 4.2 - Functional Diagram of the 3-Probe Reflection Coefficient Determination

The main part is the determination of reflection coefficient. It is based on the equations (2-58) and (2-59). From these equations the square of the magnitude, the real- and the imaginary part of the reflection coefficient are determined. For the output the magnitude is calculated from its square and from the real- and imaginary part with equation (4-1). The angle is calculated from the real- and imaginary part with equation (4-2).

$$|\Gamma| = \sqrt{\Gamma_R{}^2 + \Gamma_I{}^2} \qquad (4\text{-}1)$$

$$\varphi = arctan\left(\frac{\Gamma_I}{\Gamma_R}\right) \qquad (4\text{-}2)$$

For the reflection coefficient output there were two different files that were both saved after calculation. One file was for the development and the other one was an s1p-file that can be read by Microwave Office®. The file format that was used for the development is shown in Tab. 4.2.

The index SQ and RI at the magnitude of the reflection coefficient stand for the magnitude of the reflection coefficient calculated from the square of the magnitude or from the real and imaginary part.

f_1/GHz	$\|\Gamma_1\|_{SQ}$	$\|\Gamma_1\|_{RI}$	φ_1/°
f_2/GHz	$\|\Gamma_2\|_{SQ}$	$\|\Gamma_2\|_{RI}$	φ_2/°
f_3/GHz	$\|\Gamma_3\|_{SQ}$	$\|\Gamma_3\|_{RI}$	φ_3/°
...	...	...	...

Tab. 4.2 - Reflection Coefficient File Format for Development

The standardised s1p-file format is subdivided into a header part and a data part. The header used in my program is listed below.

```
!freq-unit  param-type  data-format  keyword  impedance-ohms
# GHZ           S          MA           R         50
!-------------------------------------------------------------------------
!Freq         MagS11       AngS11
```

Directly below this header there is the data part that is formatted as shown in Tab. 4.3. For this file format the magnitude was calculated from the real- and imaginary part.

f_1/GHz	$\|\Gamma_1\|_{RI}$	φ_1/°
f_2/GHz	$\|\Gamma_2\|_{RI}$	φ_2/°
f_3/GHz	$\|\Gamma_3\|_{RI}$	φ_3/°
...	...	...

Tab. 4.3 - Data Part of the s1p-File Format

LMS-Algorithm

The Least-Mean-Square-Algorithm uses all five power values measured at the five ports of the standing wave probe. The measured powers are normalized to the incident wave power measured at the output of the directional coupler.

Calibration Coefficient Determination

The determination of the calibration coefficients for the LMS algorithm is similar to the 3-Probe Algorithm for the part where the input data is read. This is also shown in the functional diagram depicted in Fig. 4.3.

What is different between the two algorithms is the method for determining the reflection coefficients. The first step is to calculate the intermediate values given by equations (2-85) to (2-90) and equation (2-92). The calibration coefficients are derived in the next step using equation (2-91). The calculated calibration coefficients are written to a file with the format shown in Tab. 4.4.

As in the 3-Probe-Algorithm the calibration coefficients are subdivided into bulks that contain the coefficients for the same frequencies. Each array contains 30 values in five columns. The first column shows the frequency and must be the same for the whole array. The second to the fourth columns contain the calibration coefficients. In the last column there is the number of the port used for normalisation purposes which has to be the same for one array. The different arrays are subdivided by one empty row. These saved calibration coefficients are read by the second part of the algorithm, the reflection coefficient determination that is described in the next subsection.

f_1/GHz	Q_0 @ f_1	a_0 @ f_1	b_0 @ f_1	Norm. Port @ f_1
f_1/GHz	Q_1 @ f_1	a_1 @ f_1	b_1 @ f_1	Norm. Port @ f_1
f_1/GHz	Q_2 @ f_1	a_2 @ f_1	b_2 @ f_1	Norm. Port @ f_1
f_1/GHz	Q_3 @ f_1	a_3 @ f_1	b_3 @ f_1	Norm. Port @ f_1
f_1/GHz	Q_4 @ f_1	a_4 @ f_1	b_4 @ f_1	Norm. Port @ f_1
f_1/GHz	Q_5 @ f_1	a_5 @ f_1	b_5 @ f_1	Norm. Port @ f_1
f_2/GHz	Q_0 @ f_2	a_0 @ f_2	b_0 @ f_2	Norm. Port @ f_2
f_2/GHz	Q_1 @ f_2	a_1 @ f_2	b_1 @ f_2	Norm. Port @ f_2
…	…	…	…	…

Tab. 4.4 - Format of the Calibration Coefficient File of the LMS Algorithm

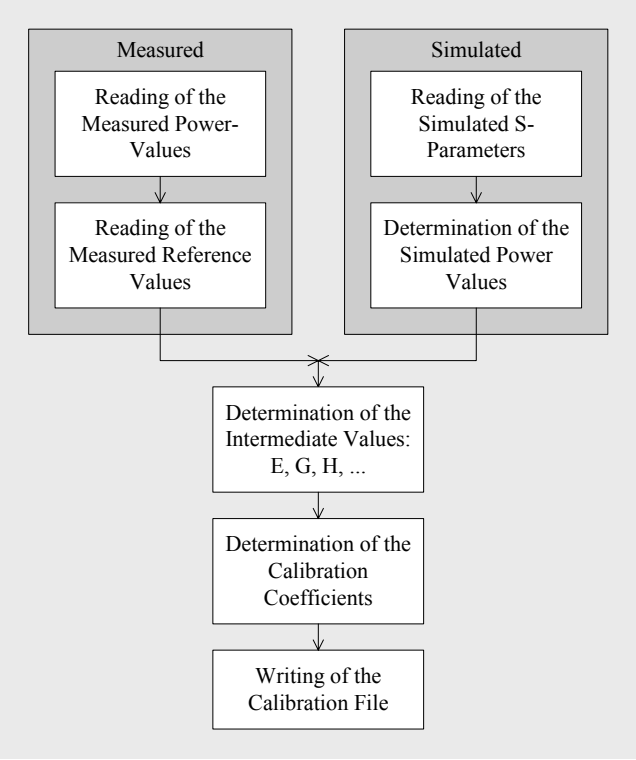

Fig. 4.3 - Determination of the Calibration Coefficients for the LMS-Algorithm

Reflection Coefficient Determination

The principal functional diagram of the reflection coefficient determination is shown in Fig. 4.2, which is the same for the 3-Probe-Algorithm and the LMS-Algorithm.

The difference is that the determination of the reflection coefficient was done using equations (2-73), (2-77), (2-78) and (2-81). The inverse matrix was calculated with a gaussian elimination algorithm.

The output procedure is equal to the 3-Probe-Algorithm. For this algorithm there were also two different file formats: one for the development and an s1p-file for Microwave Office®.

4.1.3 Simulation Results

The aim of the simulations was to proof the sensitivity of the algorithms to errors of power measurements. For that reason the S-parameters were simulated without error and read into the simulation algorithms described before. From that simulated S-parameters the simulated power values were calculated. The deviated power value was calculated from the correct power value with equation (4-3).

$$P_{Err} = P_{Corr} \cdot (1 + \eta \cdot \varepsilon) \qquad (4\text{-}3)$$

In this equation ε stands for the error coefficient. The variable η is chosen randomly and defines the influence of the error. η can have a value of -1, 0 or 1. For example if ε is chosen as 1 % then P_{Err} can be either 99 % of P_{Corr}, equal to P_{Corr} or 101 % of P_{Corr}.

The simulations were made for two different scenarios. On the one hand the error was applied just to power values used for determination of the reflection coefficient and the power values for the determination of the calibration coefficients stayed unchanged. On the other hand the error was applied just to the power values that were used for determination of the calibration coefficient and the power values for the determination of the reflection coefficient stayed unchanged.

The simulations were made in a frequency range from 0.5 GHz up to 6.5 GHz with a frequency step of 250 MHz, what results in 25 frequency points. The reflection coefficient was chosen to have a magnitude of 0.5 and an angle of 153°. This value of magnitude is in the middle between load and short or open what should be a good value for these tests. The angle should not matter for these tests.

For the comparison of the algorithms the same input values were used. Also the same sequence of η was used what leads to the same deviated power values for both algorithms. Because of that reason differences between the simulation results of the different algorithms depend only on the sensitivity of the algorithm and not on different error vectors.

3-Probe-Algorithm

The simulation results for a ε value of 1 % are shown in the following graphs. Fig. 4.4 shows the relative error of the magnitude if the determination power values are faulty and the calibration coefficients are errorless. The according absolute error of the angle is shown in Fig. 4.5. It can be seen from the simulations that the relative error of the magnitude goes up to 10 %. But the greatest problem is, that there is one value with an error of about 40 %. This value cannot be tolerated in a serious measurement system. The angle shows similar behaviour, because there were some values that have a large error compared to the others.

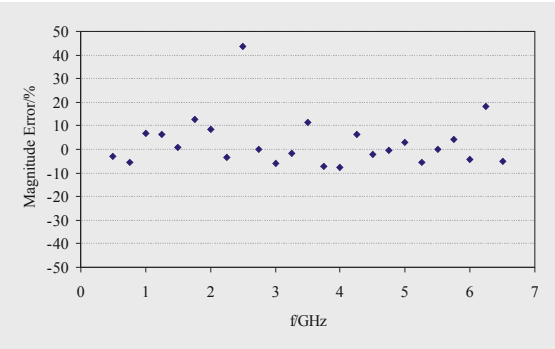

Fig. 4.4 - Error Magnitude – Determination

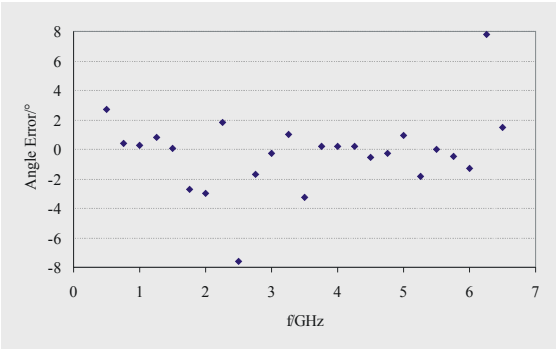

Fig. 4.5 - Error Angle - Determination

Fig. 4.6 and Fig. 4.7 show the relative error of the magnitude and the absolute error of the angle, respectively, if the calibration values were faulty and the determination powers are errorless. In these simulations there is the same behaviour as before. For some frequencies the error is much larger than the average error. Because such a behaviour is not tolerable for a measurement system this algorithm was not used in the final implementation.

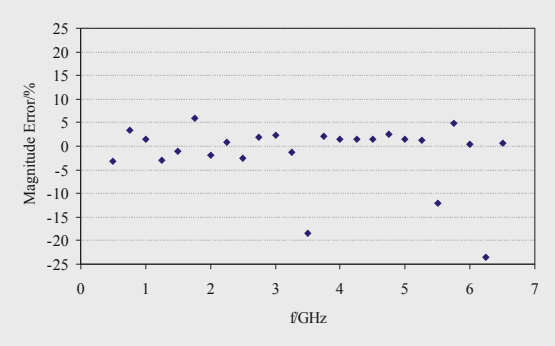

Fig. 4.6 - Error Magnitude – Calibration

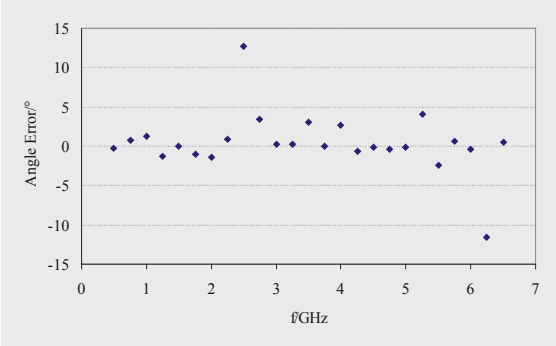

Fig. 4.7 - Error Angle – Calibration

LMS-Algorithm

As mentioned before the simulations of the LMS-Algorithm were made with the same power values as for the 3-Probe-Algorithm. For the determination part exactly the same power values were used. For the calibration part the same error vector was used but since different calibration methods were used with different standards there were also different power values.

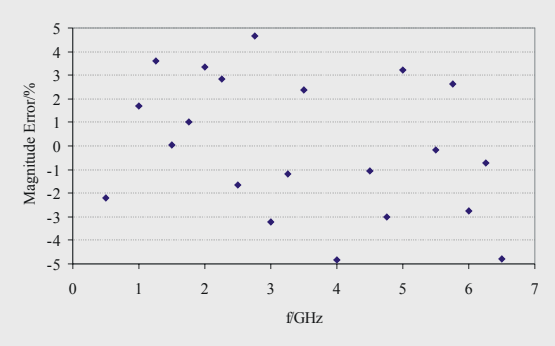

Fig. 4.8 - Error Magnitude - Determination

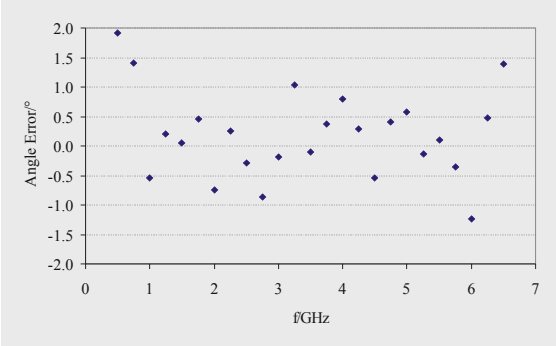

Fig. 4.9 - Error Angle - Determination

Fig. 4.8 shows that the relative error of the magnitude is always less than 5 %, what is good. In Fig. 4.9 the absolute error of the angle is always less than 2 °. Both simulations were for an error of the power values used for the determination. The power values used for the calibration and therefore the calibration coefficients were errorless.

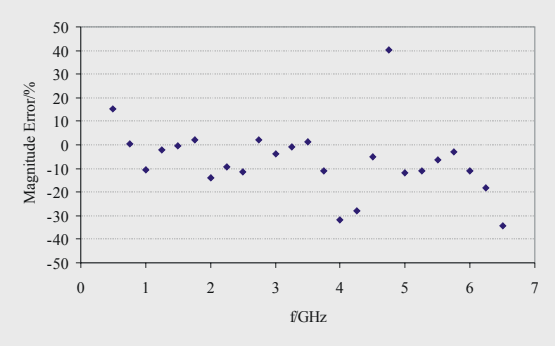

Fig. 4.10 - Error Magnitude - Calibration

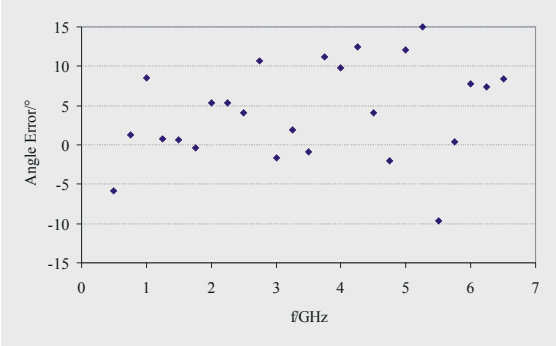

Fig. 4.11 - Error Angle - Calibration

Fig. 4.10 shows the relative error for deviated powers used for the calibration. This automatically leads to deviated calibration coefficients. In Fig. 4.11 the absolute error of the angle is shown for the same scenario. From those two figures it can be seen that the LMS algorithm is very sensitive to errors in the calibration coefficients. This circumstance had to be taken care of, when the calibration coefficients were determined. For the implementation of this algorithm in the final measurement software two different methods for determining the calibration coefficients are described.

4.2 Implementation of the Measurement Software

In the simulations of the error sensitivity the LMS algorithm had shown the better performance so this algorithm was used in the final implementation of the reflectometer. From the theory it is known that five different standards are used for the calibration of the LMS algorithm, four standards that lie on the unit circle of the smith chart and one 50 Ω-load. The load is available as a standard component. Two of the other standards are a short and an open. The other two standards were realised by sliding shorts. The four standards should be equipartioned on the unit circle, what means that there should be about 90 ° between consecutive standards. Since the angle of the sliding short is only valid for one frequency the position of the sliding short must be corrected for every frequency. Since this is a very involving method, different positions of the sliding short were measured and the best values were selected by a special program part. To implement this calibration method four different program parts were used.

4.2.1 Power Measurement Program

This program is used to measure the power values at the different ports. For that reason it has to control the signal source, the multiposition switch and the power meter. This program part is not used if the powers are simulated, because it contains no part of the reflection coefficient determination algorithm or from the calibration coefficient determination algorithm.

The user interface window is shown in Fig. 4.12. It is subdivided into four main parts: the source control, the power meter control, the measurement part and the power value part.

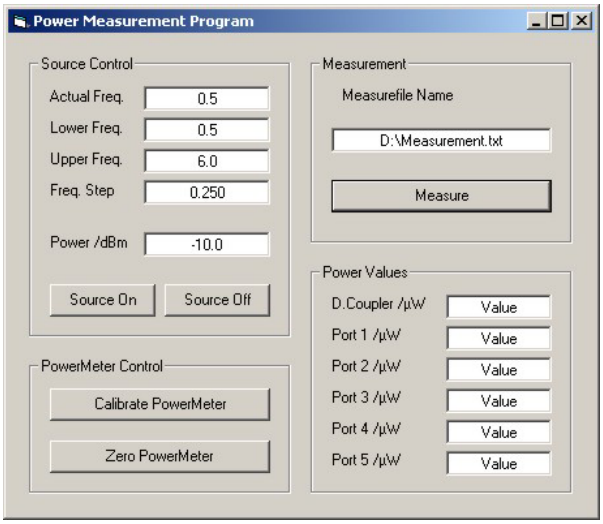

Fig. 4.12 - User Interface: Power Measurement Program

The source control has input fields for the lower and upper frequency limit and the frequency step size. The actual measurement frequency is shown in an output field. The power is controlled

by the power input field. With two buttons the output of the power source can be turned on or off manually. Normally the power source is controlled automatically by the measurement program. How this is done will be explained later.

In the measurement part the filename of the output file is defined. With the measurement button the automatically measurement is started.

With the power meter control the used power meter can be calibrated or zeroed. The calibration has to be done once before the measurement is started. The zeroing can be done additionally, but within the automatical measurement it is done once before the measurement is started anyway.

The power value part is used just to show the actually measured power values in µW. The powers of the directional coupler and of the five sampling ports are shown.

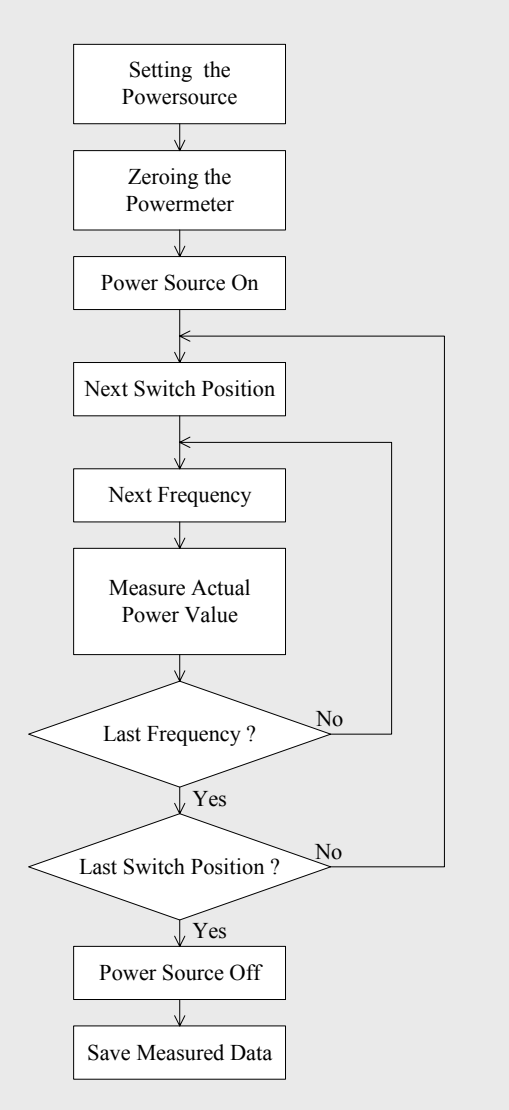

Fig. 4.13 - Power Measurement Program

The functional diagram of the automatical measurement program is shown in Fig. 4.13. The program starts with the initialisation and setting of the values of the power source. Next the power meter is initialised and zeroed. Within the zeroing process no power is applied to the power meter and so the correct offset to the zero value could be found. To start the measurements the power source has to be turned on.

Since the mechanical multiposition switch has to be toggled as less often as possible I decided to measure a whole frequency sweep at every single switch position. At the beginning the switch is initialised to the first position and the power source is set to the first frequency.

Starting with the lowest frequency the frequency is increased by the frequency step size every cycle. When the upper frequency limit is reached the multiposition switch is toggled to the next position. When all six switch positions are measured at every frequency the measurement is finished. Finally the signal source is turned off and the measured data are saved.

The data are saved with the following format. In the first column the actual frequency is stored. In the second the power value of the directional coupler and in the third to the seventh column the power values of the different coupling ports are stored. The powers are stored in µW.

4.2.2 Calibration Standard Definition Program

The calibration standard definition program is used to extract the calibration data that are used for the calibration of the LMS-Algorithm from the measured data. In the measurement program this program part is only used when measured data are used for the calibration.

From the theory it is known that four standards on the unit circle of the smith chart are used plus an additional load. The load and short and open can be measured easily, so two more standards on the unit circle have to be used. These standards are determined from measurements with a sliding short as termination. The reference measurements were made with a HP 8510 C network analyser and stored in *.s1p files.

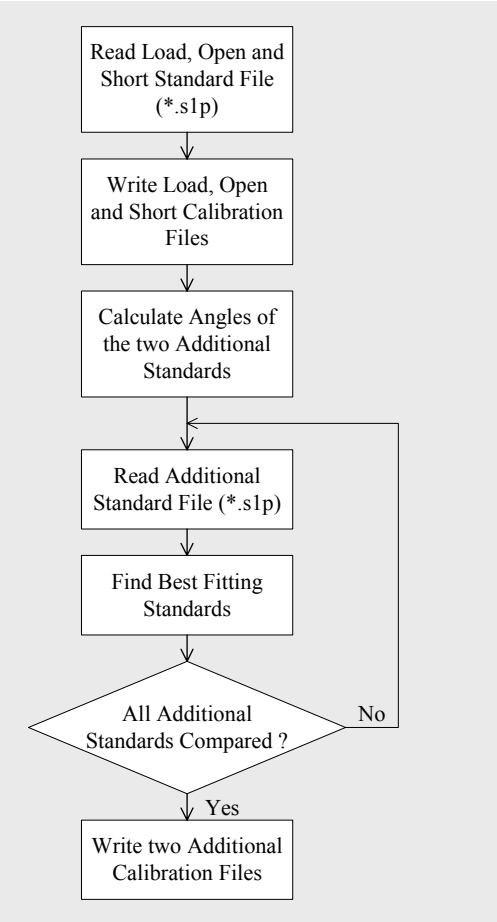

Fig. 4.14 - Standard Definition Program

The functional diagram of the algorithm is shown in Fig. 4.14. It starts with the reading of the reference files of short, load and open. In the next step the calibration files for these three

standards are written to disk, one for each standard. The calibration files have the following format. For every frequency there is one row with nine values in it that are separated by tabs. The first value is the frequency, the second the power value of the directional coupler, the third to the seventh the power values of the sampling ports. The last two values are the magnitude and the angle of the reference measurement.

The angles for the two additional standards on the unit circle are calculated from the angle of the short and the open at a certain frequency. The angle between short and open should be 180 °. As measurements showed this was fulfilled very good for all frequencies. The additional angles were chosen exactly in the middle between short and open with an angle of 180 ° between them. So there were four standards with an offset of about 90 ° between two consecutive standards.

Since those two additional standards are just the best calculated possibility, they have to be compared with the really measured reference standards. For the choice of the best available reference standard two selections were made. The first selection chooses those standards that have a magnitude greater than a fixed limit. The second selection chooses those two standards that are closest to the calculated optimum angles. This selection procedure is applied to all additional standards for every single frequency. If all standards were compared and the best were chosen the two additional calibration files are written using the file format explained above.

The user interface of the standard definition program is depicted in Fig. 4.15. The first three input fields are used for the filenames of the short, the open and the load. Here the power files and the reference files have to have the same filenames. The power files have to have no extension and the reference files have to have the extension ".s1p". The input field: "General-Filename" is used for the additional standard. These files have to be named with the general filename plus a number from one to the maximum number of standards that follows directly after the filename. The extensions as explained before have to be used. The input field has to contain the path where all files are located. The "Number of Files" input field has to contain the maximum number of additional standards. The number of used frequencies has to be written in the according input field. The tolerance value field contains the minimum magnitude of the reflection coefficient that is accepted for the choice of the additional standards. With the "Define" button the standard definition starts. The so determined five calibration files are used for the determination of the reflection coefficients explained in the next subsection.

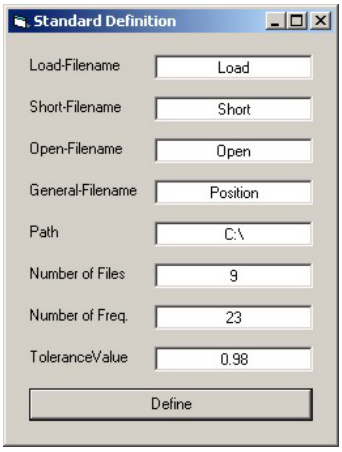

Fig. 4.15 - User Interface: Standard Definition Program

4.2.3 Calibration Coefficient Determination Program

This program part is used to determine the calibration coefficients either from the measured or the simulated data. If measured data are used, the input files have to be determined using the standard definition program and the according calibration files, which have to have the following names "calshort.txt", "calopen.txt", "calload.txt", "calfile1.txt" and "calfile2.txt". They have to

be located at the entered path. If simulated data are used the reflection coefficients have to be simulated in Microwave Office®. The magnitude of the reflection coefficient should always be equal to 1, the angles should be 0 °, 60 °, 120 ° and 180 °. The files have to be named "Sim_Power_*Mag*_*Ang*.txt", where *Mag* stands for the values of the magnitude and *Ang* stands for the angle of the reflection coefficient. For example if a short as termination is simulated the according file should be named "Sim_Power_1_180.txt". The used load has to be simulated with a magnitude of 0 and an angle of 0 ° and named in the way explained above.

The error value makes it possible to simulate an error of the power values that is calculated with equation (4-3), where ε is the error value. The number of used frequencies can be calculated by the difference of the upper frequency limit and the lower frequency limit divided by the frequency step size. It has to be equal to the number of simulated or measured power and reference values.

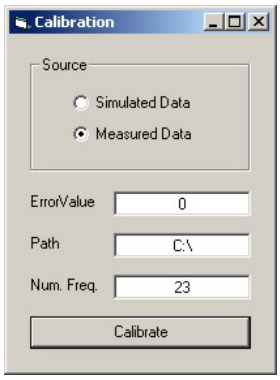

Fig. 4.16 - User Interface: Calibration Coefficient Determination Program

4.2.4 Reflection Coefficient Determination Program

The reflection coefficient determination program determines the reflection coefficient for the used number of frequencies. The frequencies and with that the number of frequencies have to be equal for the reflection coefficient files and the measured or simulated power files.

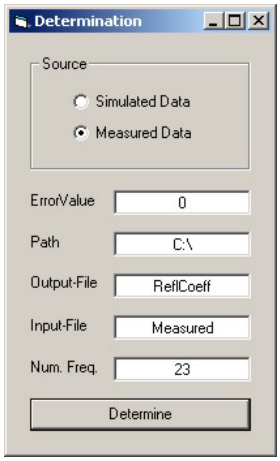

Fig. 4.17 - User Interface: Reflection Coefficient Determination Program

The error value is used in the same way as in the calibration coefficient determination program. The path specifies the location of the input-, output- and calibration coefficient files. With a radiobutton the data source (simulated or measured) can be selected. The determined reflection coefficients for all frequencies are stored in a text-file and also in an s1p-file that can be read by Microwave Office®.

5 Measurements

This chapter gives an overview of the measurement setup, explains a sequence of measurement and discusses the obtained results of measurements made with the reflectometer for different test terminations.

5.1 Measurement Setup

The measurement setup of the reflectometer depicted in Fig. 5.1 is principally equal to Fig. 1.1 in the introduction. The difference is that in this picture the used measurement devices are shown. As signal generator a SME 06 from Rohde & Schwarz was used. The generator frequency range was from 5 kHz to 6 GHz, what constraint the frequency range of the reflectometer at the upper end. The directional coupler and the standing wave probe were built myself and were described in detail in the former chapters. The directional coupler and the standing wave probe were connected together directly by a coaxial double male interconnection. To the signal source the directional coupler was connected by a coaxial cable. The DUT was directly connected to the standing wave probe.

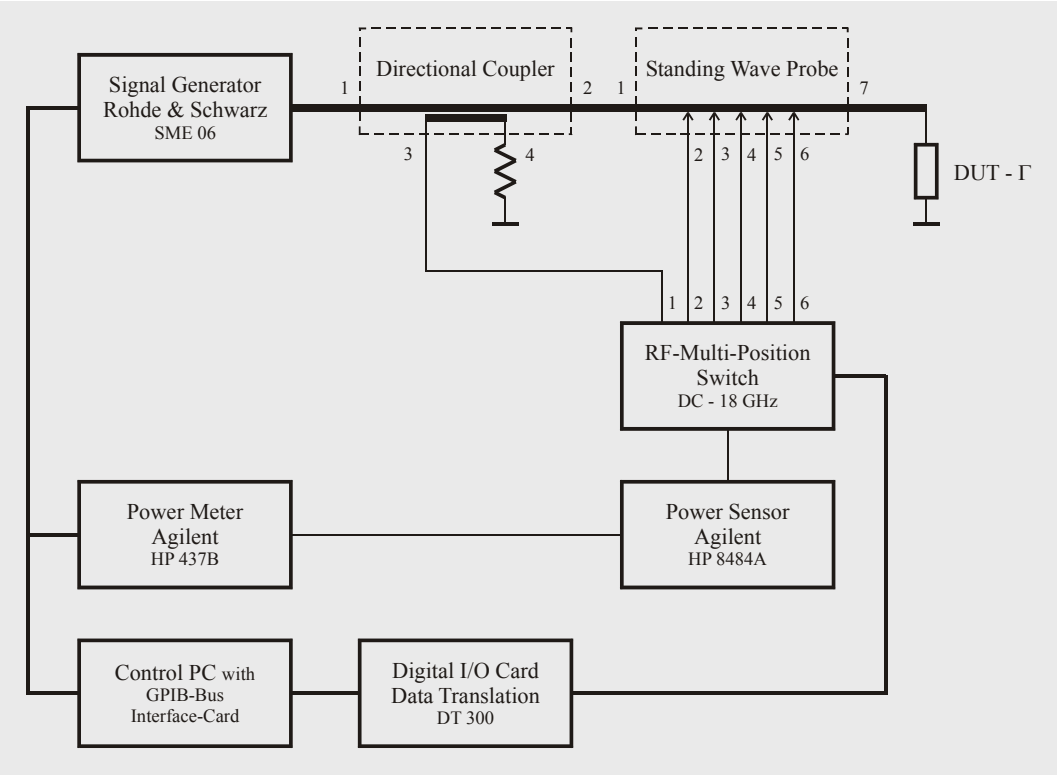

Fig. 5.1 - Measurement Structure of the Reflectometer

The isolated port of the directional coupler was terminated with a load. Via coaxial cables the coupled port and the sampling ports of the standing wave probe were connected to the RF-multiposition switch. The control of the RF-multiposition switch was done by the digital I/O card DT 300 from Data Translation. The output of the multiposition switch was connected to a HP 8484 A power sensor from Agilent. This power sensor can measure power in a range from -70 dBm to -20 dBm. The measured power was determined with a HP 437 B power meter from Agilent.

The control PC contained two interface cards: the digital I/O Card and a GPIB-Bus interface card. The digital I/O card controlled the RF-multiposition switch. The signal source and the power meter were controlled by GPIB-bus.

The reference measurements were made with an HP 8510 C network analyser from Agilent that was calibrated with a standard SOLT calibration. The measured data were stored in the HP-CITI format.

The reflectometer measurement frequency range was chosen from 0.5 GHz to 6 GHz, according to the upper frequency limit of the signal source, with a frequency step size of 250 MHz. The reference measurement frequency range was from 0.5 GHz to 8.5 GHz with 801 frequency points. The used input power was -5 dBm at the output of the signal source, what led to a good power levels at the input of the power sensor.

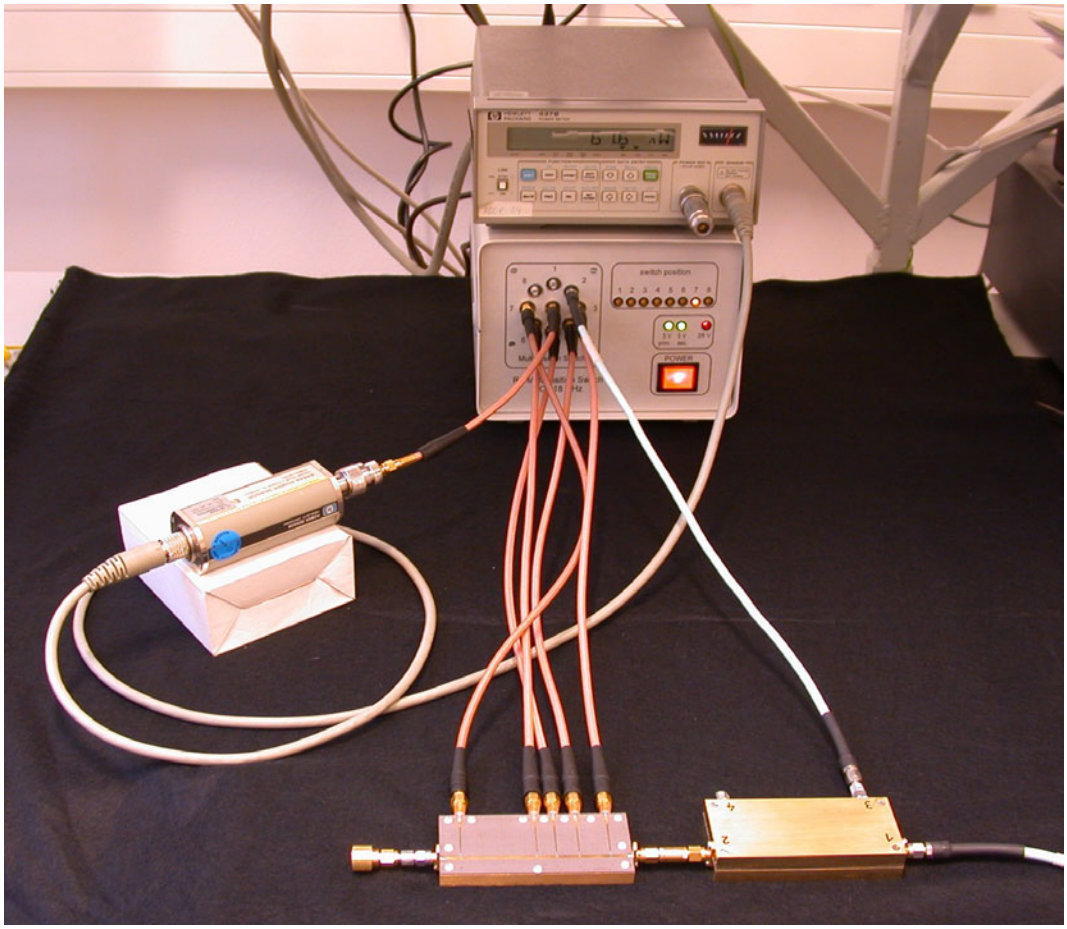

Fig. 5.2 - Measurement Setup

Fig. 5.3 - Signal Source

A photography of the setup of the reflectometer is shown in Fig. 5.2. In the background there is the multiposition switch with the power meter on top. On the left side one can see the power sensor and in front the directional coupler and the standing wave probe with a reference termination connected. With the cable connected on the right side the reflectometer was connected to the signal source shown in Fig. 5.3.

5.2 Sequence of a Measurement

Reference Measurement – SXP-File-Converter

As explained before the measured reference data are stored in the HP-CITI format. To convert this data into the s1p-format that is readable with Microwave Office® the SXP-file-converter tool, described in Appendix A, is used. Input-filename, output-filename and path were set accordingly. Since a one port measurement is performed the number of ports has to be set to 1.

Reflection Coefficient Measurement – Power Measurement Program

The powers at the output of the directional coupler and the standing wave probe are sampled with the power measurement program. It is initialised with the power- and frequency values given above. First of all the power meter is calibrated. For that reason the power sensor has to be connected to the calibration source of the power meter. Important is that the 30 dB reference attenuator is used for this measurement. After the power sensor is connected to the output of the multiposition switch and the output file name is defined the measurement starts.

Firstly the powers for the determination of the calibration coefficients and afterwards the test loads are measured. For an example the measured power file for a short as a termination is shown below. In the first column there is the frequency in GHz, in the second the power value at the output of the directional coupler and in the third to the seventh there are the powers measured at the five different sampling points. The first row is the header, the others are data. The shown power values are in µW.

Freq /GHz	DC	S1	S2	S3	S4	S5
0.50	0.00060400	0.00173000	0.00166000	0.00144000	0.00121000	0.00024600
0.75	0.00122600	0.00101700	0.00172000	0.00199000	0.00203000	0.00062400
1.00	0.00134000	0.00003200	0.00052000	0.00129000	0.00192000	0.00113100
1.25	0.00172000	0.00125000	0.00009290	0.00018600	0.00091400	0.00171000
1.50	0.00142000	0.00270000	0.00156000	0.00024500	0.00008370	0.00227000
1.75	0.00140000	0.00159000	0.00308000	0.00174000	0.00033600	0.00299000
2.00	0.00101400	0.00007600	0.00180000	0.00238000	0.00131000	0.00272000
2.25	0.00085000	0.00160000	0.00042000	0.00273000	0.00311000	0.00329000
2.50	0.00079700	0.00311000	0.00039200	0.00088900	0.00299000	0.00312000
2.75	0.00074100	0.00133000	0.00188000	0.00001750	0.00144000	0.00201000
3.00	0.00075000	0.00003840	0.00275000	0.00086300	0.00034100	0.00157000
3.25	0.00084300	0.00103800	0.00111000	0.00171000	0.00005420	0.00076100
3.50	0.00099500	0.00233000	0.00006960	0.00223000	0.00082200	0.00034400
3.75	0.00101900	0.00111000	0.00055900	0.00127000	0.00196000	0.00009310
4.00	0.00099400	0.00003010	0.00157000	0.00013200	0.00201000	0.00000091
4.25	0.00098600	0.00101800	0.00174000	0.00019300	0.00131000	0.00005880
4.50	0.00092100	0.00207000	0.00068600	0.00130000	0.00042600	0.00025600
4.75	0.00058400	0.00070400	0.00001900	0.00153000	0.00000752	0.00045900
5.00	0.00067200	0.00005100	0.00087200	0.00153000	0.00057100	0.00109900
5.25	0.00069100	0.00101900	0.00174000	0.00048100	0.00126000	0.00128000
5.50	0.00052000	0.00206000	0.00140000	0.00001580	0.00157000	0.00183000
5.75	0.00066300	0.00130000	0.00037000	0.00080100	0.00176000	0.00253000
6.00	0.00050000	0.00005540	0.00014100	0.00185000	0.00057400	0.00271000

Reflection Coefficient Measurement – Standard Definition Program

After the power values at the sampling ports and the reference values for the different terminations are measured the calibration files are determined. As described in the former chapter the measured data of the load, the short, the open and the different positions of the

sliding short were used for that reason. With these calibration files the calibration coefficients are derived as described in the next step.

Reflection Coefficient Measurement – Calibration Coefficient Determination Program

The calibration coefficients are determined from two different sources. On the one hand from the measured power values and the according reference terminations and on the other hand from the simulated power values.

To derive the calibration coefficients from the measured source, the used five calibration files are determined using the program parts explained above. In the calibration coefficient determination program the switch is set to measured data.

For the calculation of the calibration coefficients based on the simulated data the S-parameters of the directional coupler connected together with the standing wave probe including all cables have to be determined. To do this the S-parameters between each two ports of this setup have to be measured using the measurement rules of the SXP-File-Converter that are explained in Appendix A. With this tool the measured data are linked together to an eight-port S-parameter file. Basing on this eight-port S-parameter file of the measurement setup the power values for the simulation are derived using Microwave Office®. This means if simulated data are used, the power values are simulated but they base on the measured characteristics of the reflectometer. Using these simulated power values the calibration coefficients of the reflectometer are derived with the calibration coefficient determination program.

Both calibration processes are complicated and use a VNA but they have to be performed only one time for a reflectometer. After the calibration coefficients are determined they can be stored and used every time the reflectometer is used again. This means the reflectometer has to be calibrated just once and not before any single measurement.

Reflection Coefficient Measurement – Reflection Coefficient Determination Program

The reflection coefficient is always determined from measured power values. The calibration coefficients are either determined from measured data or from simulated data. The results for different test terminations are shown in the next subchapter.

5.3 Measurement Results

Calibration Coefficients Determined from the Measured Data

If the calibration coefficients derived from the measured data are used for the determination of the reflection coefficients the results are not good. This means that the error of magnitude was for some frequencies larger than 100 % for different terminations. Since no correlation between these errors and the frequency or termination was found this method of calibration is not applicable for practical measurements.

The most probable reason for this behaviour might be the imperfect calibration standards. This can be explained like that: As the sliding short terminations do not have a perfect short at the end as assumed in the calibration algorithm there is a systematic error in the calibration. This error can be kept small since the accepted minimum magnitude of the sliding short can be set in the standard definition program but it cannot be eliminated since there has to be a possibility to choose between different angles. If the limit for the reflection coefficient magnitude is set to lower values the angles can be chosen more accurate but unfortunately the magnitude error increases. Together with the error sensitivity of the measurement to inaccuracies of the calibration coefficients the large errors can be explained.

Calibration Coefficients Determined from the Simulated Data

The following measurement results shown in Fig. 5.4 to Fig. 5.15 were determined using simulated calibration data, this means that the calibration coefficients were exact and the errors of the determined reflection coefficients only depend on the inaccuracies of the measured power values. The left pictures show the magnitudes determined with the reflectometer compared to the values measured with a HP 8510C network analyser. The right pictures show the comparison of the angles measured with the reflectometer and with the VNA, respectively

As one can see from these comparisons the angle was always determined with a maximum absolute error of 5° for all terminations over the whole frequency range.

The absolute error of the linear magnitude is for all frequencies and terminations less than 0.2. This is not very good, but this fact will be explained later. The range of the absolute error is equal for all magnitudes, what means that the relative error increases when the reflection coefficient magnitude goes to 0.

The explanation of the errors could be found together with the calibration method. The standards for the determination of the calibration coefficients were four reflective standards what means they are all located on the unit circle of the smith chart. Because there is just one magnitude used in the calibration this may be the reason for the errors of the magnitude.

Also the good results for the phase could be explained together with the calibration method. Since four different angles are used for the calibration good results could be expected for the phase and as it is shown they were reached too.

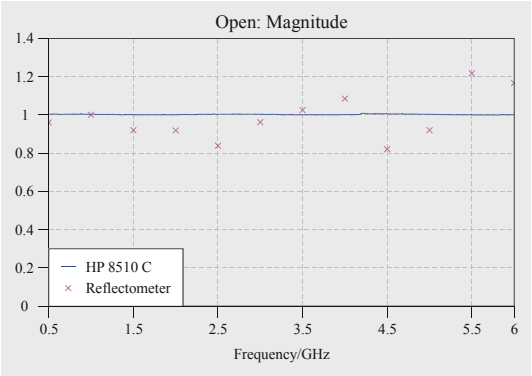

Fig. 5.4 Open: Magnitude

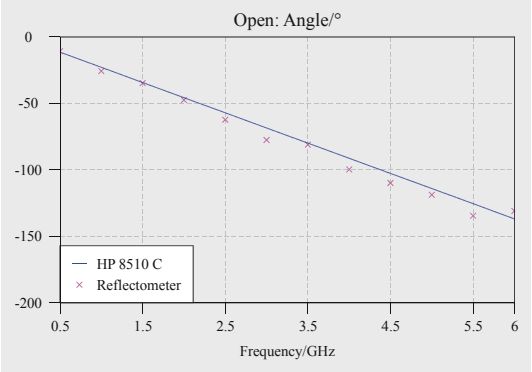

Fig. 5.5 Open: Angle

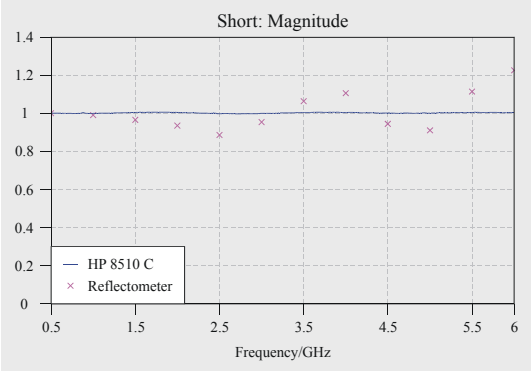

Fig. 5.6 - Short: Magnitude

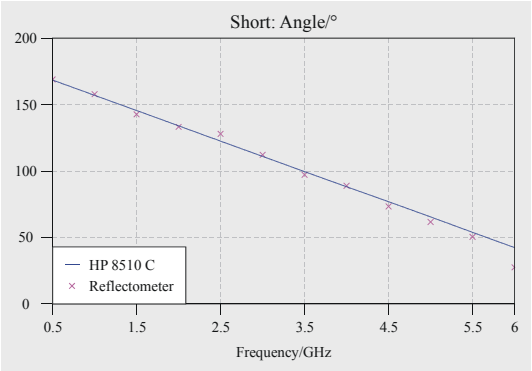

Fig. 5.7 - Short: Angle

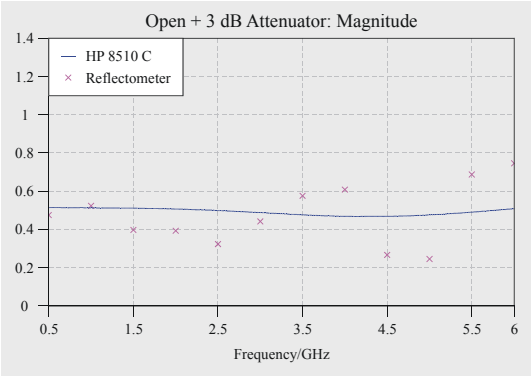

Fig. 5.8 - Open + 3 dB Attenuator: Magnitude

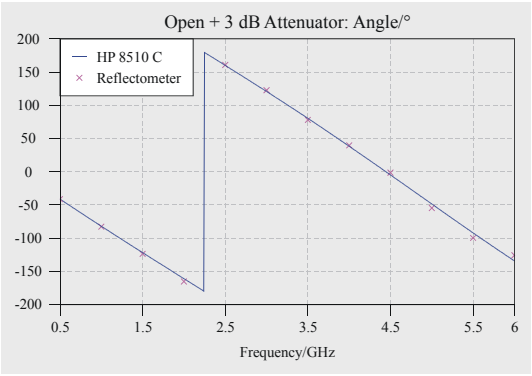

Fig. 5.9 - Open + 3 dB Attenuator: Angle

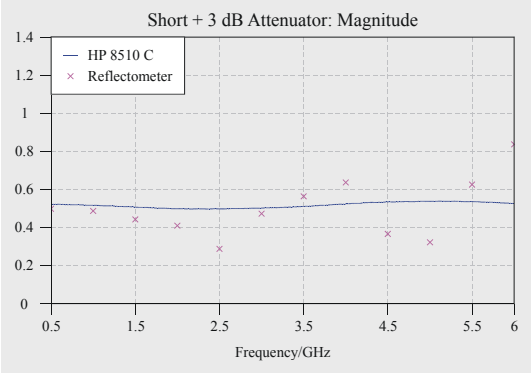

Fig. 5.10 - Short + 3 dB Attenuator: Magnitude

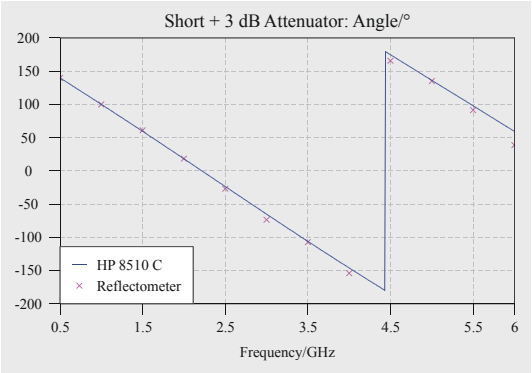

Fig. 5.11 - Short + 3 dB Attenuator: Angle

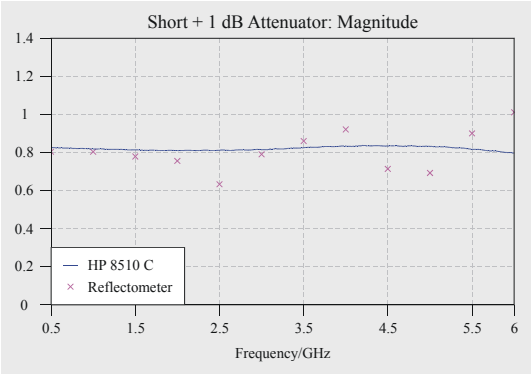

Fig. 5.12 - Short + 1 dB Attenuator: Magnitude

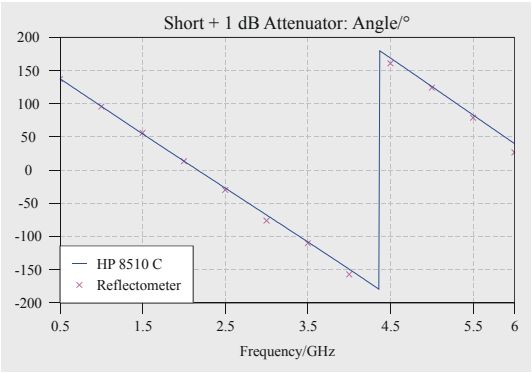

Fig. 5.13 - Short + 1 dB Attenuator: Angle

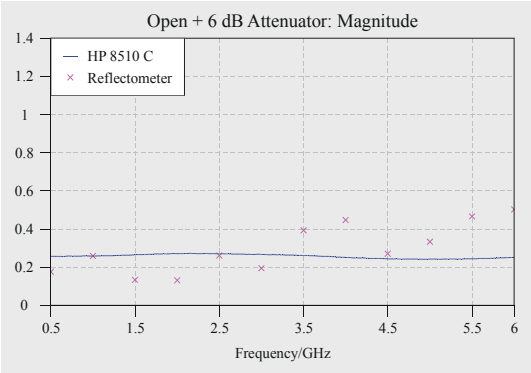

Fig. 5.14 - Open + 6 dB Attenuator: Magnitude

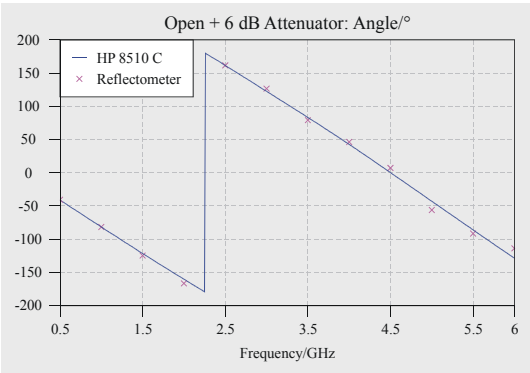

Fig. 5.15 - Open + 6 dB Attenuator: Angle

The consequences of these measurement results to the low impedance reflectometer will be discussed in the following Summary.

6 Summary

The reflectometer that I have built in my diploma thesis consists of two main components: the directional coupler and the standing wave probe. Additionally I implemented the whole software to control the measurement and determine the reflection coefficient.

The measurements of the single hardware components showed that the implementation is very critical. For the standing wave probe this means that it was very hard to design it in a way that the coupling is equal over the whole frequency range together with a low insertion loss. The design of the directional coupler is very sensitive to manufacturing inaccuracies due to the small physical dimensions, especially in the upper frequency range.

The two algorithms I have implemented and tested are both sensitive to measurement inaccuracies. The three-probe version is very sensitive to inaccuracies from power measurements for the determination of the reflection coefficient and the LMS version does not work well with inaccuracies that occur during the calibration procedure.

The test measurements I made with my reflectometer showed that the phase can be measured very accurately, but there are inaccuracies when measuring the magnitude of the reflection coefficient. Both facts could be explained by the used calibration procedure.

As explained before the used calibration algorithm has great influences to the accuracy of the measurement. The problem is that only calibration standards with a magnitude of 1 are used. The accuracy will increase if the algorithm is adapted to use also calibration standards with other magnitudes. Of course it was tried to adapt the algorithm in that way but this leads to very sophisticated mathematical methods that would have grown over the scope of this thesis.

To adapt the reflectometer to a low impedance measurement system the principle of the standing wave probe can be used as implemented within this work. According to the lower transmission line impedance the properties should even increase. The implementation of a directional coupler that has a low impedance between ports 1 and 2 and a impedance of 50 Ω at the ports 3 and 4 will be very hard but it should be possible. Perhaps it will be easier to implement the coupler with a low impedance at all four ports and the transformation to 50 Ω is done externally.

Finally it can be said that this kind of reflectometer can be applied to a low impedance measurement system if the hardware components are designed well and if a more sophisticated calibration method is developed.

7 References

The following articles and books were used in this diploma thesis:

[1] G. Magerl: “Vorlesungsskriptum: Hochfrequenztechnik 1”, Institut für Nachrichten- und Hochfrequenztechnik, Technische Universität Wien, Juni 1998

[2] G. F. Engen: “The Six-Port Reflectometer: An Alternative Network Analyzer”, IEEE Transaction on Microwave Theory and Techniques, vol. MTT-25, pp 1075-1080, Dec. 1977

[3] J. Hu Chia-Lun: “A Novel Approach to the Design of Multiple-Probe High-Power Automatic Impedance Measuring Schemes”, IEEE Transaction on Microwave Theory and Techniques, vol. MTT-28, pp. 1422-1428, Dec. 1980

[4] R. Mongia, I. Bahl, P. Bhartia: “RF and Microwave Coupled-Line Circuits”, Artech House Publishers, ISBN 0-89006-830-5, 1999

[5] G. Madonna, A. Ferrero, M. Pirola: “Design of a Broadband Multiprobe Reflectometer”, IEEE Transaction on Instrumentation and Measurement, vol. 48, pp 622-625, Apr. 1999

[6] S. Ülker, R. M. Weikle: “A Millimeter-Wave Six-Port Reflectometer Based on the Sampled-Transmission Line Architecture“, IEEE Microwave and Wireless Components Letters, vol. 11, pp 340-342, Aug. 2001

[7] F. M. Ghannouchi, R. G. Bosisio: “An Alternative Explicit Six-Port Matrix Calibration Formalism Using Five Standards”, IEEE Transaction on Microwave Theory and Techniques, vol. MTT-36, pp 494-498, Mar. 1988

[8] S. Li, R. G. Bosisio: “Calibration of Multiport Reflectometers by Means of Four Open/Short Circuits”, IEEE Transaction on Microwave Theory and Techniques, vol. MTT-30, pp 1085-1090, Jul. 1982

Appendix A – MatLab® Functions

A.1 MatLab® Functions

A.1.1 Standing Wave Probe Optimisation

For the optimisation of the Standing Wave Probe two MatLab® functions were used, one for the calculation of the condition number for the optimisation function and one to plot the condition number over frequency.

First of all the MatLab® internal function 'fmincon' and its parameters should be explained. This function is used to optimise the positions of the couplers according to the condition number. The following MatLab® instruction was used:

```
X=fmincon('DistDet',[1 2 4 8]·rand+10,A,C,B,C,ones(4,1)·10,ones(4,1)·150)
```

X is a column vector that saves the results of the optimisation which are the distances between the first and the other four couplers. 'DistDet' is a scalar function that delivers the condition number that has to be minimised according to **X**. The second term is a start value for minimisation. **A** and **C** are matrices and **B** is a vector that defines the constraints. These constraints are defined as $\mathbf{A} \cdot \mathbf{X} \leq \mathbf{B}$ and $\mathbf{C} \cdot \mathbf{X} = \mathbf{B}$. **A** is a 4 x 4 negative unit matrix and **B** is a 4 x 1 zero-vector, so all distances have to be positive. **C** is a 4 x 4 zero matrix so this results in no constraint. The penultimate and the last term are the lower and the upper limit for the distances, defined by 4 x 1 one-vectors multiplied with the minimum and maximum length, respectively. The used scalar MatLab® function DistDet is listed below. The input value is a 4 x 1 vector containing the distances between the first and the other four couplers. The return value is the overall condition number.

MatLab®-Function: DistDet - Listing

```
% MatLab-File for determination of the condition number of coupler distances
% written by Rainer Hornstein for diploma thesis "Broadband Reflectometer", 2001
% the input parameter is a vector with the four distances from port 1 to port 2,
% port 1 to port 3, port 1 to port 4 and port 1 to port 5
function[minimum]=DistDet(Dist)     % function definition as DistDet
N=70;                               % number of frequency steps
c=2.997*1e8;                        % speed of light in free space
d12=Dist(1)*1e-3;                   % input parameter redefinition
d13=Dist(2)*1e-3;
d14=Dist(3)*1e-3;
d15=Dist(4)*1e-3;
erg=0;                              % sum variable
for i=0:N                           % for all frequency points
   f=(0.5+0.1*i)*1e9;               % actual frequency
   beta2=4*pi/c*f;                  % 2*beta
   r1=[1 1 1 1 1]';                 % first column of the coefficient matrix
   r2=[2 2*cos(beta2*d12) 2*cos(beta2*d13) 2*cos(beta2*d14) 2*cos(beta2*d15)]';%second
   r3=[0 -2*sin(beta2*d12) -2*sin(beta2*d13) -2*sin(beta2*d14) -2*sin(beta2*d15)]'%third
   Z=[r1 r2 r3];                    % matrix creation
   X=transpose(Z)*Z;                % \
   Y=inv(X)*transpose(Z);           %  calc of the condition number for one frequency
   cond=norm(Z,2)*norm(Y,2);        % /
   erg=erg+cond^2;                  % sum of all squared condition numbers
end
minimum=erg/(N+1);                  % calculation of the overall condition number
```

The second MatLab® function was used for the plot of the condition number over frequency. It was partly similar to the function "DistDet" and uses the same input vector. The output is a plot of the condition number over frequency in a MatLab® plot window. In the MatLab® interface window the distances between two consecutive couplers are returned. The distances between the couplers one and two, two and three, three and four, and four and five are calculated for a

microstrip line with an effective dielectric constant of 2.1085 what is the characteristic value of the used material.

MatLab®-Function: DistPlot - Listing

```
% MatLab-File for plot of the condition number and calculation of coupler distances
% written by Rainer Hornstein for diploma thesis "Broadband Reflectometer", 2001
% the input parameter is a vector with the four distances from port 1 to port 2,
% port 1 to port 3, port 1 to port 4 and port 1 to port 5
function[minimum]=DistPlot(Dist)    % function definition as DistPlot
N=7000;                             % number of frequency steps
c=2.997*1e8;                        % speed of light in free space
d12=Dist(1)*1e-3;                   % input parameter redefinition
d13=Dist(2)*1e-3;
d14=Dist(3)*1e-3;
d15=Dist(4)*1e-3;
erg=0;                              % sum variable
test=zeros(1,N+1);                  % vector of the condition numbers for all frequencies
for i=0:N                           % for all frequencies
   f=(0.5+0.001*i)*1e9;             % calculation of the actual frequency
   beta2=4*pi/c*f;                  % 2*beta
   r1=[1 1 1 1 1]';                 % definition of the 1st column of the coeff matrix
   r2=[2 2*cos(beta2*d12) 2*cos(beta2*d13) 2*cos(beta2*d14) 2*cos(beta2*d15)]';% 2nd
   r3=[0 -2*sin(beta2*d12) -2*sin(beta2*d13) -2*sin(beta2*d14) -2*sin(beta2*d15)]';% 3rd
   Z=[r1 r2 r3];                    % matrix creation
   X=transpose(Z)*Z;                % \
   Y=inv(X)*transpose(Z);           %  calc of the condition number for actual frequency
   cond=norm(Z,2)*norm(Y,2);        % /
   test(i+1)=cond;                  % saving actual condition number
   if test(i+1)>10                  % \
      test(i+1)=10;                 %  if condition number greater than limit set to limit
   end                              % /
   erg=erg+cond^2;                  % calculation of the sum of condition numbers
end
minimum=erg/(N+1);                  % overall condition number
plot(500:N+500,test);               % plot condition number over frequency
Dist=sort(Dist);                    % sort the distances
D1=Dist(1)/sqrt(2.1085)             % calculation of distance between port 1 and 2
D2=(Dist(2)-Dist(1))/sqrt(2.1085)   % calculation of distance between port 2 and 3
D3=(Dist(3)-Dist(2))/sqrt(2.1085)   % calculation of distance between port 3 and 4
D4=(Dist(4)-Dist(3))/sqrt(2.1085)   % calculation of distance between port 4 and 5
```

A.1.2 Directional Coupler

This MatLab® function was used for the development of the directional coupler on an ideal substrate. For this function no input value is needed, since there are so many parameters, that they are chosen by definitions on the beginning of the function. The most important are the *Z*-values, the bandwidth and the number of segments, which are chosen according to theory. The transmission line impedance, the lower frequency and the relative dielectric constant have to be set according to the requirements. The output values are the overall length of the coupler, the length of one element and the lower-, upper- and centre-frequency of the directional coupler. In a table the even- and odd-mode impedances and the accompanying physical dimensions of the coupler at certain positions are displayed. With these values the physical layout of the coupler can be implemented.

MatLab®-Function: DirCoupler - Listing

```
% MatLab function for the determination of a directional coupler
% written by Rainer Hornstein for the diploma thesis "Broadband Reflectometer", 2001
% no input values needed
function[]=DirCoupler()             % function definition as DirCoupler
Elem=20;                            % number of elements of one half
C=20;% coupling between port 1-3,2-4 respectively, in dB
%Z=[1.00555 1.01529 1.03447 1.07471 1.21931];% Z-values for C=20 and B9
%Z=[1.00886 1.02054 1.04153 1.08328 1.22965];% Z-values for C=20 and B11
%Z=[1.01187,1.02485,1.04700,1.08974,1.23748];% Z-values for C=20 and B13
Z=[1.01474 1.02871 1.05175 1.09527 1.24426];% Z-values for C=20 and B15
%Z=[1.01753,1.03232,1.05608,1.10028,1.25049];% Z-values for C=20 and B17
```

```
Z0=50;                              % reference transmission line impedance
%B=9.061;                           % bandwidth value B9
%B=11.571;                          % bandwidth value B11
%B=13.697;                          % bandwidth value B13
B=15.674;                           % bandwidth value B15
%B=17.588;                          % bandwidth value B17
N=9;                                % number of reference segments
er=2.5;                             % relative dielectric constant of the substrate
b=2*0.762e-3;                       % overall height of the substrate
n=(N+1)/2;                                      % number of Z-values
fu=8e8                              % lower frequency limit
fo=fu*B                             % upper frequency limit
f0=(fu+fo)/2                        % centre frequency
R=10^(-C/20);                       % linear coupling factor
w=zeros(1,5);                       % weighting factor vector
L=n*pi/2/pi*3e8/f0/sqrt(er)*1e3;    % overall length
LElem=round(100*L/Elem/2)/100       % element length rounded to 2 decimals
LGes=2*Elem*LElem                   % overall length rounded to 2 decimals
for i=0:3,                          % \
   w(1+i)=(2*i+1)*pi/4/R*log(Z(5-i)/Z(4-i));%  weighting factor
end                                 %  calculation
w(5)=9*pi/4/R*log(Z(1));            % /
syms u                              % MatLab definition for integration
Winkelteil=10*pi/Elem;              % integration steps
DirCoupler=zeros(Elem+1,6);         % field definition
for i=0:Elem,                       % for all segments
Winkel=-10*pi+i*Winkelteil;         % integration area
   Sum=0;                           % summing variable
   for j=1:5,                       % for all weighting factors
      if Winkel>((j-5)*2*pi)        % integral parts according to the different
                                    % weighting factors
         Sum=Sum+w(6-j)*int((sin(u/2))^2/(u/2),(j-6)*2*pi,(j-5)*2*pi);%
      elseif and((Winkel>(j-6)*2*pi),(Winkel<=(j-5)*2*pi)) %
         Sum=Sum+w(6-j)*int((sin(u/2))^2/(u/2),(j-6)*2*pi,Winkel);%
      else                          %
         Sum;                       %
      end                           %
   end                              % end of integration
   DirCoupler(i+1,1)=Winkel;        % angular position -10*pi .. 0
   DirCoupler(i+1,2)=-L/2+i*LElem;  % absolute position - L/2 .. 0
   Sum=-Sum*R/pi*2;                 % intermediate value
   DirCoupler(i+1,3)=Z0*exp(Sum);   % even-mode impedance at determined position
   DirCoupler(i+1,4)=Z0*Z0/DirCoupler(i+1,3);% odd-mode impedance at determined position
end                                 % phys. shape accomp. with odd- and even-mode imp.
for i=1:Elem+1,                     % for all elements
   [ke1,ko1]=solve('DirCoupler(i,3)*sqrt(er)=30*3.1415*3.1415/log(2*(1+sqrt(ke1))/
   (1-sqrt(ke1)))', 'DirCoupler(i,4)*sqrt(er)=30*3.1415*3.1415/
   log(2*(1+sqrt(ko1))/(1-sqrt(ko1)))');
   [ke2,ko2]=solve('DirCoupler(i,3)*sqrt(er)=30*log(2*(1+sqrt(sqrt(1-ke2^2)))/(1-
   sqrt(sqrt(1-ke2^2))))','DirCoupler(i,4)*sqrt(er)=
   30*log(2*(1+sqrt(sqrt(1-ko2^2)))/(1-sqrt(sqrt(1-ko2^2))))');
   ke1=eval(ke1);                   %
   ko1=eval(ko1);                   %
   ke2=eval(abs(ke2(1)));           %
   ko2=eval(abs(ko2(1)));           % evaluation of the equations explained in
   if and((ke1^2>=0.5),(ke1^2<=1))  % the theory of the directional coupler
      ke=ke1;                       %
   else                             %
      ke=ke2;                       %
   end                              %
   if and((ko1^2>=0.5),(ko1^2<=1))  %
      ko=ko1;                       %
   else                             %
      ko=ko2;                       %
   end                              %
   DirCoupler(i,5)=round(100*b*2/pi*atanh(sqrt(ke*ko))*1e3)/100; % even impedance
                                    % rounded to 2 decimals
DirCoupler(i,6)=round(50*b*2/pi*atanh((1-ko)/(1-ke)*sqrt(ke/ko))*1e3)/50; % odd impedance
end                                 % rounded to 2 decimals
DirCoupler                          % output of all values
```

A.2 SXP-Fileconverter

This tool is for the conversion of HP-CITI 2-Port-Files measured with a HP Network-Analyser to *N*-Port-Files that are readable for Microwave Office®. The structure of a *N*-Port-Network that has to be measured is shown in Fig A.1.

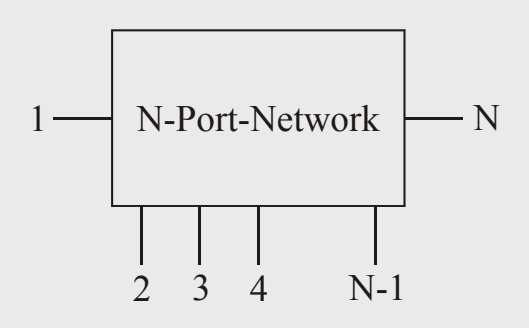

Fig. A.1 - Structure of the Measurement N-Port

The following 2-Port-Files have to be measured: From port 1 to every other port up to port *N*, from port 2 to every higher port up to *N*, from port 3 to every higher port up to port *N* and so on. The last measurement has to be made from port *N*-1 to port *N*. In total $\frac{N\cdot(N-1)}{2}$ files have to be measured. The files have to be named as entered in the input mask field "Input-Filename" shown in Fig. A.2. As an example: If a 4-Port-Network should be created the following files as shown in Tab A.1 have to be measured.

Filename	Network Analyser Port 1	Network Analyser Port 2
DD_S12	1	2
DD_S13	1	3
DD_S14	1	4
DD_S23	2	3
DD_S24	2	4
DD_S34	3	4

Tab. A.1 - Example 4-Port-Network

The input mask for the conversion program is shown in Fig A.2. It contains just four input fields that have to be filled in before the conversion is started by pressing the convert button. The help button gives a little help on the input fields.

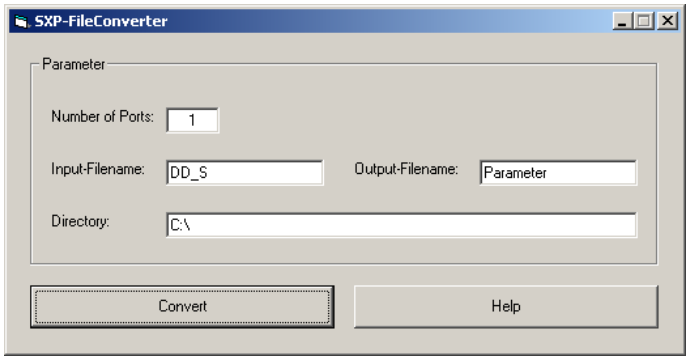

Fig. A.2 - Input Mask of the SXP-FileConverter

The following input fields have to be filled in as explained below for a successful program use:

Number of Ports: This field contains the number of ports of the output file, which should be *N*, the maximum number of ports that were measured. If the number of ports equals 1 the file of port 1 of the input file is created.

Input-Filename: The name of the input file. For 1- and 2-Port files the whole filename has to be specified. For 3 and more ports all files have to be named equal with the number of the first and the second port as index. For example if the files are named *DD_S* and a specific file was measured with port 3 at port 1 and port 5 at port 2 of the network analyser this file has to be named *DD_S35*. In the "Input-Filename" field only *DD_S* has to be specified. The indices are added automatically according to the measurement rules.

Output-Filename: Contains the name of the output file. As extension *.sxp is added automatically, where *x* equals the number of ports *N*.

Directory: This field has to contain the whole path where the input files are located. Also the output file is stored there.

Appendix B - Mechanical Drawings

This chapter shows the mechanical drawings used for the production of the brass carriers for the standing wave probe and the upper- and lower brass carrier of the directional coupler.

Standing Wave Probe

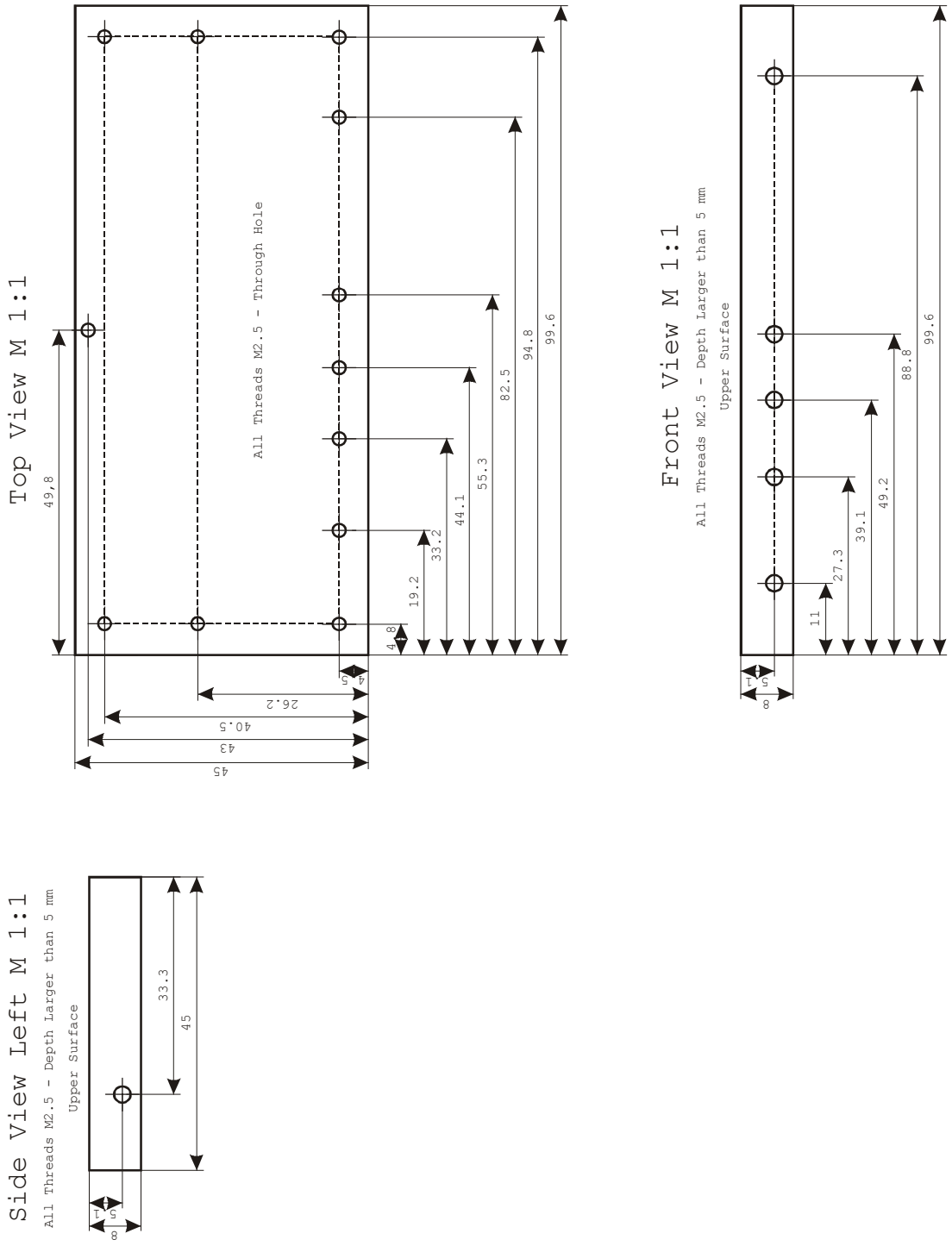

Directional Coupler – Upper Part

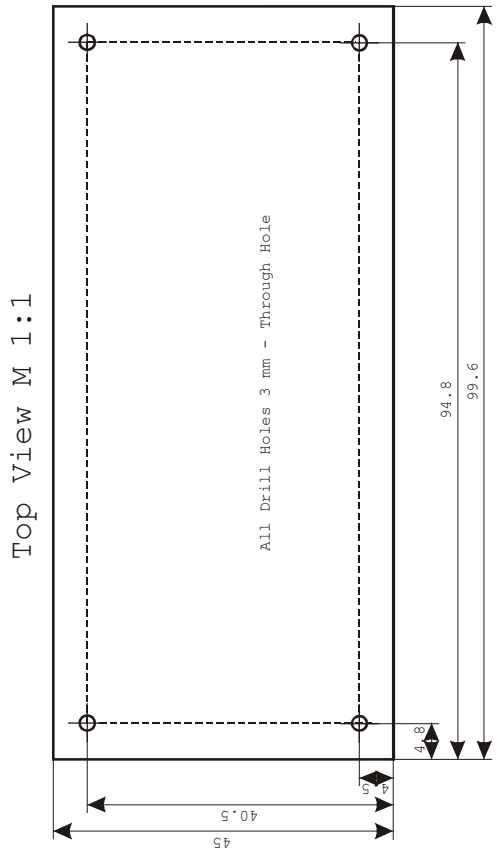

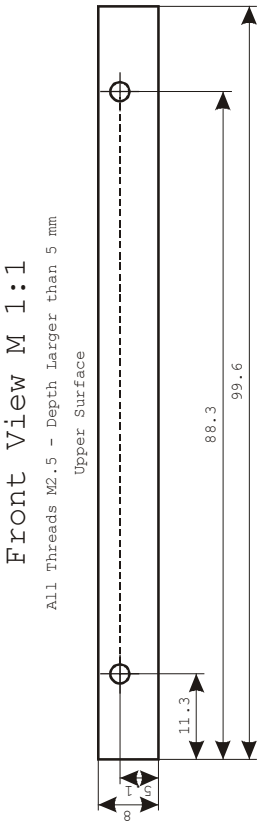

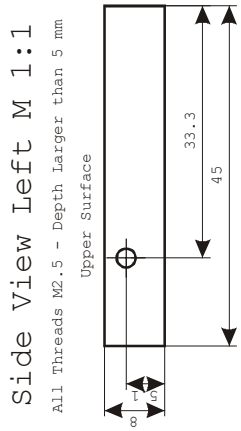

Directional Coupler – Lower Part

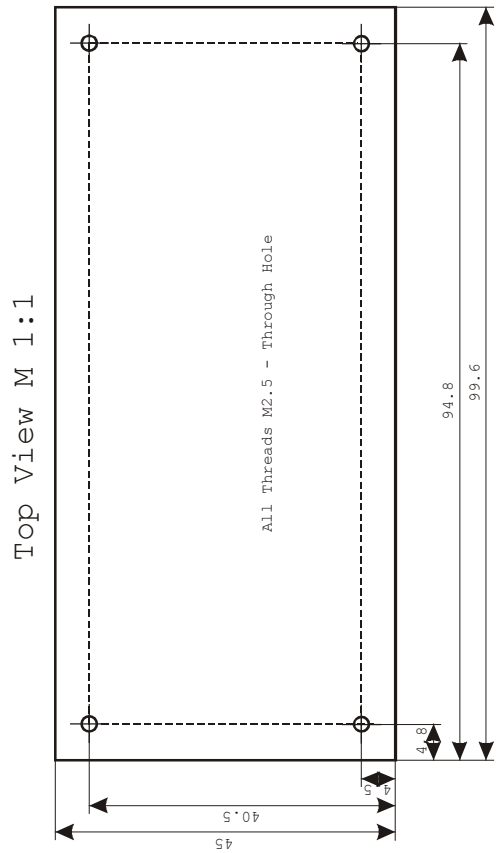

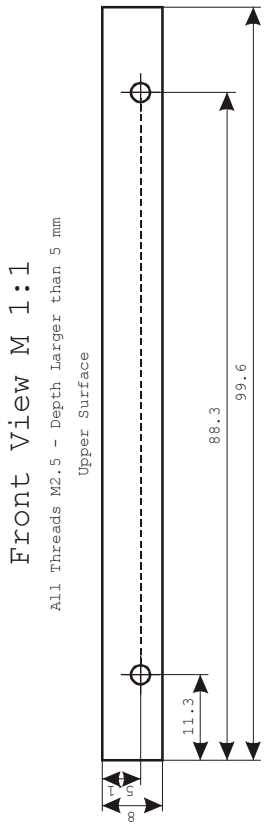

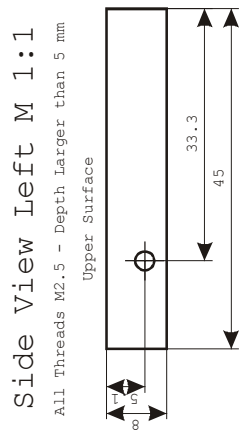

Appendix C - Directional Coupler - Table 6.1

In the following table 6.1 from [4] that was used to design the directional coupler is displayed.

Table 6.1
Tables of parameters for symmetrical TEM-mode coupled-transmission-line directional couplers

δ	Z_1	Z_2	w	B
(a) Normalized even-mode impedances for equal-ripple symmetrical 3.01-db couplers of three sections ($Z_{4-i} = Z_i$)				
0.05	1.14888	3.16095	0.86101	2.51187
0.10	1.17135	3.25984	1.00760	3.03063
0.15	1.9039	3.34049	1.10168	3.45275
0.20	1.20776	3.41242	1.17199	3.83085
0.25	1.22415	3.47932	1.22844	4.18429
0.30	1.23992	3.54311	1.27572	4.52271
0.35	1.25528	3.60495	1.31645	4.85178
0.40	1.27036	3.66560	1.35225	5.17521
0.45	1.28527	3.72563	1.38420	5.49559
0.50	1.30008	3.78546	1.41305	5.81489
0.60	1.32984	3.90585	1.46353	6.45816
0.70	1.35942	4.02894	1.50670	7.10860
0.80	1.38970	4.15648	1.54440	7.77966
0.90	1.42073	4.29005	1.57788	8.47591
1.00	1.45274	4.43120	1.60798	9.20361
(b) Normalized even-mode impedances for equal-ripple symmetrical 6-db couplers of three sections ($Z_{4-i} = Z_i$)				
0.10	1.10298	2.09445	0.91996	2.70356
0.20	1.12090	2.14693	1.07404	3.31984
0.30	1.13625	2.18999	1.17223	3.83226
0.40	1.15038	2.22865	1.24518	4.29931
0.50	1.16381	2.26488	1.30345	4.74258
0.60	1.17680	2.29968	1.35201	5.17291
0.70	1.18952	2.33366	1.39364	5.59673
0.80	1.20208	2.36724	1.43006	6.01830
0.90	1.21454	2.40072	1.46241	6.44068
1.00	1.22698	2.43431	1.49150	6.86621
(c) Normalized even-mode impedances for equal-ripple symmetrical 8.34-db couplers of three sections ($Z_{4-i} = Z_i$)				
0.05	1.06661	1.69824	0.76021	2.22636
0.10	1.07434	1.71858	0.89286	2.61290

(Continued)

Table 6.1 *(Continued)*

δ	Z_1	Z_2	w	B
0.15	1.08073	1.73468	0.97882	2.91703
0.20	1.08644	1.74864	1.04355	3.18211
0.25	1.09171	1.76127	1.09583	3.42397
0.30	1.09670	1.77299	1.13986	3.65041
0.35	1.10146	1.78405	1.17796	3.86595
0.40	1.10606	1.79461	1.21159	4.07347
0.45	1.11054	1.80478	1.24170	4.27495
0.50	1.11490	1.81463	1.26898	4.47178
0.55	1.11918	1.82424	1.29391	4.66502
0.60	1.12339	1.83365	1.31688	4.85550
0.65	1.12754	1.84289	1.33817	5.04386
0.70	1.13164	1.85200	1.35801	5.23063
0.75	1.13570	1.86101	1.37658	5.41623
0.80	1.13973	1.86993	1.39403	5.60103
0.85	1.14373	1.87878	1.41049	5.78534
0.90	1.14770	1.88759	1.42607	5.96943
0.95	1.15166	1.89636	1.44084	6.15354
1.00	1.15560	1.90510	1.45488	6.33787
(d) Normalized even-mode impedances for equal-ripple symmetrical 10-db couplers of three sections ($Z_{4-i} = Z_i$)				
0.20	1.06945	1.57423	1.03140	3.12968
0.40	1.08475	1.60708	1.19816	3.98852
0.60	1.09817	1.63470	1.30282	4.73738
0.80	1.11075	1.66014	1.37959	5.44739
1.00	1.12290	1.68458	1.44020	6.14545
(e) Normalized even-mode impedances for equal-ripple symmetrical 20-db couplers of three sections ($Z_{4-i} = Z_i$)				
0.20	1.02070	1.14914	1.00980	3.03956
0.40	1.02497	1.15617	1.17423	3.84396
0.60	1.02866	1.16197	1.27772	4.53804
0.80	1.03208	1.16720	1.35381	5.19011
1.00	1.03534	1.17213	1.41398	5.82570
$Z_{0e1} = Z_1 Z_2$, $Z_{0e2} = Z_2 Z_3$, $Z_{0e3} = Z_3 Z_0$				

(Continued)

Table 6.1 (*Continued*)

δ	Z_1	Z_2	Z_3	w	B
(f) Normalized even-mode impedances for equal-ripple symmetrical 3.01-db couplers of five sections ($Z_{s-i} = Z_i$)					
0.05	1.05972	1.32624	3.81243	1.20488	4.03071
0.10	1.07851	1.37268	3.97615	1.32559	4.93114
0.15	1.09451	1.40890	4.10191	1.39889	5.65437
0.20	1.10921	1.44029	4.21023	1.45184	6.29714
0.25	1.12314	1.46883	4.30864	1.49333	6.89474
0.30	1.13659	1.49551	4.40089	1.52744	7.46462
0.35	1.14973	1.52091	4.48917	1.55639	8.01698
0.40	1.16266	1.54541	4.57491	1.58152	8.55845
0.45	1.17547	1.56926	4.65912	1.60371	9.09367
0.50	1.18822	1.59265	4.74253	1.62357	9.62609
0.60	1.21370	1.63864	4.90924	1.65791	10.69292
0.70	1.23941	1.68425	5.07867	1.68691	11.77568
0.80	1.26555	1.73013	5.25363	1.71196	12.88720
0.90	1.29235	1.77678	5.43655	1.73402	14.03860
1.00	1.31998	1.82466	5.62978	1.75370	15.24047
(g) Normalized even-mode impedances for equal-ripple symmetrical 6-db couplers of five sections ($Z_{s-i} = Z_i$)					
0.10	1.04501	1.21972	2.38181	1.25446	4.34522
0.20	1.06052	1.25302	2.46010	1.37766	5.45738
0.30	1.07392	1.27919	2.52068	1.45202	6.29953
0.40	1.08633	1.30203	2.57332	1.50548	7.08866
0.50	1.09818	1.32294	2.62159	1.54720	7.83386
0.60	1.10969	1.34262	2.66727	1.58135	8.55462
0.70	1.12099	1.36148	2.71142	1.61023	9.26242
0.80	1.13217	1.37978	2.75470	1.63520	9.96482
0.90	1.14328	1.39772	2.79760	1.65716	10.66721
1.00	1.15438	1.41542	2.84048	1.67673	11.37370
(h) Normalized even-mode impedances for equal-ripple symmetrical 8.34-db couplers of five sections ($Z_{s-i} = Z_i$)					
0.05	1.02538	1.14102	1.85802	1.11764	3.53328
0.10	1.03211	1.15690	1.89019	1.23184	4.20727
0.15	1.03770	1.16899	1.91418	1.30256	4.73524

(*Continued*)

Table 6.1 (*Continued*)

δ	Z_1	Z_2	Z_3	w	B
0.20	1.04271	1.17918	1.93414	1.35395	5.19150
0.25	1.04737	1.18822	1.95170	1.39442	5.60527
0.30	1.05179	1.19648	1.96764	1.42783	5.99090
0.35	1.05602	1.20417	1.98243	1.45627	6.35662
0.40	1.06012	1.21142	1.99635	1.48104	6.70767
0.45	1.06412	1.21833	2.00960	1.50296	7.04761
0.50	1.06803	1.22497	2.02232	1.52262	7.37898
0.55	1.07187	1.23138	2.03462	1.54043	7.70370
0.60	1.07565	1.23760	2.04658	1.55670	8.02323
0.65	1.07939	1.24367	2.05826	1.57168	8.33872
0.70	1.08309	1.24960	2.06971	1.58554	8.65112
0.75	1.08675	1.25542	2.08098	1.59844	8.96119
0.80	1.09039	1.26114	2.09210	1.61050	9.26959
0.85	1.09401	1.26678	2.10310	1.62182	9.57685
0.90	1.09761	1.27235	2.11401	1.63247	9.88347
0.95	1.10119	1.27785	2.12484	1.64253	10.18985
(i) Normalized even-mode impedances for equal-ripple symmetrical 10-db couplers of five sections ($Z_{s-i} = Z_i$)					
1.00	1.10476	1.28331	2.13562	1.65206	10.49635
0.20	1.03418	1.14316	1.70922	1.34442	5.10148
0.40	1.4784	1.16808	1.75305	1.47118	6.56407
0.60	1.05996	1.18815	1.78805	1.54675	7.82513
0.80	1.07140	1.20606	1.81943	1.60053	9.01322
1.00	1.08249	1.22280	1.84912	1.64210	10.17639
(j) Normalized even-mode impedances for equal-ripple symmetrical 20-db couplers of five sections ($Z_{s-i} = Z_i$)					
0.20	1.01016	1.04183	1.17873	1.32734	4.94656
0.40	1.01406	1.04855	1.18767	1.45350	6.31936
0.60	1.01747	1.05386	1.19463	1.52888	7.49038
0.80	1.02066	1.05851	1.20073	1.58261	8.58338
1.00	1.02371	1.06280	1.20638	1.62420	9.64410

$Z_{oe1} = Z_1Z_0$, $Z_{oe2} = Z_2Z_0$, $Z_{oe3} = Z_3Z_0$
$Z_{oe4} = Z_4Z_0$, $Z_{oe5} = Z_5Z_0$

(*Continued*)

Table 6.1 (*Continued*)

δ	Z_1	Z_2	Z_3	Z_4	w	B
(k) Normalized even-mode impedances for equal-ripple symmetrical 3.01-db couplers of seven sections ($Z_{s-i} = Z_i$)						
0.05	1.03635	1.14905	1.50280	4.39954	1.40024	5.6693
0.10	1.05240	1.18406	1.56753	4.61180	1.49705	6.9531
0.15	1.06643	1.21166	1.61640	4.77112	1.55447	7.9780
0.20	1.07950	1.23581	1.65795	4.90662	1.59539	8.8860
0.25	1.09201	1.25786	1.69523	5.02872	1.62715	9.7283
0.30	1.10419	1.27860	1.72975	5.14254	1.65308	10.5302
0.35	1.11615	1.29840	1.76238	5.25103	1.67497	11.3064
0.40	1.12798	1.31754	1.79367	5.35611	1.69388	12.0666
0.45	1.13975	1.33622	1.82400	5.45909	1.71051	12.8174
0.50	1.15149	1.35457	1.85365	5.56097	1.72534	13.5637
0.60	1.17505	1.39069	1.91172	5.76434	1.75090	15.0578
0.70	1.19890	1.42654	1.96915	5.97094	1.77238	16.5728
0.80	1.22323	1.46258	2.02682	6.18437	1.79087	18.1270
0.90	1.24820	1.49918	2.08545	6.40775	1.80710	19.7360
1.00	1.27399	1.53668	2.14566	6.64407	1.82155	21.4147
(l) Normalized even-mode impedances for equal-ripple symmetrical 6-db couplers of seven sections ($Z_{s-i} = Z_i$)						
0.10	1.02686	1.10756	1.32930	2.62516	1.44052	6.1494
0.20	1.04246	1.13419	1.37278	2.72038	1.53802	7.6583
0.30	1.05449	1.15540	1.40584	2.79246	1.59558	8.8908
0.40	1.06580	1.17408	1.43416	2.85438	1.63645	10.0026
0.50	1.07670	1.19128	1.45977	2.91078	1.66806	11.0505
0.60	1.08735	1.20755	1.48367	2.96391	1.69378	12.0628
0.70	1.09787	1.22318	1.50642	3.01511	1.71541	13.0553
0.80	1.10831	1.23839	1.52841	3.06523	1.73404	14.0396
0.90	1.11872	1.25331	1.54989	3.11486	1.75036	15.0232
1.00	1.12915	1.26805	1.57104	3.16446	1.76487	16.0119
(m) Normalized even-mode impedances for equal-ripple symmetrical 8.34-db couplers of seven sections ($Z_{s-i} = Z_i$)						
0.05	1.01460	1.06403	1.21141	1.99183	1.32568	4.9319
0.10	1.02033	1.07694	1.23301	2.03194	1.42127	5.9117

(*Continued*)

Table 6.1 (*Continued*)

δ	Z_1	Z_2	Z_3	Z_4	w	B
0.15	1.02519	1.08680	1.24872	2.06076	1.47818	6.6655
0.20	1.02963	1.09518	1.26167	2.08436	1.51889	7.3140
0.25	1.03379	1.10266	1.27297	2.10489	1.55059	7.9005
0.30	1.03778	1.10953	1.28316	2.12339	1.57653	8.4458
0.35	1.04163	1.11595	1.29256	2.14044	1.59848	8.9622
0.40	1.04538	1.12204	1.30136	2.15641	1.61749	9.4572
0.45	1.04905	1.12786	1.30969	2.17156	1.63423	9.9360
0.50	1.05265	1.13346	1.31764	2.18606	1.64919	10.4022
0.55	1.05621	1.13889	1.32528	2.20004	1.66270	10.8588
0.60	1.05972	1.14417	1.33267	2.21361	1.67500	11.3077
0.65	1.06320	1.14933	1.33984	2.22683	1.68629	11.7507
0.70	1.06666	1.15438	1.34684	2.23979	1.69672	12.1891
0.75	1.07009	1.15934	1.35368	2.25251	1.70640	12.6240
0.80	1.07350	1.16423	1.36040	2.26506	1.71543	13.0563
0.85	1.07689	1.16904	1.36700	2.27746	1.72389	13.4870
0.90	1.08028	1.17381	1.37351	2.28975	1.73184	13.9165
0.95	1.08365	1.17852	1.37993	2.30194	1.73934	14.3456
1.00	1.08702	1.18319	1.38629	2.31408	1.74643	14.7747
(n) Normalized even-mode impedances for equal-ripple symmetrical 10-db couplers of seven sections ($Z_{8-i} = Z_i$)						
0.20	1.02360	1.07622	1.20802	1.81699	1.51198	7.1965
0.40	1.03597	1.09725	1.23839	1.86715	1.61028	9.2638
0.60	1.04718	1.11444	1.26213	1.90649	1.66773	11.0383
0.80	1.05786	1.12991	1.28298	1.94149	1.70815	12.7059
1.00	1.06834	1.14444	1.30229	1.97446	1.73917	14.3359
(o) Normalized even-mode impedances for equal-ripple symmetrical 20-db couplers of seven sections ($Z_{8-i} = Z_i$)						
0.20	1.00697	1.02256	1.05976	1.20128	1.49853	6.9766
0.40	1.01052	1.02846	1.06767	1.21112	1.59672	8.9188
0.60	1.01369	1.03320	1.07372	1.21863	1.65421	10.5678
0.80	1.01669	1.03740	1.07894	1.22515	1.69472	12.1029
1.00	1.01958	1.04129	1.08368	1.23116	1.72584	13.5903

$Z_{0ei} = Z_i Z_0$

(*Continued*)

Table 6.1 (*Continued*)

δ	Z_1	Z_2	Z_3	Z_4	Z_5	w	B
(p) Normalized even-mode impedances for equal-ripple symmetrical 3.01-db couplers of nine sections ($Z_{10-i} = Z_i$)							
0.05	1.02680	1.09163	1.24706	1.66958	4.93133	1.5218	7.365
0.10	1.04112	1.12024	1.29488	1.74863	5.18240	1.6012	9.030
0.15	1.05391	1.14328	1.33137	1.80742	5.36886	1.6478	10.356
0.20	1.06598	1.16366	1.36260	1.85696	5.52654	1.6807	11.528
0.25	1.07763	1.18248	1.39075	1.90116	5.66814	1.7062	12.615
0.30	1.08904	1.20027	1.41691	1.94192	5.79985	1.7269	13.649
0.35	1.10030	1.21737	1.44168	1.98035	5.92523	1.7444	14.648
0.40	1.11149	1.23397	1.46548	2.01711	6.04655	1.7594	15.627
0.45	1.12264	1.25023	1.48856	2.05271	6.16540	1.7728	16.594
0.50	1.13379	1.26625	1.51114	2.08747	6.28296	1.7844	17.554
0.60	1.15624	1.29789	1.55536	2.15551	6.51769	1.8046	19.475
0.70	1.17904	1.32941	1.59902	2.22278	6.75634	1.8216	21.423
0.80	1.20234	1.36117	1.64277	2.29038	7.00316	1.8362	23.421
0.90	1.22630	1.39348	1.68712	2.35918	7.26188	1.8490	25.488
1.00	1.25107	1.42660	1.73250	2.42995	7.53602	1.8604	27.644
(q) Normalized even-mode impedances for equal-ripple symmetrical 6-db couplers of nine sections ($Z_{10-i} = Z_i$)							
0.10	1.02201	1.06888	1.17282	1.42807	2.83542	1.5550	7.989
0.20	1.03437	1.09137	1.20736	1.47877	2.94305	1.6345	9.943
0.30	1.04554	1.10967	1.23393	1.51676	3.02373	1.6809	11.535
0.40	1.05615	1.12599	1.25686	1.54902	3.09269	1.7136	12.969
0.50	1.06645	1.14117	1.27768	1.57805	3.15533	1.7389	14.319
0.60	1.07658	1.15561	1.29716	1.60504	3.21427	1.7594	15.622
0.70	1.08662	1.16957	1.31574	1.63070	3.27103	1.7765	16.900
0.80	1.09661	1.18320	1.33370	1.65546	3.32658	1.7913	18.166
0.90	1.10661	1.19661	1.35125	1.67962	3.38161	1.8042	19.431
1.00	1.11663	1.20989	1.36852	1.70342	3.43663	1.8157	20.702
(r) Normalized even-mode impedances for equal-ripple symmetrical 8.34-db couplers of nine sections ($Z_{10-i} = Z_i$)							
0.05	1.01032	1.03838	1.10598	1.27508	2.10668	1.4599	6.406
0.10	1.01536	1.04904	1.12341	1.30048	2.15200	1.5392	7.681

(*Continued*)

Table 6.1 (*Continued*)

δ	Z_1	Z_2	Z_3	Z_4	Z_5	w	B
0.15	1.01974	1.05735	1.13622	1.31862	2.18413	1.5858	8.658
0.20	1.02379	1.06452	1.14687	1.33341	2.21025	1.6190	9.498
0.25	1.02764	1.07099	1.15622	1.34622	2.23285	1.6446	10.256
0.30	1.03134	1.07697	1.16469	1.35771	2.25315	1.6656	10.960
0.35	1.03494	1.08261	1.17253	1.36825	2.27180	1.6832	11.627
0.40	1.03846	1.08798	1.17989	1.37809	2.28925	1.6985	12.265
0.45	1.04193	1.09314	1.18687	1.38738	2.30577	1.7119	12.883
0.50	1.04534	1.09813	1.19356	1.39622	2.32156	1.7238	13.484
0.55	1.04872	1.10298	1.19999	1.40471	2.33677	1.7346	14.072
0.60	1.05206	1.10771	1.20622	1.41290	2.35152	1.7444	14.650
0.65	1.05538	1.11234	1.21228	1.42085	2.36589	1.7534	15.221
0.70	1.05868	1.11689	1.21819	1.42858	2.37996	1.7617	15.785
0.75	1.06196	1.12137	1.22398	1.43615	2.39378	1.7694	16.345
0.80	1.06523	1.12579	1.22966	1.44356	2.40740	1.7766	16.901
0.85	1.06849	1.13018	1.23525	1.45084	2.42087	1.7833	17.455
0.90	1.07174	1.13448	1.24076	1.45802	2.43421	1.7896	18.008
0.95	1.07498	1.13877	1.24620	1.46511	2.44745	1.7955	18.560
1.00	1.07823	1.14302	1.25158	1.47211	2.46063	1.8011	19.111
(s) Normalized even-mode impedances for equal-ripple symmetrical 10-db couplers of nine sections ($Z_{10-i} = Z_i$)							
0.20	1.01889	1.05161	1.11743	1.26387	1.90628	1.6133	9.345
0.40	1.03041	1.07004	1.14313	1.29777	1.96074	1.6927	12.016
0.60	1.04103	1.08543	1.16344	1.32390	2.00313	1.7386	14.303
0.80	1.05127	1.09945	1.18139	1.34672	2.04073	1.7708	16.450
1.00	1.06133	1.11271	1.19805	1.36779	2.07614	1.7954	18.547
(t) Normalized even-mode impedances for equal-ripple symmetrical 20-db couplers of nine sections ($Z_{10-i} = Z_i$)							
0.20	1.00555	1.01529	1.03447	1.07471	1.21931	1.6024	9.061
0.40	1.00886	1.02054	1.04153	1.08328	1.22965	1.6818	11.571
0.60	1.01187	1.02485	1.04700	1.08974	1.23748	1.7278	13.697
0.80	1.01474	1.02871	1.05175	1.09527	1.24426	1.7601	15.674
1.00	1.01753	1.03232	1.05608	1.10028	1.25049	1.7848	17.588

$Z_{0ei} = Z_i Z_0$

Appendix D - Substrate Taconic TLX 9

Following 3 sheets present the data sheet of the used substrate. The material is a TLX 9 substrate of Taconic with a thickness of 0.03'' and a copper cladding of 1 oz./sq. ft.

TLX

APPLICATIONS

LNAs, LNBs, and LNCs
PCS/PCN Large Format Antennas
High Power Amplifiers
Passive Components

Taconic has over 35 years of experience coating fiberglass fabric with PTFE (polytetrafluoroethylene). This enables Taconic to manufacture copper clad PTFE/woven glass laminates with exceptionally well controlled electrical and mechanical properties.

The dielectric constant (Dk) range is 2.45 to 2.65. The Dk can be specified anywhere within this range with a tolerance of ±.04. The dissipation factor is approximately .0019 when measured at 10 GHz.

See "How to Order" on back page for a complete product listing.

TLX laminates can be sheared, drilled, milled and plated using standard methods for PTFE/woven fiberglass materials. The laminates are dimensionally stable, and exhibit virtually no moisture absorption during fabrication processes.

TLX laminates are generally ordered clad on one or both sides with 1/2, 1, or 2 oz. electrodeposited copper. Contact our Customer Service Department for alternate claddings.

Typical applications for TLX laminates include radar systems, phased array antennas, mobile communication systems, microwave test equipment, microwave transmission devices and RF components.

The copper-clad laminates meet the latest revision of MIL-S-13949/9, type GXN and IPC-L-125.

TLX laminates are tested in accordance with IPC-TM-650. A Certificate of Compliance containing actual test data accompanies each shipment.

TLX-9 TYPICAL VALUES

Property	Test Method	Units	Value	Units	Value
Dielectric Constant @ 10 GHz	MIL-P-13949		2.50		2.50
Dissipation Factor @ 10 GHz	MIL-P-13949		0.0019		0.0019
Moisture Absorption	IPC-TM-650,2.6.2.1	%	<.02	%	<.02
Dielectric Breakdown	IPC-TM-650,2.5.6	kV	>60	kV	>60
Volume Resistivity	IPC-TM-650,2.5.17.1	Mohm/cm	10^7	Mohm/cm	10^7
Surface Resistivity	IPC-TM-650,2.5.17.1	Mohm	10^7	Mohm	10^7
Arc Resistance	IPC-TM-650,2.5.1	Seconds	>180	Seconds	>180
Flexural Strength Lengthwise	IPC-TM-650,2.4.4	psi	>23,000	N/mm²	>159
Flexural Strength Crosswise	IPC-TM-650,2.4.4	psi	>19,000	N/mm²	>131
Peel Strength (1 oz. ED)	IPC-TM-650,2.4.8	lbs./in.	12.0	N/mm	2.1
Thermal Conductivity	Cenco-Finch	BTU/in./hr/ft²/°F	2.34	W/m/K	0.34
x-y CTE	TMA	ppm/°C	9-12	ppm/°C	9-12
z CTE	TMA	ppm/°C	130-145	ppm/°C	130-145
UL-94 Flammability Rating	UL-94		V-0		V-0

Type		Dk
TLY-5A		2.17
TLY-5		2.20
TLY-3		2.33
TLT-0	TLX-0	2.45
TLT-9	TLX-9	2.50
TLT-8	TLX-8	2.55
TLT-7	TLX-7	2.60
TLT-6	TLX-6	2.65
TLE-95		2.95
TLC-27		2.75
TLC-30		3.00
TLC-32		3.20
CER-10		10.0

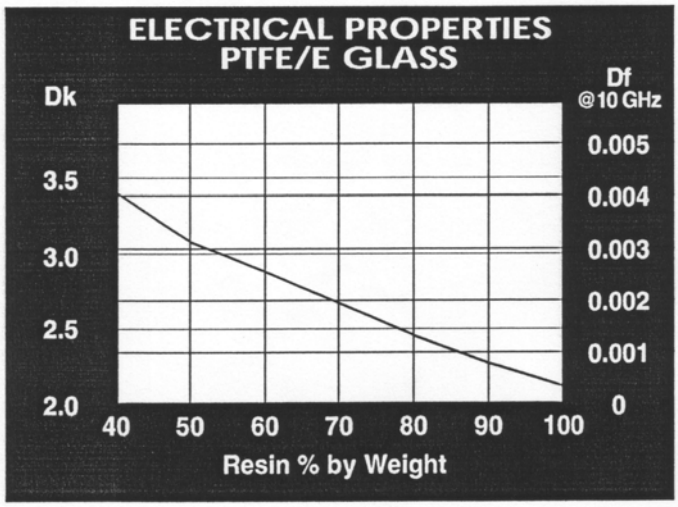

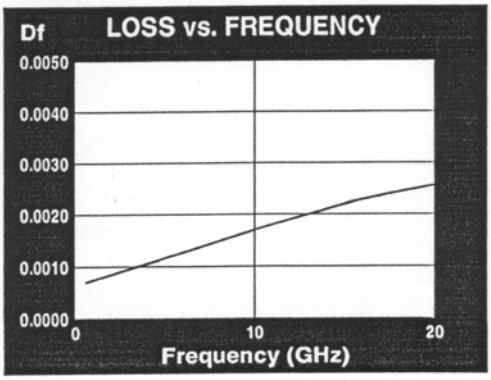

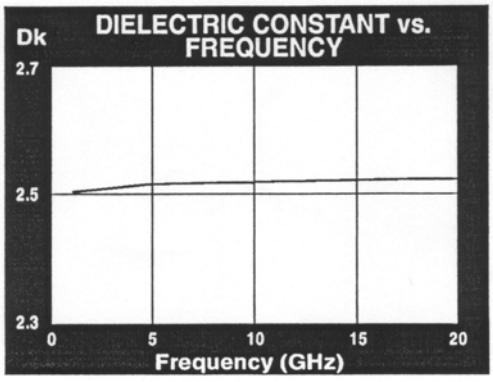

3/98

How to Order

Designation	Dielectric Constant	Dielectric Thickness	Dielectric Thickness
TLX - 0	2.45 +/– .04	.0050" - .0190"	0.13mm – 0.48mm
		.0200" - .0300"	0.50mm – 0.76mm
		.0310" and up	≥ 0.80mm
TLX - 9	2.50 +/– .04	.0050" - .0190"	0.13mm – 0.48mm
		.0200" - .0300"	0.50mm – 0.76mm
		.0310" and up	≥ 0.80mm
TLX - 8	2.55 +/– .04	.0050" - .0190"	0.13mm – 0.48mm
		.0200" - .0300"	0.50mm – 0.76mm
		.0310" and up	≥ 0.80mm
TLX - 7	2.60 +/– .04	.0050" - .0190"	0.13mm – 0.48mm
		.0200" - .0300"	0.50mm – 0.76mm
		.0310" and up	≥ 0.80mm
TLX - 6	2.65 +/– .04	.0050" - .0190"	0.13mm – 0.48mm
		.0200" - .0300"	0.50mm – 0.76mm
		.0310" and up	≥ 0.80mm

Standard sheet size is 36" x 48" (914mm x 1220mm). Please contact our Customer Service Department for the availability of other sizes of certain products and for other types of copper foil and thick metal claddings.

TLX can be ordered with the following electrodeposited copper:

Designation	Weight	Copper Thickness	Copper Thickness
CH	1/2 oz./sq. ft.	~ .0007"	~18 µm
C1	1 oz./sq. ft.	~ .0014"	~ 35 µm
C2	2 oz./sq. ft.	~ .0028"	~ 70 µm

Panels may be ordered cut to size

Typical Panel Sizes	
12" x 18"	304mm x 457mm
16" x 18"	406mm x 457mm
18" x 24"	457mm x 610mm
16" x 36"	406mm x 914mm
24" x 36"	610mm x 914mm
18" x 48"	304mm x 508mm

An example of our part number is: TLX-9-0310-CH/CH-18" x 24" (TLX-9-0310-CH/CH-457mm x 610mm)

TACONIC
ADVANCED DIELECTRIC DIVISION

P.O. Box 69 • 136 Coonbrook Road
Petersburgh, New York 12138 • USA
TEL: 518-658-3202 • FAX: 518-658-3988
TOLL FREE: 800-833-1805 • FAX: 800-272-2503

Lynn Industrial Park
Mullingar, Co. Westmeath,
Republic of Ireland
TEL: +353-44-40477 • FAX: +353-44-44369

Na-906-2, APT Factory 148
Yatap-dong, Bundang-ku
Sungnam-si, Kyung'gi-do, Republic of Korea
TEL: +82-342-704-1858/9 • FAX: +82-342-704-1857